

Thesis

Jens Steckert

“Design, implementation and setup of an automated quantum efficiency measurement system for charge-coupled devices”

version_8_final_print_b

Contents

1	Introduction and Overview.....	7
1.1	The SNAP Project.....	7
1.1.1	Theoretical background.....	7
1.1.1.1	Measurements done with supernovae data.....	7
1.1.1.2	Reasons for a space telescope.....	8
1.1.2	The SNAP Satellite.....	8
1.1.3	The SNAP CCD.....	9
1.2	Quantum efficiency (QE).....	11
1.2.0.1	Wavelength versus Absorption length.....	11
1.2.0.2	Internal and external quantum efficiency.....	12
1.3	Specifications of the QE test setup.....	13
1.4	System architecture.....	13
1.4.1	Planned extensions.....	15
2	The Test Setup.....	16
2.1	The light source.....	16
2.1.1	QTH source.....	16
2.1.2	Arc lamps.....	16
2.1.3	The housing.....	17
2.1.3.1	Standard housing.....	17
2.1.3.2	Elliptic reflector housing.....	18
2.1.3.3	Selected housing.....	18
2.1.4	Shutter.....	19
2.2	The monochromator section.....	20
2.2.1	Monochromator.....	20
2.2.1.1	Theory of operation.....	20
2.2.2	The stray light problem.....	22
2.2.3	Filters.....	24
2.2.3.1	Dielectric short pass filters.....	25
2.2.3.2	Dielectric long pass filters.....	25
2.2.3.3	Colored glass band pass filters.....	26
2.3	Integrating sphere section.....	27
2.3.1	Dimensions of the sphere.....	28
2.4	Black Box.....	30
2.5	Dewar.....	30

2.6	Light monitoring.....	31
2.6.1	Photo Diode.....	32
2.6.1.1	Temperature dependency of the photo diode.....	32
2.6.1.2	Photo diode mount.....	33
2.6.1.3	Operation.....	34
2.6.1.4	Secondary light monitoring PD.....	34
2.7	Mechanics.....	35
2.7.1	The height problem.....	35
2.7.2	Adapters.....	35
2.7.2.1	Focusing lens - shutter adapter.....	35
2.7.2.2	Shutter – filter wheel adapter.....	36
2.7.2.3	Monochromator – Integrating sphere adapter.....	36
2.7.2.4	Integrating sphere – black box connector.....	37
2.7.2.5	Black box – dewar adapter.....	38
2.7.3	Detector housing.....	39
3	Dimensioning and performance checks.....	40
3.1	Throughput Estimation.....	40
3.1.1	Calculation of light flux into the monochromator.....	40
3.1.2	Calculation of light flux into the Integrating Sphere.....	42
3.1.3	Calculation of the light flux on the Detector.....	43
3.2	Spectral dependence of the throughput.....	44
3.3	Noise Measurements	45
3.3.1	Noise measurement of the photo diode.....	45
3.3.1.1	Signal-to-noise ratio at 960nm.....	47
3.3.1.2	Signal-to-noise current ratios for different wavelengths.....	48
3.3.1.3	Measurement strategies vs. Noise.....	49
3.4	System Setup and performance measurements.....	51
3.4.1	Light generation and manipulation system set up.....	51
3.4.1.1	Set up of the filter wheels.....	51
3.4.1.2	Light source set up.....	51
3.4.2	Light detection system setup.....	52
3.4.3	Measurement of the dark level.....	53
3.4.4	Measurement of the light output.....	54
3.4.4.1	Light output vs wavelength.....	54
3.4.4.2	Explanation of the UV drop.....	55
3.4.5	Uniformity measurement.....	58

3.4.5.1	Horizontal scan.....	58
3.4.5.2	Vertical scan.....	59
3.4.5.3	Conclusion.....	59
4	Automation.....	61
4.0.1	The VOODOO software.....	61
4.0.1.1	Architecture.....	61
4.0.1.2	The VOODOO.qe add-on.....	62
4.0.1.3	VOODOO script.....	67
4.0.1.4	Script controlled mode.....	68
4.0.2	IDL program.....	70
5	QE measurements and error calculation.....	71
5.1	QE Measurements.....	71
5.1.1	Reflectivity vs QE.....	71
5.1.2	Gain measurement.....	71
5.1.2.1	The 55Fe method.....	71
5.1.2.2	Results of the Gain measurement.....	72
5.1.3	Measurement of QE vs wavelength.....	73
5.1.3.1	Measurement of the QE on a low voltage (lv) device.....	73
5.1.3.2	Measurement of the QE on a high voltage (hv) device.....	76
5.1.3.3	Re-measuring the first device.....	78
5.1.4	Conclusion.....	79
5.2	Error Calculation.....	80
5.2.1	Sources of errors and correction factors.....	80
5.2.1.1	Error caused by lamp and Housing.....	80
5.2.1.2	Error caused by the shutter.....	80
5.2.1.3	Error caused by the filter wheels.....	81
5.2.1.4	Sources of error in the monochromator.....	82
5.2.1.5	Error contribution by the integrating sphere.....	82
5.2.1.6	Error contribution by light leaks in the setup.....	82
5.2.1.7	Errors caused by the reference photo diode.....	82
5.2.1.8	Measurement error of the Keithley 6485 picoammeter.....	82
5.2.1.9	Maximum exposure time.....	83
5.2.2	Summary.....	84
6	Conclusion.....	86
7	Appendix.....	87

7.1 Hardware.....	87
7.1.1 Pictures of the test setup.....	87
7.1.2 Parts list.....	90
7.1.3 Additional Autocad drawing of the mechanical parts.....	92
7.1.4 Wiring diagram of the setup.....	93
7.2 Software.....	94
7.2.1 Qe measurement script.....	94
7.2.2 VOODOO qe script log file.....	97
7.2.3 IDL Program for calculation of the QE.....	98
7.2.4 Selected parts of the VOODOO extensions.....	100
7.2.4.1 VOODOO.QE.Main.setLightLevel_closedSlit.....	100
7.2.4.2 VOODOO.QE.Calc.....	102
7.2.4.3 VOODOO.QE.Mono.SendCommand.....	106
7.2.5 Software Screenshots.....	107

ABSTRACT

The SNAP group at LBNL developed backside illuminated high resistivity p-channel charge-coupled devices (CCDs). An important parameter of these devices is the quantum efficiency (QE)

A test setup was designed and implemented to measure the quantum efficiency (QE) of these CCDs.

Several existing designs of other groups had been reviewed to develop an own improved setup which is able to perform fully automated high precision QE measurements with a wavelength range from 300 to 1100nm.

The setup consist of the following main components:

- Light source (100W xenon)

- Monochromator (Oriel MS257)

- Integrating sphere (LabSphere CSTM US2000SF)

- Dewar (hosting the CCD and the reference photo diode)

- Control PC (controls the setup and provides full automatic operation)

This design features a highly uniform (>99% uniformity) source of monochromatic light. The light intensity is measured with a photo diode on the focal plane next to the CCD inside the dewar.

Due to the placing of the diode and measuring times covering >90% of the exposure time, the results are independent of light intensity variations and other optical sources of error.

The QE of a LBNL CCD was measured successfully. The results had been verified by a reflectivity measurement done at Lick Observatory.

The measurement values were reproductive and explainable, hence the setup is considered to be working. However further work in error analysis and detail refinements will have to be done.

1 INTRODUCTION AND OVERVIEW

1.1 The SNAP Project

The goal of the SNAP collaboration is to build a satellite telescope which is able to make high resolution and broad spectral bandwidth images of type Ia supernovae.

1.1.1 Theoretical background

Type Ia supernovae are astronomical light standards. This type of supernova occurs only in double star systems where one star is a carbon-oxygen white dwarf and the other is usually an evolving red giant. As the white dwarf accrete matter from the nearby companion its mass increases. When the Chandrasekhar limit is reached, the white dwarf collapses. Due to the increasing pressure inside the white dwarf, the fusion of carbon and oxygen to ^{56}Ni starts. This fusion process stops the contraction of the white dwarf and turns it into an explosion. This explosion produces an enormous amount of visible and infrared light. Since this type of supernova shows a typical spectrum and has a definite absolute brightness it can be used as an astronomical “standard candle” [1].

1.1.1.1 Measurements done with supernovae data

By measuring the irradiance of such a supernova, its distance from earth can be estimated. From the distance the time elapsed since the supernova event happened can be derived.

The redshift of the light provides the speed of the object relative to the earth. Properly calibrated and sorted into classes, several thousand of such supernova images will provide a database from which important cosmological parameters can be extracted [2].

Knowing the distance and speed of supernovae, it is possible to learn about the size and shape of space.

One of the questions has to do with the expansion of the space. Before 1998 it was common sense that the expansion of space was slowing down. Then, by observation of supernovae, the LBNL group and another independent group discovered that the expansion is accelerating. The problem right now is that only 70 supernovae per year are detected by ground based telescopes. With the SNAP satellite it should be possible to observe around 2000 of these events each year [3].

1.1.1.2 Reasons for a space telescope

There are several advantages of a space telescope like SNAP. Due to the lack of any atmosphere there is no IR cutoff which is often caused by water molecules. Another benefit is a better brightness calibration because there is no atmosphere which can cause variations in the light intensity. Another issue is the spectral calibration of the telescope. Inside the atmosphere there are always variations in humidity, temperature and pressure. These variations can influence the observed spectrum. In space none of these occur.

1.1.2 The SNAP Satellite

The main design goals for the SNAP satellite are a large field of view (fov), adequate spectral range, and maximal optical resolution. SNAP will be equipped with a three-mirror, two-meter diameter reflecting telescope. The focal length of the optics is 21.6m. The fov will be about 0,34 arcmin for visible and near infrared (NIR) observations. The spectral sensitivity range will be from 350-1000 nm for the CCD imagers and 900-1700 nm for the HgCdTe infrared detectors.

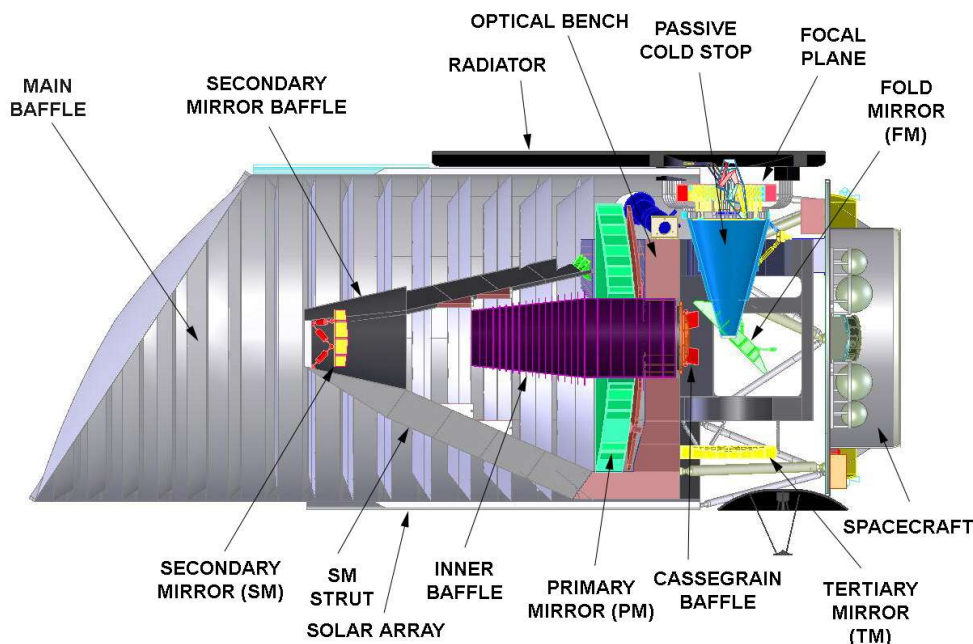


Fig. 1 Cross section of the SNAP satellite [2]

Fig. 1 shows a cross section of the actual satellite design. The focal plane, holding 36 CCDs and 36 IR sensors is located below the primary mirror [2]. The focal plane is connected with thermal links to a radiator which maintains an

operating temperature of 140K. The CCDs and HgCdTe sensors will be located on the focal plane in an alternating pattern. Each CCD will be equipped with 4 broadband color filters. Since the focal plane has only illumination in a ring-shape area, scanning across the observation area is required. To achieve good signal quality, the CCD Read Out IC (CRIC) is also located on the focal plane. The amplified signals from the sensors are then transferred to the electronics boxes on both sides of the plane. Fig. 2 shows an exploded drawing of the SNAP imaging system.[4]

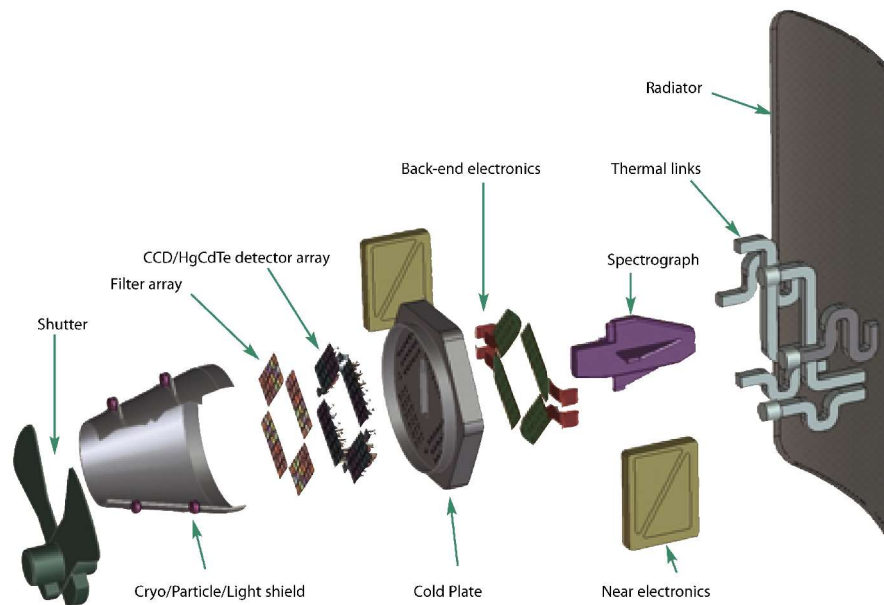


Fig. 2 Exploded drawing of the SNAP imager [4]

1.1.3 The SNAP CCD

To meet the demands of the astronomers, the SNAP CCD has to have excellent VIS/NIR response. The IR response up to more than 1000 nm is achieved by making the sensitive area of the CCD very thick (200 nm). A good blue response is reached by choosing a back illuminated design so that no gate structure absorbs the UV light. Since the thickness of the SNAP CCD is about 200 um an electric field on the substrate is needed to achieve a good resolution. Otherwise, the charge transfer from the backside to the gate structure on the front side is too slow and the charge has time to spread laterally. Since the main purpose of the CCD is the observation of "point-like" objects, this point spread function is very important. Experiments have shown that bias voltages up to 100 V applied to a 200 um CCD are possible. Fig. 3 shows a schematic cross section of the LBNL CCD compared

with other conventional designs.

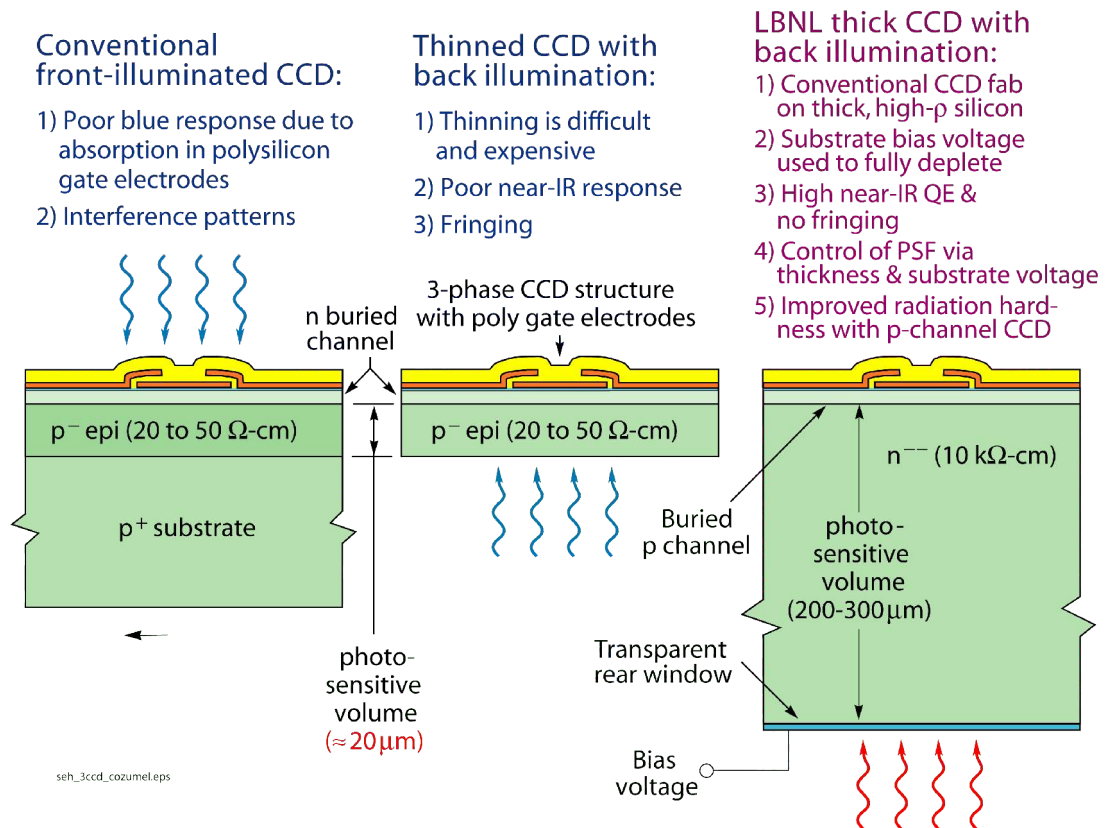


Fig. 3 Different types of CCDs

As shown in Fig. 3 conventional CCD designs as front illuminated and thin back illuminated CCDs have several design-based problems. The SNAP CCD inherits the advantages of both conventional designs without inheriting most of their problems.

The CCD is made on very high resistivity (10k Ω -cm) n-type silicon. Unlike conventional CCDs the charge carriers are holes, not electrons. This also improves the radiation hardness [5].

The backside has a 3-layer coating. The first layer is a very thin (10nm) layer of n⁺ doped poly-Si used as an interface layer. This layer is followed by a layer of Indium Tin oxide (ITO). The top layer consist of 100nm SiO₂. Both outer layers are transparent for UV/Vis light and the thickness of the SiO₂ and the ITO was chosen to minimize reflection. The ITO layer is also used as electrode to apply the bias voltage.

1.2 Quantum efficiency (QE)

The quantum efficiency (QE) is the probability that an incident photon produces an e-h pair which is collected. In the range of near UV to IR it is simply the percentage of light detected by the CCD. The quantum efficiency is dependent of several parameters, such as the material, the architecture, and the geometry of the CCD. A silicon CCD is capable of detecting light from about 300 to nearly 1100 nm. Fig. 4 shows the measured quantum efficiency of a SNAP CCD vs. wavelength.

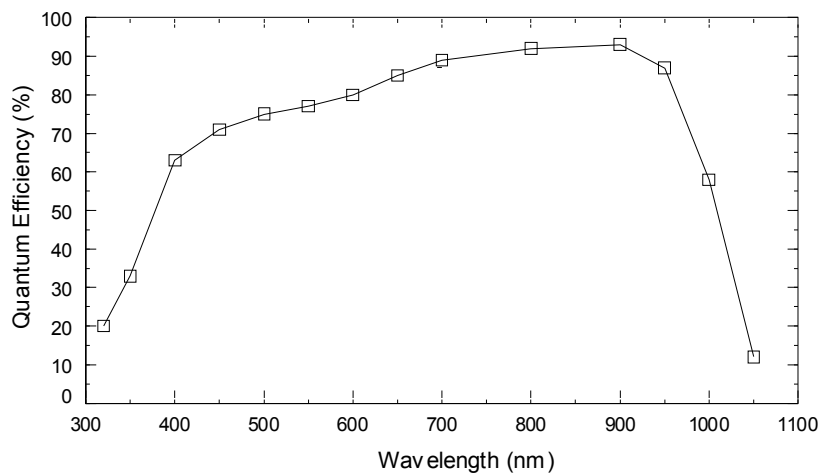


Fig. 4 Quantum efficiency of a LBNL CCD vs. wavelength [6]

1.2.0.1 Wavelength versus Absorption length

The QE is wavelength dependent. This dependency is directly related to the energy of the photons (see Fig. 5). If a photon has higher energy it gets absorbed in a shorter distance. The absorption length is quite short for UV and long for infrared light. This absorption length is directly related to the wavelength of the photon and the band gap of the silicon. If the photon has a lower energy than the band gap it is not able to generate any electron-hole pair in the CCD; the CCD becomes transparent for these longer wavelengths. If the photon has a high energy, it is able to push electrons of different energies from the valence band into the conduction band. That means that a photon “find” an e⁻ in an appropriate energy level is higher for high than for low energy photons. At lower photon energies, the probability of “finding” an e⁻ with a appropriate energy decreases and the absorption length increases. When the photon energy reaches the band gap energy, the photon is only able to push the electrons in the valence band with the highest energy levels into the conduction band. This leads to a dramatic

decrease in the QE at a certain wavelength. When $E_{\text{photon}} < E_{\text{band gap}}$ the quantum efficiency reaches zero. This explains the drop of the QE curve of silicon at the red end of the spectrum. Fig. 5 shows the absorption length of photons in silicon for different wavelengths and temperatures.

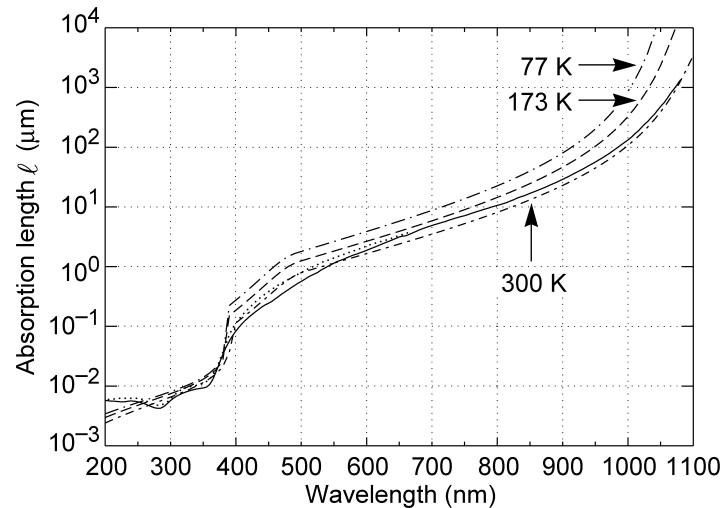


Fig. 5 Absorption length of photons in Si vs. wavelength [6]

1.2.0.2 Internal and external quantum efficiency

In this setup the external quantum efficiency is measured. The external quantum efficiency includes reflection at the surface of the device and other absorption processes. Therefore the external QE is always lower than the internal QE. This factor describes the QE of the device for the case that the photons arrive the sensitive region and the charge does not recombine.

A good example which shows the difference of internal and external QE is the illumination of the CCD with UV light. Due to the high energy of the UV photons the probability that they generate an e-h pair is very high, the absorption length is very short. A high rate of generated e-h pairs would lead to a good QE. Measurements on CCDs show the opposite behavior. The reason for that is the structure of the CCD. As mentioned above the gate structure on conventional front illuminated CCD absorbs most of the higher energy photons, the sensitivity decreases. The back illuminated designs have, due to the lack of an interfering gate structure, a better UV performance. But, compared to visible light the QE for UV light is still low. The reason for this behavior is the backside coating of the CCD. The poly-Si layer absorbs most of the UV light and is responsible for the low QE at 300nm [6].

1.3 Specifications of the QE test setup

The test setup should perform the following tasks:

- Automatic computer controlled measurement of the QE
- Capability to measure the QE up to a CCD size of 6x6cm
- Perform a QE measurement with an absolute error less than 3%
- Relative error less than 1%
- Repeatability of the measured values.
- Spectral range from 300nm to nearly 1100nm
- Optional reflection measurement should be possible

To achieve this performance, a test setup consisting of different components was built. To meet the first specification, the automatic computer controlled measurement of the QE, every motorized part which has to be adjusted during measurement is connected to a PC running control software. The second specification is met by using an integrating sphere with a distance of ~90 cm from the CCD, this provides an uniform light source over the 6x6cm area. The error requirements are met through the selected components and the design of the setup. The spectral range is guaranteed by the chosen lamp and optical components while a dual output monochromator gives the flexibility to integrate a reflectivity measurement device into the setup.

1.4 System architecture

The main system architecture is derived from QE test setups of other groups. The setups of 3 other groups were reviewed to design an architecture of our setup. All of these systems are similar. There are differences in the use and placing of the different components. In particular the integrating sphere sizes varied from 8" to 20". The choices of monochromators and light sources were also different. The group at ESO (European Southern Observatory) uses a W lamp instead of an arc lamp. The existing test systems do not meet our specifications in terms of accuracy in the measurement, so we had to think about the refinement of the existing designs. [7][8][9]

The main task of the system is to provide a nearly monochromatic light source (10 nm bandwidth) with a highly uniform output over an area with a diameter of 10 cm. The system consists of 4 main sections: light source, monochromator, integrating sphere and the "exposure" section including the dewar with the CCD and the photo diode. In the following chapters the parts of the different sections,

the alternatives we had and reasons why choosing a specific part will be described. As shown in Fig. 6 the whole setup will be assembled on two "breadboards". These rigid boards with threaded holes in a regular array are arranged in a L-shape and mounted with brackets. On one board are the light source, filter wheels and monochromator. The monochromator has two output ports. One is used for the QE measurement the other will be used for the reflectivity measurement. The integrating sphere is located in the corner of the L shape. Here the the optical path changes direction by 90 degrees. After the integrating sphere there is a black box, approximately 80cm long. The dewar with the CCD is located at the opposite end of the box. By placing the dewar some distance of the integrating sphere, the exact positioning of the CCD is uncritical. Since the CCD is located inside a dewar, the light has to pass through a window. This window will not decrease the performance of the setup because the reference photo diode will be also placed behind this window.

The placing of the temperature controlled reference diode next to the CCD inside the dewar is one of the key features of the setup and is the main advancement to the other reviewed setups.

QE Test Setup

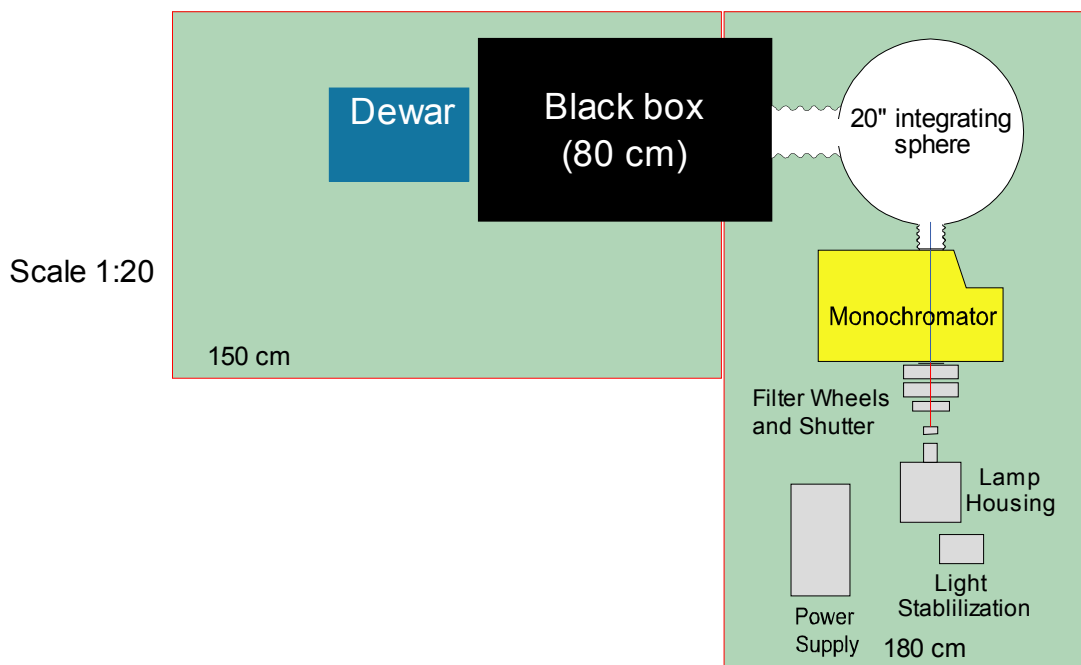


Fig. 6 Block diagram of the QE test bench

Fig. 7 Shows the actual QE setup.



Fig. 7 Photo of the QE setup

As shown in Fig. 7 the QE setup is fairly large. The 90° design helps to arrange it in the lab. Other pictures of the setup can be found in the appendix.

1.4.1 Planned extensions

Since the light source in the setup provides monochromatic, highly stabilized and controlled light, it can be used for other purposes. One measurement which is essential for the characterization of CCDs and which can verify the results of the QE measurement is the measurement of the reflectivity. Therefore an optical fiber will be used to guide light from the secondary output of the monochromator into the black box, where the reflectivity measurement device will be located.

Another useful application for using the light is an advanced pinhole projector. This device can be also placed into the black box using the same optical fiber bundle.

2 THE TEST SETUP

This section will show the hardware which is used in the QE setup. Every part will be discussed and described. The description follows the light beam from its generation in the light source to the absorption in the CCD.

2.1 The light source

The first part of every QE measurement system is a light source. Since there are several light sources available it is important to make a good choice. The necessary wavelength range extends from 300 to 1100 nm. There are basically two big groups of scientific light sources available: Quartz tungsten halogen (QTH) lamps and arc lamps.

2.1.1 QTH source

A tungsten halogen lamp consist of a quartz bulb filled with a halogen gas and a tungsten filament. A QTH light source acts nearly as a black body, which means that the spectral distribution changes with the temperature of the filament. The spectrum of a QTH lamp is quite smooth and without emission lines. Its spectral range reaches from 240 to 2700 nm. The disadvantage of this lamp is the relatively low UV output and the short lifetime of approximate 50 h at a color temperature of 3300 K. At a wavelength of 300nm the output is only 2% of the maximum output, which occurs at around 900nm. Since the QE of the CCD at 300nm is about 5%, a higher photon flux is required to reach the required level of charge in a pixel at a given exposure time. To achieve this flux with a QTH lamp a high wattage lamp has to be used. An other fact is the limited sensitivity of the photo diode (PD) at the low wavelength end of the spectrum The lifetime of a QTH lamp is dependent upon its operating temperature. Lowering the operating temperature will increase the lifetime of the bulb dramatically. Since high UV output is mandatory, there is no way to lower the operating temperature. Another aspect of QTH sources is the size of the filament. The light source has to illuminate the input slit of a monochromator. A typical size for an input slit is 2mm x 20mm. The filament of a 100W QTH source is 2.3mm x 4.2mm. This relatively large-area light source leads to a light source image much bigger than the input slit. [10]

2.1.2 Arc lamps

Arc lamps are based on a electric discharge between two electrodes. The excited gas between the electrodes emits light. Since the light-emitting part in an

arc lamp is very small, the light density is relatively high. An arc lamp consists of two electrodes (cathode and anode) in a quartz tube, filled with an inert gas like xenon. By adding metals like sodium the spectrum of the emitted light can be changed (sodium causes the strong yellow color of some street lights). The useful spectrum of common arc lamps spans 250-2400 nm. The light intensity distribution over the spectrum in the limits of 300-1100 nm changes by approximately 60%, which is a good value comparing to QTH lamps. That means a xenon arc lamp is an ideal light source for our purposes. The only problem of this source are emission lines of xenon. The excited atoms in the arc emit light at specific wavelengths (aka. emission lines). The spectrum of a typical xenon “ozone free” lamp is relatively free of these lines from 300 to around 800nm. In the rest of the spectrum from about 800 to 1100 nm are many pressure broadened emission lines, which are often 30 times brighter than the average of the spectrum. Since the light intensity is measured in the integrating sphere and the dewar, the absolute brightness of these lines is not a problem. The more critical effect is the stray light in the monochromator caused by this lines. The out of band light is 10^{-5} less than the in band light, a strong emission line of 3000% the base intensity next to the desired band is visible as stray light with 0.03 % of the in band light. Since there are several emission lines in the spectrum, additional filters have to be used to reduce this effect [10]. Spectra of other arc lamps filled with Hg, or HgXe etc. showed much more emission lines so the pure Xe lamp was the best choice.

2.1.3 The housing

Every scientific light source needs to have an appropriate housing. Since we had the choice between two different lamp types we had also the choice between different housing models. There are two different housing types available: Housings based on a condenser and an additional lens which matches the acceptance cone of the monochromator, and housings which employ a parabolic mirror to focus the light and matching the acceptance cone.

2.1.3.1 Standard housing

The “traditional” housings based on the condenser lens system have the big disadvantage that they are inefficient. Only a small solid angle of the “light sphere” around the light source is converted to usable output. In the *Oriel Book of Photon Tools* [10] the efficiency of the housing is described by a “lens conversion factor”. To calculate the light output of the housing the irradiance of the lamp has

to be multiplied with this factor (1).

$$L_{out} = Irrad * LCF \quad (1)$$

Where L_{out} is the light light emitted by the housing, *Irrad* is the irradiance of the lamp and *LCF* is the lens conversion factor. For standard housings (either arc or QTH lamp housings) this factor is ~ 0.11 . That means that only 11% of the light emitted by the lamp leaves the housing. The other big disadvantage of the condenser/focal length matching lens system is the magnification factor of the light source on the monochromator entrance slit. This magnification reduces the light density of the image projected on the slit. When the image of the light source is larger than the monochromator entrance slit, light loss occurs. Especially when using QTH lamps with their large filaments, high light loss occurs by this vignetting factor. By using arc lamps with a very small light emitting area the magnified image on the slit is still smaller than the slit. That means a bigger fraction of the light light falling onto the slit gets into the monochromator [10].

2.1.3.2 Elliptic reflector housing

The other housing type is based on a elliptic reflector which is available in different focal lengths to match the acceptance cone of the monochromator. Like in a car headlight, most light of the lamp is collected by the mirror and focused onto the monochromator entrance slit. The “lens conversion factor” of this housing (Oriel PHOTOMAX) is around 0.7. This means 70% of the light emitted by the source leaves the housing and is focused onto the monochromator entrance slit. This type of housing has several disadvantages. It requires water cooling when using arc lamps as sources. It also produces an bigger image of the source on the slit due to imperfect focusing [10].

2.1.3.3 Selected housing

The light throughput estimation of the whole system shows that even with a conventional housing the amount of light arriving the CCD is sufficient. In our system we use a standard housing which has an better focus on the input slit of the monochromator than the PHOTOMAX. With the combination of a standard housing and an arc lamp we can avoid too much vignetting of the light beam at the monochromator input slit. A picture of the housing chosen for the QE setup is shown in the appendix (Fig. 53)

2.1.4 Shutter

To achieve exact exposure times the light flux has to be interrupted by a shutter system. The usual exposure times will be between 5 and 50 seconds (see section 5.2.1.2 for possible exposure times).

For absolutely light-tight operation the shutter has double-overlapped blades. The Uniblitz model VS25 was chosen. This shutter with double-overlapping, and reflecting blades provides a very high light suppression. The other benefit is the ability of high speed operation. The shutter is controlled and driven by the timing board of the Leach¹ controller. The reflective blades protect the shutter from overheating while the shutter is closed.

¹ Leach controller: The standard CCD controller at LBNL which operates the CCD and is controlled by the VOODOO software

2.2 The monochromator section

This component of the QE setup has the task of producing a beam of monochromatic light. Our goal is to produce a light beam with a spectral width of $\sim 10\text{nm}$. This can be achieved by either using narrow-band filters or a monochromator. Since the monochromator provides the most flexible way to create nearly monochromatic light, it is used in our setup. The second part of the monochromator is a motorized filter wheel.

2.2.1 Monochromator

A monochromator is an optical device which uses the wavelength dispersion of a diffraction grating to filter light. The dispersion is achieved by the ruled surface of the grating. An Oriel MS257 monochromator was chosen for this setup. Fig. 52 (Appendix) shows the opened monochromator.

2.2.1.1 Theory of operation

The grating equation describes the dispersing property of the grating

$$m \cdot \lambda = g \cdot (\sin A - \sin B) \quad (2)$$

Where m is an integer (the order), λ is the wavelength, g is the distance between two grooves in the grating, B is the angle of the incident ray to the grating normal, A is the angle of the reflected ray to the grating normal. If the path difference between the reflected rays 1' and 2' is equal to any integer multiple of the wavelength λ , constructive interference occurs.

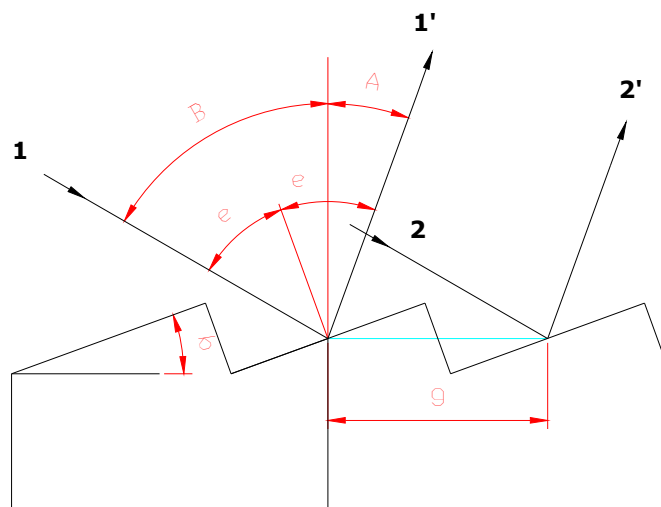


Fig. 8 Illustration of an optical grating. The angle b is the blaze angle

The grating equation is satisfied for $m=0$, $m=1$, $m=2\dots$. This leads to the problem that the unwanted “higher orders” have to be suppressed (see filter wheel discussion below).

A parabolic mirror projects the dispersed light onto the output slit. By varying the slit width the optical bandpass width is selected. The spectral position of the bandpass is determined by the angle of the grating to the incident light. In this way a monochromator can select a specific wavelength band of the spectrum. The light which is not leaving the monochromator through the output slit has to be absorbed in the monochromator. There is always a small amount of light (out of the selected band) which is able to leave the monochromator. This out-of-band light is called stray light. One number which indicates the quality of a monochromator is the stray light rejection. Other important numbers are the reflectivity of the mirrors, the grating efficiency, and its dispersion. To get maximal throughput an low f-number and a large input width is required. Since the optical bandwidth is defined to be 10nm, the only way to use wide slits is the usage of a grating with a high dispersion. The standard gratings available have 300,600 and 1200 lines per cm. To achieve maximum dispersion, a 1200 line grating is chosen.

A single monochromator has 4 mirrors, each with a reflectivity of about 92% which leads to an overall attenuation of about $0.92^4 = 72\%$ by the mirrors. At the point of highest efficiency a 1200 lines/mm grating reaches approximately 80%.

$$Efficiency = E_{mirror}^{(number\ of\ mirrors)} * E_{grating}^{(number\ of\ gratings)} \quad (3)$$

The overall efficiency of a monochromator as shown in (3) decreases with the number of mirrors and gratings in the beam line.

2.2.1.1.1 The grating

The key part of a monochromator is the grating. The grating disperses the incident light and projects the spectrum onto the output slit. The grating is made of an optical substrate which is coated with a reflective surface such as an aluminum alloy. A practical grating has a surface structure like a sawtooth. The angle of this pattern to the normal of the grating determines the “blaze wavelength”². At this wavelength the grating has the highest efficiency. To cover the spectral range of our setup, we chose a grating with a 350nm blaze³ and one

² Blaze wavelength: wavelength with highest reflection, determined by the blaze angle.

³ Blaze angle: see Fig. 8

with a 750nm blaze wavelength. With these two gratings we are able to cover the whole spectral range with a grating efficiency which is never below 50%. [10] The grating efficiencies of the chosen gratings over wavelength is shown in Fig. 9.

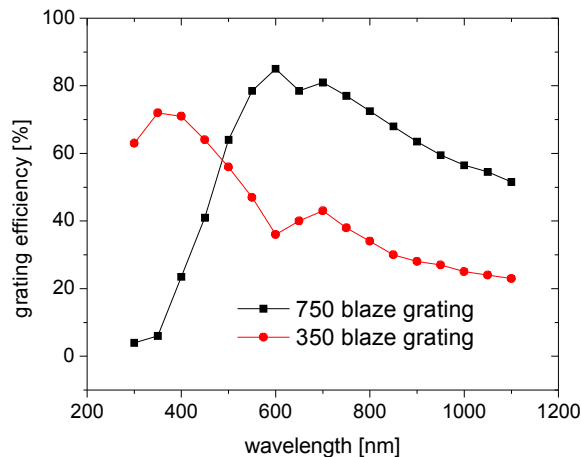


Fig. 9 Grating efficiencies of the used gratings

2.2.1.1.2 Filter wheel

Another part which also belongs to this section is a motorized filter wheel. The filter wheel is used for order sorting. Since the grating equation (2) is fulfilled for different wavelengths, the unwanted higher orders have to be suppressed. To avoid second order effects, the light has to be band limited before it reaches the monochromator. A second-order effect occurs when light with double the desired wavelength falls onto the grating. This light is reflected into the same angle than the desired light, hence it comes out of the output slit. To prevent this, order sorting filters which block higher wavelengths are used. Bandpass filters with a width of ~150-200 nm are a good choice for blocking higher order effects and reducing the amount of stray light.

2.2.2 The stray light problem

Between the different monochromator models we compared, the stray light rejection varied from 3×10^{-4} to 1×10^{-9} . That means out-of-band light incident in the monochromator is suppressed by this factor. To estimate the influence of stray light on the output signal of the CCD a calculation was done.

As a first step the total amount of light coming into the monochromator has to be quantified. This is partially done in the throughput calculation. The amount of

incident light calculated in (14) has to be multiplied by the bandwidth of the input. To avoid as much stray light as possible, 150nm wide bandpass filters were placed in front of the monochromator. Each of these filters consist of a short and a long wavelength pass filter. The following equation quantifies the total amount of light coming through the input slit [10].

$$L_{MonoIn} = L_{out} * LC * Ref * Fm * Fw * Vi * Bw \quad (4)$$

L_{out} is the light output of the source

LC is the Lens Conversion Factor

Ref is the gain through the reflector

Fm is the attenuation through the focusing lens

Fw is the attenuation through the filter

Vi is the vignetting factor and is calculated by formula (2)

Bw is the bandwidth of the light (defined by the filters)

The stray light rejection factor suppresses all out-of-band light. This factor is provided by the makers of the monochromator The total amount of stray light is given by

$$SL = L_{MonoIn} * StrayReject \quad (5)$$

SL is the stray light

L_{monoIn} is the light coming into the monochromator

$StrayReject$ is the Stray light rejection factor

Since the absolute amount of stray light is known, it's possible to calculate the stray light in the output beam which leaves the mono. This is then

$$SLRel = \frac{(SL * 100)}{Light} \quad (6)$$

$SLRel$ is the Stray light relative to the desired light output of the Monochromator in percent

SL is the Stray light

$Light$ is the desired light in the band pass

The effect of the stray light in the CCD output signal is given by

$$SLS = \frac{(SL * QE_{FilterBand})}{(L_{MonoOut} * QE_{(10nm)})} \quad (7)$$

Where SL is the stray light, $QE_{FilterBand}$ is the average QE for the stray light, $L_{MonoOut}$ is the output of the monochromator and QE_{10nm} is the QE in the desired band.

The result of these calculations is shown in Fig. 10.

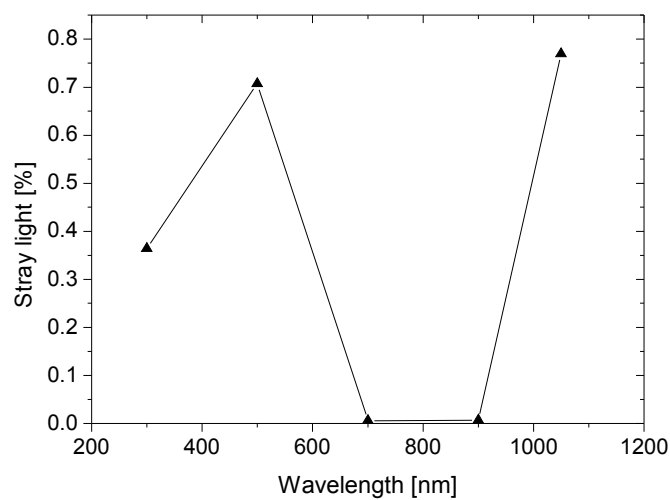


Fig. 10 Stray light vs wavelength

As shown in Fig. 10 the maximal contribution of the stray light to the signal is $\sim 0.8\%$. This case occurs when the QE of the CCD for the desired light is low and high for the stray light.

To avoid the stray light problem, a double monochromator could be used. Double monochromators are expensive and lower the intensity of the light. A single Oriel MS257 monochromator is used in our design. This gives the flexibility to upgrade the system to a double monochromator if the error caused by the stray light is found to be a problem. To reduce the error in the QE, the stray light could be measured.

2.2.3 Filters

To avoid the second order effects of the monochromator as well as the most of the stray light, it is advisable to use a filter wheel with bandpass filters to limit the

out of band light caused by these effects. In our setup we have two filter wheels with five positions each. That means there is an overall capacity of eight filters (one position on each wheel left blank to use all filters independently). Since the spectral range is about 800nm, eight 100nm band passes would cover it. The problem is that there are no 100nm wide bandpass filters available. We therefore made our own bandpass filters by stacking of a short wave- and a long wave pass filter. This combination is shown in Fig. 11.

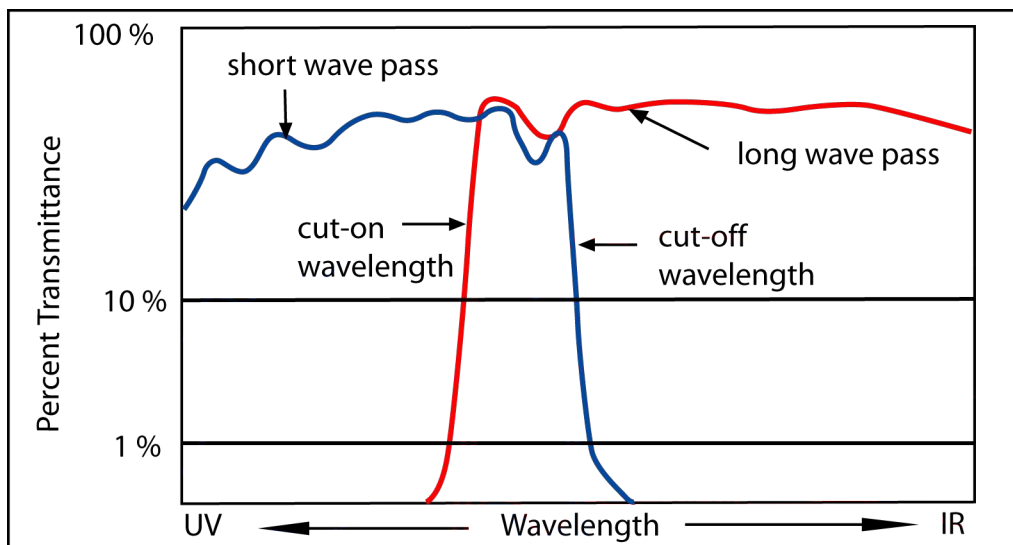


Fig. 11 Bandpass resulting of the combination of a short wave pass and a long wave pass filter

The second critical issue is the cut-on / cutoff slope of these filters. To get the same transmission at every wavelength the filter bands must overlap. Since we have 8x 100nm there is no reserve for overlapping the bands. To get overlapping areas we increased the bands to 150nm. With 150nm bands its possible to cover the whole spectral range with 50nm overlap.

2.2.3.1 Dielectric short pass filters

These filters consist of a substrate which is coated by a multilayer thin film coating which defines the cut off transition edge. Longer wavelengths are rejected with several layers of dielectric reflectors. The problem with these filters is the limited transmission range. The minimum wave length which is transmitted is about 415nm. In this case they cannot be used for the two lowest wavelength bandpass filters.

2.2.3.2 Dielectric long pass filters

These filters consist of a substrate which is coated by thin films which define

the cut-on point of the filter. The transmittance range reaches from the cut on wavelength up to more than 1200nm. The transmittance is about 80% in the transmissive and $<1 \cdot 10^{-3}$ in the blocked area.

2.2.3.3 Colored glass band pass filters

Colored glass produces the bandpass. The slope at the turn on frequency is often not as sharp as a dielectric or dichroic filter but they are the only type of filters available for the blue.

All three filter types are used in the setup. The combination of a short and a long pass filter creates a band pass filter. These combination filters are used from 450-1000nm. The glass filters are used for the two bandpass filters at the short end of the spectrum. The area from 950-1100 is covered by a single long pass. For wavelengths over 1100 nm there is no need of any blocking because the CCD does not have any sensitivity to light. Fig. 12 shows the different bandpass filters chosen over the desired wavelength range.

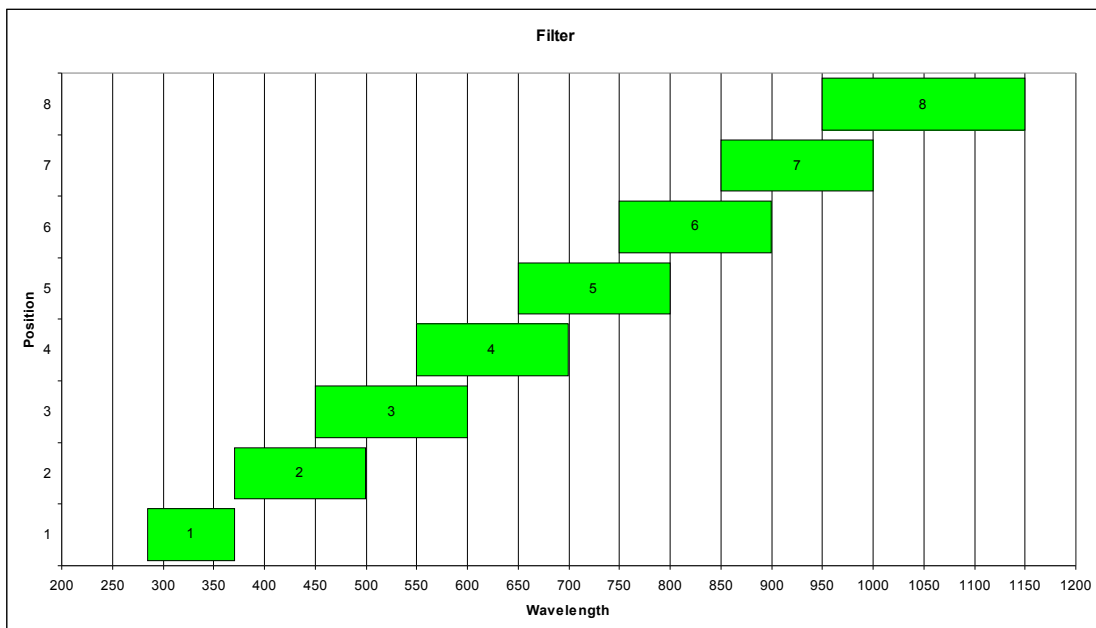


Fig. 12 The bandpass filters used

2.3 Integrating sphere section

After the monochromator the light is monochromatic (10nm band) but not uniformly illuminating the area of the CCD. An integrating sphere is used to convert the small-dimensional light beam into an uniform diffuse light source. An integrating sphere is a sphere whose interior is covered with a diffuse reflective material. The input and output port are arranged in such a way that no light from the input port is able to reach the output port after one reflection. Often internal baffles are used to achieve at least two or more reflections of the light between in and output port. By having multiple diffuse reflections inside the sphere the light becomes uniformly distributed and the output port appears as a diffuse uniform light source. Among other parameters, the uniformity of the light leaving the sphere is determined by the port-fraction (8) [11]

$$f = \frac{A_{ports}}{A_{sphere}} \quad (8)$$

The ratio between reflective surface (A_{sphere}) and port area (A_{ports}) determines the size (diameter of the sphere). There is no equation which describes the uniformity as a function of the port fraction. A “thumbs rule” given by the maker of the sphere, LabSphere, quotes good uniformity at a port fraction of < 0.05 . To reach better uniformity a smaller port-fraction is required. In our case we chose a port- fraction of 0.01. A second parameter which influences the uniformity is the distance of the object from the output port. The dependency of the uniformity from the distance is given by:

$$IU = \cos^4 \left(\arctan \left(\frac{D/2}{x} \right) \right) \quad (9)$$

IU is the light intensity, D is the diameter of the illuminated area and x is the distance from the output port. For an output port size of 4” (~100mm), the uniformity of the light across the illuminated area scales with distance to the port as shown in Fig. 13. This figure shows the dependency of the uniformity from the distance to the spheres' output port. A value of 1 represents maximal uniformity. Other sources of uniformity errors like imperfections in the coating or a high port fraction value are ignored in this graph. These errors in uniformity are visible at every distance from the sphere [11].

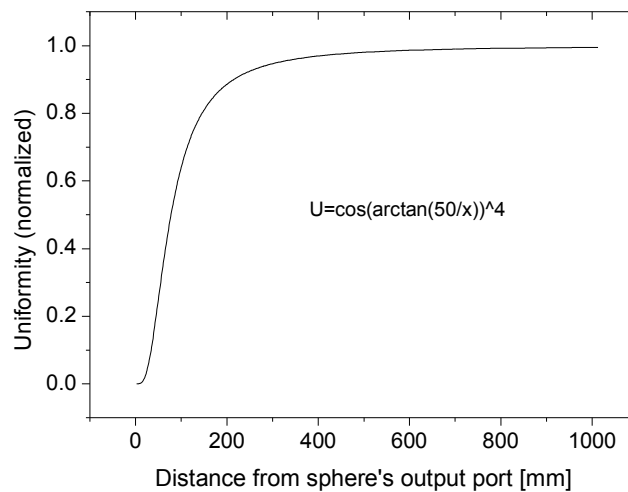


Fig. 13 Uniformity vs. distance from sphere calculated with (9)

2.3.1 Dimensions of the sphere

The size of the output port is determined by the size of the illuminated area and the brightness of illumination. The size of the largest CCD is 60x60mm. To illuminate this area the output port size was chosen to be 4" which is a good compromise between uniformity and light intensity. The input port is 2" with an option to reduce it to 1" if this diameter is not necessary. To monitor the irradiance of the sphere, two 1" detector ports are located above the output port of the sphere. Solving

$$pf = \frac{(A_{InputPort} + A_{OutputPort} + 2 * A_{DetectorPort})}{A_{Sphere}} \quad (10)$$

with a *pf* of 0.01, a sphere diameter of 20" (50 cm) is more than adequate. The main disadvantages of such a large sphere are a relatively low light output because of the large number of reflections and the high cost. Since the throughput calculation has shown a sufficient amount of light even with this diameter, the 50cm design was chosen.

Fig. 14 and Fig. 15 are showing the sphere which is used in the measurement setup.

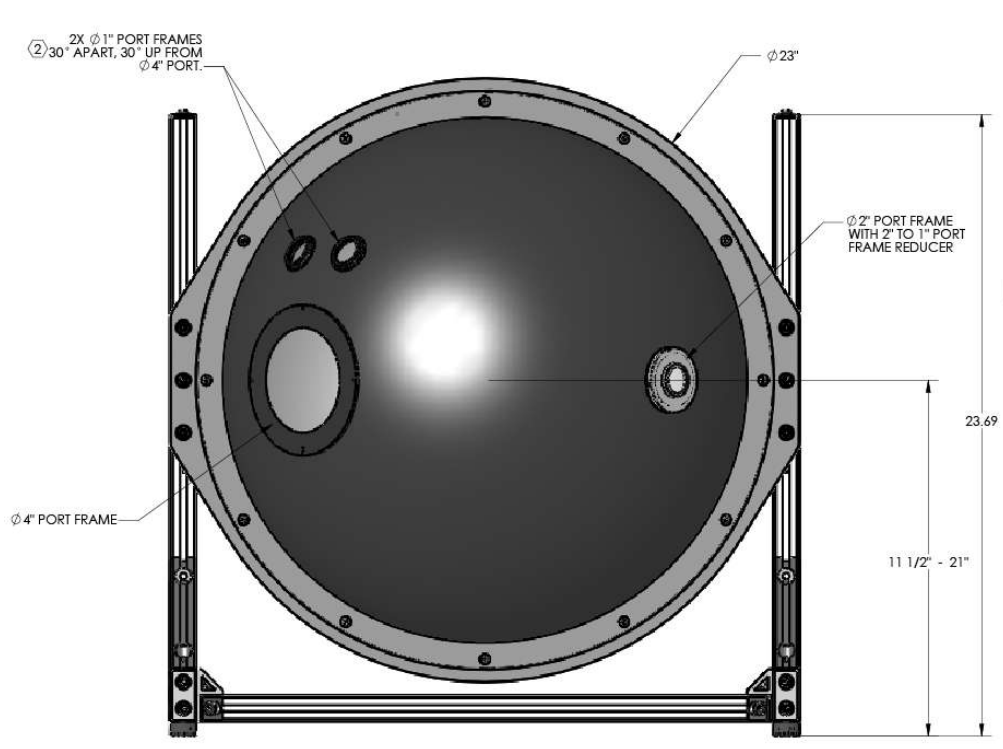


Fig. 14 Sketch of the integrating sphere



Fig. 15 Photograph of the integrating sphere

2.4 Black Box

The uniformity of the light is dependent from the distance of the output port of the sphere (see Fig. 13).

To maintain this distance a “cover” for the ~80cm drift space was developed by Don Groom. The Box is made of plywood and features a big front door. The front third of the box is mounted on a piano hinge and can be flipped upwards. The joints between door section and the rest of the box are made in a multiple tongue and groove pattern. These overlapping joints provide absolute light tightness.

The box was also used for performance measurements like the uniformity measurement. (---> section 3.4.5)

In future the box could house other experiments like a reflectivity measurement setup or the pin hole projector. Fig. 16 Shows the black box opened with attached dewar.



Fig. 16 open black box

2.5 Dewar

This part contains the CCD, the reference photo diode (PD) and some readout electronics. The dewar we use in the setup is one of our standard dewars. To adapt it to the box a special flange was made. The dewar maintains the CCD operation temperature at 140K. Since the reference diode has to be placed next to the CCD a temperature controlled photo diode mount was developed. The PD calibration was only available at a calibration temperature of 298K, so the operational temperature should be the same.

2.6 Light monitoring

The quantum efficiency (QE) is calculated as the ratio of incident photons and the e-h pairs (current) measured as output. To determine the photon flux, a calibrated sensor has to measure the amount of light arriving the CCD.

In comparison to the other QE setups the light monitoring method of this setup is unique. Instead of measuring the light somewhere in the beam line, the light intensity is measured directly on the focal plane next to the CCD. This approach makes the QE measurement independent from any variations in the light intensity and reflections on the glass window of the dewar or other interferences in the beam line. With this setup the light incident on the CCD is measured during the exposure time. Since the accumulated integration time of the picoammeter⁴ is nearly equivalent with the exposure time, all the light which reaches the CCD is monitored with the diode. With a photo diode placed next to the CCD, end-to-end monitoring of the system is ensured. Because the photodiode measures at most exactly the light intensity which arrives the CCD, attenuation between source and CCD can be ignored. Fig. 17 shows the focal plane of the QE setup in the dewar.

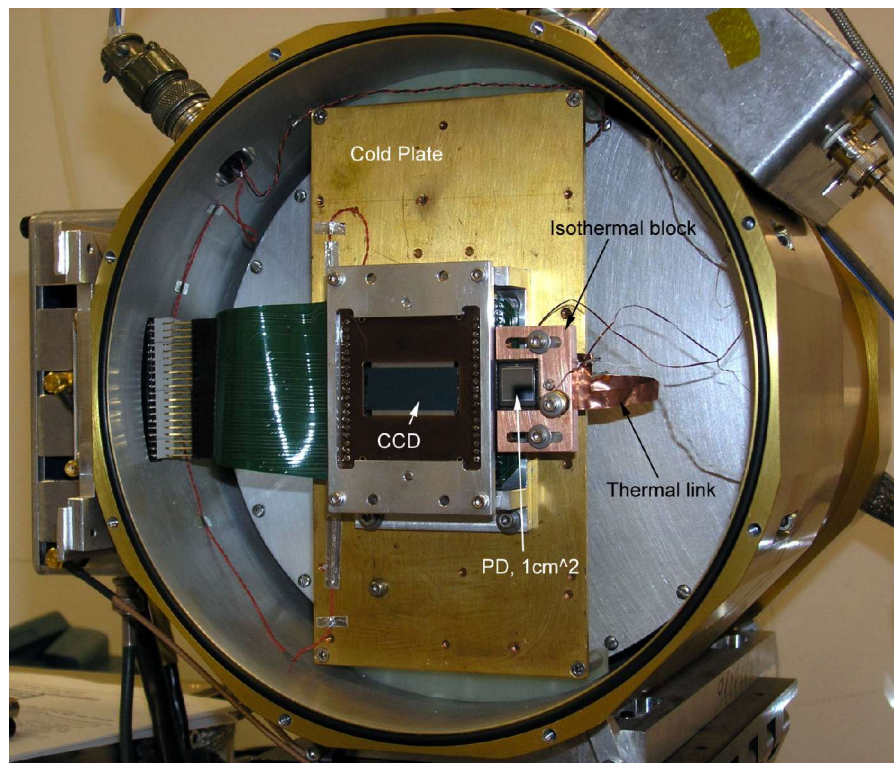


Fig. 17 Dewar with CCD and photo diode

4 Keithley 6485 "picoammeter" pico ampere meter

2.6.1 Photo Diode

A Si photodiode is one of the most sensitive photon detectors available. These devices are available with an active surface of 100mm² and a NIST⁵-traceable calibration. The large active surface provides outstanding sensitivity, ~530 mA/W peak. An other important aspect is the very low noise equivalent power (NEP) of these devices. Hamamatsu, the maker of the PDs which are used in the experiment, quotes a NEP of $2 \cdot 10^{-14}$ W/sqrt(Hz)[12]. A measurement with a Keithley 6485 picoammeter verified this value.

There are two different PDs used in the QE setup. One calibrated Hamamatsu S1337-1010BQ is used as reference diode for the QE measurement. The second PD is a Hamamatsu 2281 which features a housing and a BNC connector. This diode is used as secondary monitor in the sphere. Fig. 18 Shows a QE curve of a Hamamatsu 1337 photo diode. In comparison to a CCD the QE of the PD is relatively high at the blue end of the spectrum

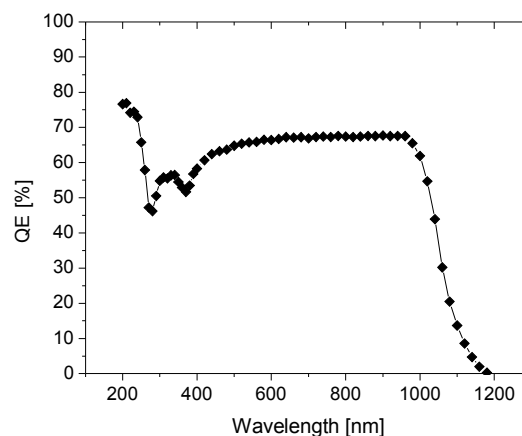


Fig. 18 Typical QE of a Hamamatsu 1010BQ photo diode

2.6.1.1 Temperature dependency of the photo diode

To ensure the values of the calibration curve the diode has to be operated at the calibration temperature. The influence of the temperature is small over the most of the spectrum. However, on the red end of the spectrum, around 1000nm, the output signal of a photo diode changes significantly with temperature. One of the diodes is placed inside the dewar next to the CCD. In this environment it is relatively easy to stabilize the operating temperature of the diode. An heating

⁵ National Institute of Standards and Technology

resistor in combination of a temperature sensor and a temperature controller maintains a stable operating temperature.

2.6.1.2 Photo diode mount

In order to mount the photo diode in the dewar next to the CCD, a temperature controlled mount was designed. The mount is made of a copper plate with a thickness of 0.25" and is mounted on the cold plate of the dewar. Two slots in the plate guarantee flexible mounting for different CCD picture frame sizes. The plate is mounted on two heat insulating nylon posts. The thermal link is realized by a strip of thin copper strip which is bolted to the diode mount and the cold plate. To regulate the temperature a heating resistor is placed on the rear side of the mount plate. The photo diode and a Si-diode temperature sensor are located on the front side. Fig. 19 shows the AutoCad drawing of the diode mount.

The heater/temp sensor in combination with a LakeShore L321 temperature controller ensures a temperature controlled operation of the PD which is calibrated at 25 °C.

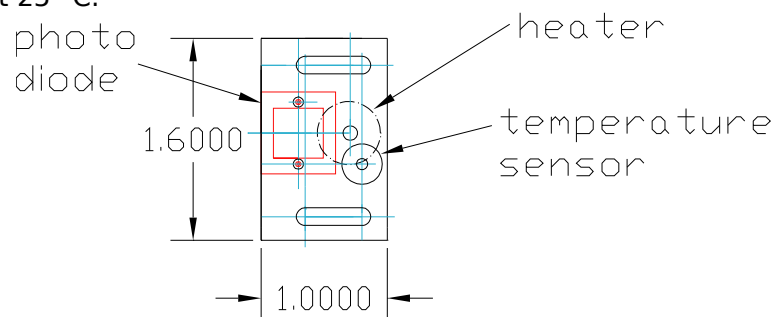


Fig. 19 Temperature controlled photo diode mount for dewar

To dimension the copper strip which is used as a cold link, the thermal conductance was calculated with (11).

$$H = -k * dT * \left(\frac{A}{l}\right) \quad (11)$$

Where H is the thermal conductance [W], k is the thermal conductivity, dT the temperature difference, A is the area and l is the length of the copper strip. With a thermal conductivity of 401 W/K*m, a temperature difference of 150K, a cross section area of $75 \cdot 10^{-6} \text{ m}^2$ and a length of 71 mm the thermal conductance is 0.63W. This values ensures a stable operating for the heater temperature sensor.

The actual thermal conductivity might be lower than the calculated value because of high thermal resistance of the joints between copper strip and cold plate/diode mount. [13]

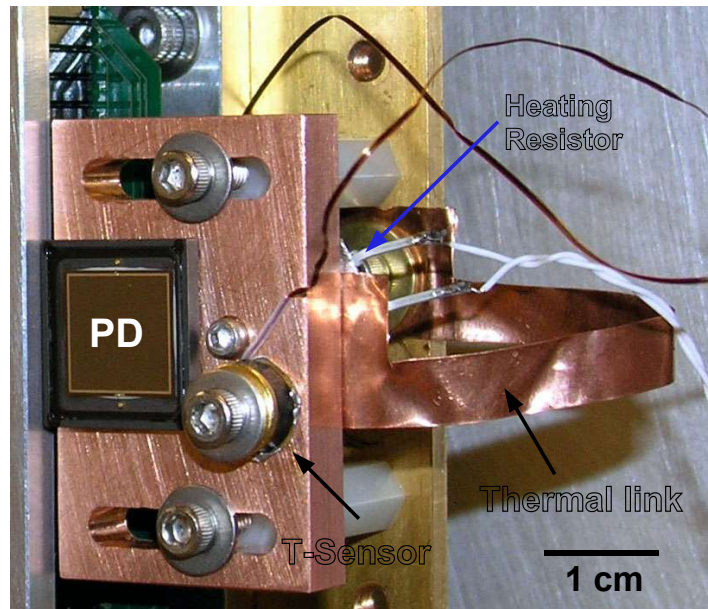


Fig. 20 PD mount built into Dewar

Fig. 20 shows the the PD mount with photo diode Si-temperature sensor and heating resistor.

2.6.1.3 Operation

The photodiode is operated in a photovoltaic mode, which means that no bias voltage is applied. In this mode we avoid all problems with biasing noise and dark current. The only disadvantage of the photovoltaic mode is the relatively high time constant of the diode. Since high-speed readout of the PD is not required, this is not a problem.

2.6.1.4 Secondary light monitoring PD

A second, uncalibrated PD is mounted on the instrument port of the integrating sphere. This diode is used for constant monitoring of the light intensity inside of the integrating sphere. Since signal of the calibrated photo diode provides our reference value which determines the QE, a second measurement for control purposes is useful. A change of the signal ratio of the pd in the sphere and the dewar can be an indicator for a light leak between sphere and dewar. If the ratio between sphere and dewar diode is stable, the sphere diode can be used as reference diode for measurements with very low light intensities.

2.7 Mechanics

In the following chapters the different mechanical parts of the test setup which had been designed are described. This chapter also covers the height problem. All measures in the technical drawings are in inches.

2.7.1 The height problem

The whole test setup relies on an uninterrupted optical path. To achieve this all components must be aligned properly. The vertical alignment is more critical than the horizontal because of the difficulty to maintain a certain height. The actual center of the optical path is on a height of 11.5". This number is determined by the largest part in the setup, the integrating sphere. All the other parts have to be vertically adjusted to this level. The height adjustment was done by variable posts underneath the main components as monochromator and the light source. The black box is made to fit into the optical path directly. The monochromator is lifted by 6,5", the light source by 7.5"

Smaller components like the shutter and filter wheels are mounted directly on the beam line. They are held in place by the adapter parts so no additional posts or fixtures are necessary.

2.7.2 Adapters

Since the test setup must be light tight, all parts must be connected properly. The connection is done using several parts which were made in the LBNL machine shop.

2.7.2.1 Focusing lens - shutter adapter

The first adapter part connects the focusing lens with the shutter. It consists of two tubes which are stacked into each other to provide an adjustable distance between the lens and the shutter. Fig. 22 shows the adapter tubes. Part one fits into the standard Oriel interconnect at the focusing lens. Part two is equipped with an inner thread which fits to the shutter. They are machined to run smoothly into each other, providing enough stability to support the shutter. Fig. 21 shows the assembled adapter in the setup

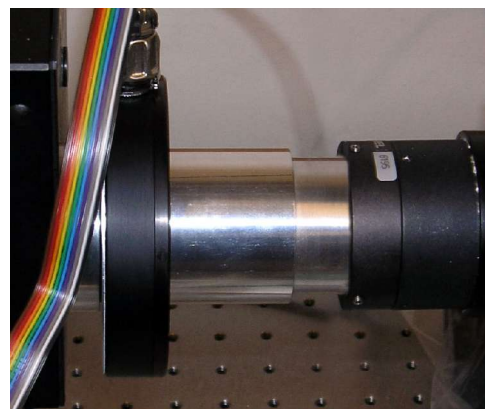


Fig. 21 Shutter- filter wheel adapter

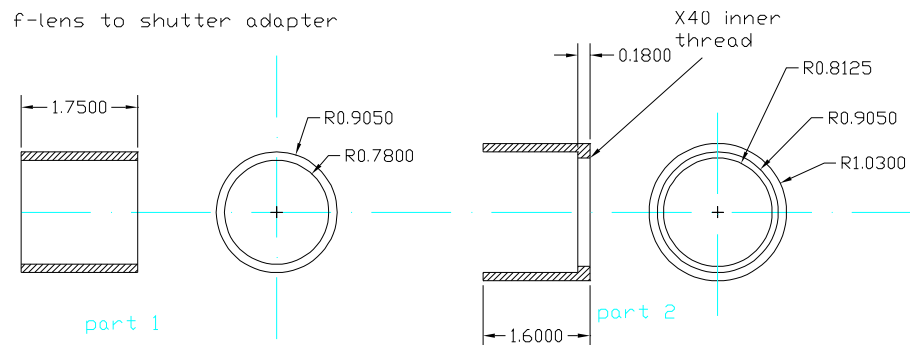


Fig. 22 Focusing lens to shutter adapter

In this adapter absolute light tightness is not required as for the adapters after the monochromator.

2.7.2.2 Shutter – filter wheel adapter

The next part to design and build was the shutter-to-filter-wheel adapter. This part is bolted on the shutter at one side and provides an female Oriol standard flange at the other side. The flange side connects with the filter wheel. Fig. 23 shows the AutoCAD drawing of this adapter. The filter wheels, as supplied, are directly connected to the monochromator.

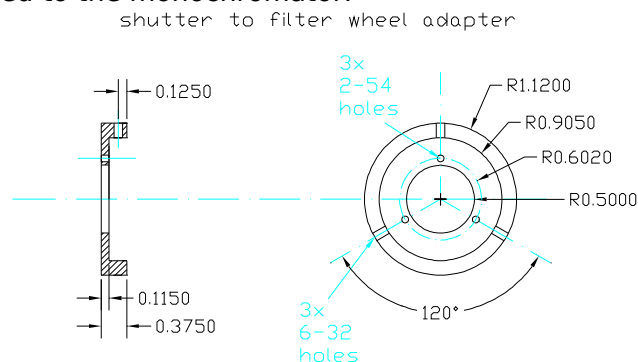


Fig. 23 Shutter-to-filter wheel adapter

2.7.2.3 Monochromator – Integrating sphere adapter

The next part to design was the connector between monochromator output port and the input port of the integrating sphere which is shown in Fig. 24. The output port of the monochromator is equipped with a male 1.5" standard Oriol flange. The input port of the sphere is equipped with a male LabSphere flange. As shown in Fig. 25 this adapter consist of two tubes, part 1 and part 2. Part one is equipped with three tapped holes on one end to connect the flange on the

monochromator. Part two is also a tube with an female flange which fit to the 2" flange on the sphere. Since this connector has to be absolutely light tight, the smaller diameter tube is equipped with an outer thread and the larger diameter tube with a matching inside thread. The tubes are screwed together and provide a length-adjustable light-tight interconnect. The only other places where a possible light leak could occur are the interconnects at the flanges. The LabSphere side of the adapter is equipped with an o-ring groove to seal this connection. At the Oriel side it is possible to place also an o-ring. With this o-rings the adapter is absolutely light-tight.

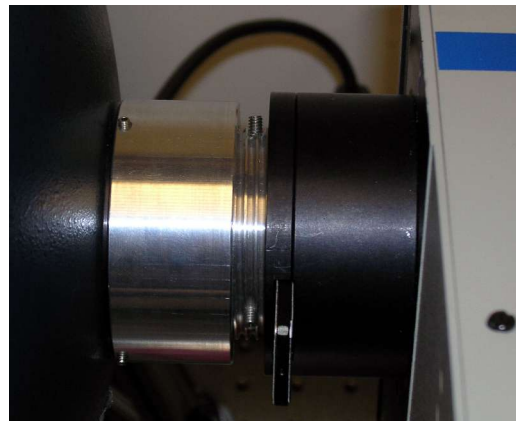


Fig. 24 Monochromator-integrating sphere adapter

Monochromator to integrating sphere adapter

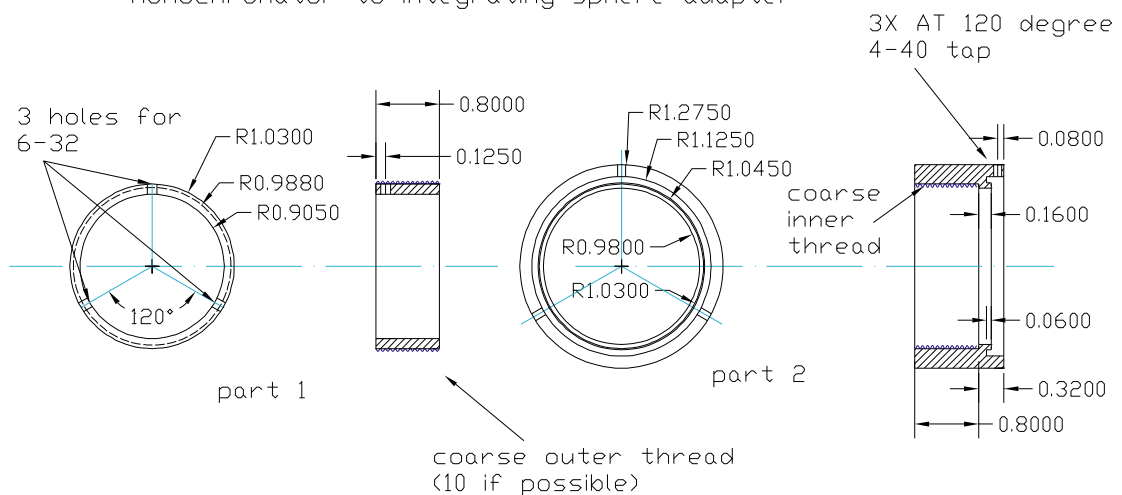


Fig. 25 Monochromator to integrating sphere adapter

2.7.2.4 Integrating sphere – black box connector

The output port of the integrating sphere is equipped with a plain ring with tapped holes. In order to connect the output of the sphere with the input of the black box with a bellows, a flange must be added. Fig. 26 shows the add-on flange for the integrating sphere and the black box. In order to maintain light tightness the flange is equipped with a groove for a 1/8" thick o-ring. An identical flange is mounted on the input port of the black box.

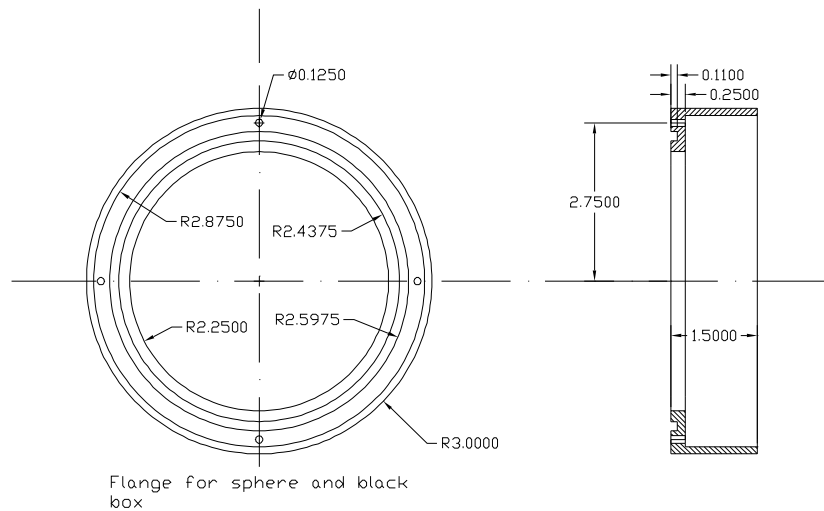


Fig. 26 Flange for sphere and black box supporting a bellows

2.7.2.5 Black box – dewar adapter

The last connection on the optical path is between the black box and the dewar. The dewar has a window on one side which is ~5" in diameter. The black-box-to-dewar connector consist of an flange which is bolted on one side of the dewar and reaches through the output port of the black-box. From the inside of the black box a nut fits over the flange and fixes the black box. As displayed in Fig. 54 this connector is equipped with three o-ring grooves to maintain light tightness. Fig. 27 shows the black box – dewar adapter attached to the dewar.

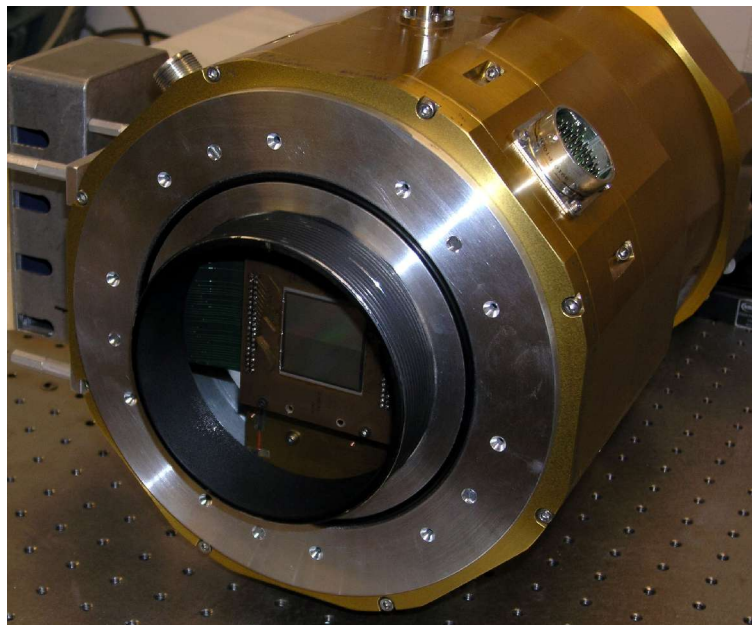


Fig. 27 Dewar with attached black box adapter flange

All these parts are designed in AutoCad and manufactured in the building 50 machine shop.

2.7.3 Detector housing

To mount the secondary light sensor, a Hamamatsu S2881 photo diode, on the integrating sphere, a special housing was necessary. The 1" detector port of the sphere is equipped with a standard male LabSphere flange. To keep the housing as simple as possible a one-piece design was chosen. On one side, the housing connects to the LabSphere flange. To avoid light leaks, this interface is equipped with an o-ring. The other side of the housing is basically a cylinder which keeps the PD in place. The space between the end of the housing and the diode is filled with black epoxy. This layer of epoxy is light tight and holds the diode in place. Fig. 28 Shows the housing (part 1) and a plug (part 2). The plug was designed to close the second detector port until a real PD is mounted there.

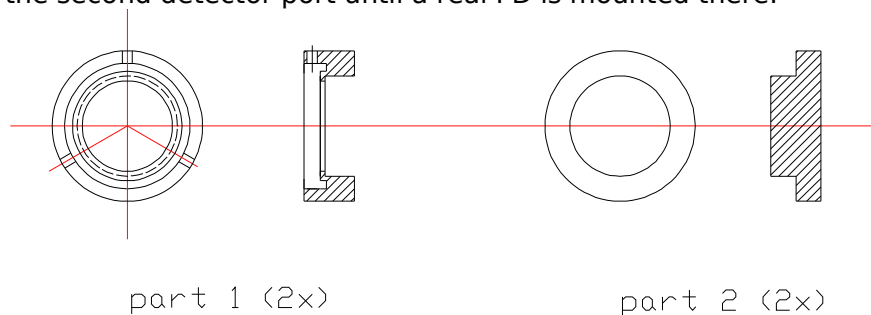


Fig. 28 Photo diode housing

3 DIMENSIONING AND PERFORMANCE CHECKS

This section shows the calculations made to dimension the system in terms of light throughput and the detector performance. This section also describes several performance measurements which were done before measuring a real CCD.

3.1 Throughput Estimation

Since the light incident on the CCD is monitored directly next to the CCD, a precise and exact optical calculation (ray tracing) was not required. However, an estimation of the light throughput was necessary to dimension the system. This estimation is based on the equations the manufacturers of the different devices provide in their catalogs.

On the following pages the light throughput of the system is calculated. The calculation follows the beam line, starts with the light source and ends with the light flux on the detector.

3.1.1 Calculation of light flux into the monochromator

The first part of the calculation is the output of the lamp. The output is given by the manufacturer of the light source in the unit [mW/m² * nm].

$$E_e = E_{spec} * Bandwidth \quad (12)$$

With (12) the total irradiance of a light source can be calculated. E_{spec} is the average spectral irradiance in the given wavelength band determined by the monochromator.

The next parameter is the efficiency of the housing (called lens conversion factor) and is given by the producer of the housing. It is dependent of the used condenser lens and the rear reflector. For the chosen F/1 condenser the efficiency is ~11%. A rear reflector gains additional ~60% from this value. A F/#⁶ matching lens after the condenser has an attenuation factor of 0.9. Positioned in front of the monochromator there are two filter wheels used for order sorting and stray light limitation. These filters cause an attenuation of the light due to their limited

⁶ F/# is the measure of the acceptance angle of an optical instrument, and is generally defined as the ratio of diameter to focal length. (#="number")

transparency, which is around 80%. The bandpass filters combined of a short and a long pass have a total transmission of 50%. To get light into the monochromator it has to be within its acceptance cone, which is determined by the $F/\#$ of the monochromator[10].

The $F/\#$ concept is only valid if the apertures of the optical elements are equal. We use a 1.5" condenser and a 1.5" focusing lens so there is no light loss due to different sized apertures.

Since the light is $F/\#$ matched and focused onto the input slit, the next important number is the vignetting factor (15). Due to the condenser/lens combination the image of the light source (in our case the arc) is magnified. The magnification is given by

$$mag = \frac{(F_2/\#)}{(F_1/\#)} \quad (13)$$

where $F_1/\#$ is the $F/\#$ of the first lens and $F_2/\#$ the $F/\#$ of the second lens. A $F/1$ condenser and a $F/4.6$ focusing lens is used, so the magnification is 4.6. The input slit of the monochromator has a maximum width of 2mm. To get as much light as possible into the monochromator the source image has to be smaller than than the slit width. The Oriel 6257 arc lamp has an arc width of 0.4 mm. When multiplied by 4.6 this leads to a 1.8 mm wide projection of the source on the slit. In this case the slit width and height do not limit the amount of light focused on the monochromator. With all these factors the amount of light coming into the monochromator can be calculated.

$$L_{MonoIn} = L_{out} * LC * Ref * Fm * Fw * Vi \quad (14)$$

Lout is the light output of the source

LC is the Lens Conversion Factor

Ref is the gain through the reflector

Fm is the attenuation through the focusing lens

Fw is the attenuation through the filter

Vi is the Vignetting Factor and is given by (15)

$$Vi = \frac{slw}{(sow * mag)} \quad (15)$$

s/w is the slit width

sow is the source width, mag is the magnification

The unit of the result (MonoInput) is still $mW/(m^2)*nm$. The result of this calculations for different wavelengths is shown in Table 1

Light source	100W Xenon	300nm	500nm	700nm	900nm	1100nm
Power @wavelength [mW/m ² *nm]		6	10	10	14	6
Lens Conversion Factor [1/m ²]		0.11	0.11	0.11	0.11	0.11
Reflector		1.6	1.6	1.6	1.6	1.6
Additional F/# matching lens		0.9	0.9	0.9	0.9	0.9
Light leaving condensor +lens [mW/nm]		0.9504	1.584	1.584	2.2176	0.9504
Magnification (f2/f1)		4.6	4.6	4.6	4.6	4.6
Filament width [mm]		0.4	0.4	0.4	0.4	0.4
Filament height [mm]		0.8	0.8	0.8	0.8	0.8
Area of filament [mm ²]		0.32	0.32	0.32	0.32	0.32
Magnified filament width [mm]		1.84	1.84	1.84	1.84	1.84
Magnified filament height [mm]		3.68	3.68	3.68	3.68	3.68
Filament Image on Slit [mm ²]		6.7712	6.7712	6.7712	6.7712	6.7712
Slit width [mm]		2	2	2	2	2
Slit height [mm]		15	15	15	15	15
Slit area [mm ²]		30	30	30	30	30
Filter Wheel	Attenuation caused by filter	0.6	0.5	0.5	0.5	0.5
Leaves the filter [mW]		0.57024	0.792	0.792	1.1088	0.4752
Vignetting factor		1	1	1	1	1
Comes into monochromator [mW]		0.57024	0.792	0.792	1.1088	0.4752

Table 1 Throughput calculation, light source section

3.1.2 Calculation of light flux into the Integrating Sphere

Now the light which falls into the integrating sphere is calculated. Therefore the light loss caused by the monochromator has to be calculated. Inside the monochromator the light is attenuated by reflection losses and the loss on the grating. The monochromator is an optical band pass. Due to this, only a small amount of the incident light in the right band leaves the monochromator. The monochromator throughput is given by [11]

$$L_{MonoOut} = L_{MonoIn} * MI^M * GI * BW \quad (16)$$

L_{monoIn} is the light coming into the monochromator

MI is the mirror loss

M is the number of mirrors

GI is the grating loss

Bw is the width of the bandpass.

The unit of the result is now [mW/m²]

Table 2 shows the results of the monochromator throughput calculation.

Monochromator	300nm	500nm	600nm	900nm	1100nm
Mirror efficiency	0.77	0.9	0.92	0.92	0.92
Grating efficiency @ 300nm	0.7	0.7	0.83	0.62	0.52
# of mirrors	4	4	4	4	4
# of gratings	1	1	1	1	1
Mirror Loss (4 mirrors)	0.35153041	0.6561	0.71639296	0.71639296	0.71639296
Gratings Loss	0.6	0.7	0.83	0.62	0.52
Bandpass	10	10	10	10	10
Leaves the monochromator [mW]	1.20274021	3.6374184	4.70928076	4.924886387	1.77023566

Table 2 Throughput calculation, monochromator section

3.1.3 Calculation of the light flux on the Detector

To calculate the the light flux on the detector the throughput of the integrating sphere has to be calculated.

The light flux inside the sphere, the radiance (light flux per solid angle), is

$$L_s = \frac{\Phi_i}{(\pi * A_s)} * \left(\frac{\rho}{(1 - \rho * (1 - f))} \right) \quad (17)$$

L_s is the radiance

Φ_i is the input flux

A_s is the active sphere surface

ρ is the reflectance of the surface

f is the port fraction which is the ratio between sphere surface and the area of the ports [11]

The second part of (17) is called the sphere multiplier and is determined by the reflectance of the coating and the port fraction. To achieve a good uniformity a port fraction of at least 0.05 (5%) is mandatory. In our design the port fraction f is 0.01 which provides superior uniformity of the light. Since the radiance L of the sphere is known, the light flux on a detector outside the sphere is then

$$D_{flux} = L_s * A_d * \Omega \quad (18)$$

D_{flux} is the light flux onto the detector

L_s is the sphere radiance

A_d is the detector area

Ω is the solid angle [11]

Since the flux onto the detector is known, it can be verified if the light flux is

sufficient for the used detector. The limiting element in the setup is not the CCD, which is designed for very low light levels, it is the calibrated reference photodiode. As said these diodes have a NEP of $2 \cdot 10^{-14}$ W/sqrt(Hz) [14]. With a readout bandwidth of max 10Hz the NEP is $2 \cdot 10^{-13}$. To achieve a good signal/noise ratio the lowest light flux should be better $100 \times \text{NEP} \cdot 10\text{Hz}$. The lowest flux is then $2 \cdot 10^{-11}$ W. The maximal flux for our setup is $\sim 9 \cdot 10^{-8}$ W which is determined by the optical attenuation factors and the lamp output. That means the light in the system can be attenuated by a factor of 4000 and will be still well above the noise floor.

Table 3 shows the results of the throughput calculation for the integrating sphere. Included the power arriving the detector.

Integrating sphere		300nm	500nm	600nm	900nm	1100nm
	reflectance	0.95	0.97	0.96	0.96	0.96
	f	0.01	0.01	0.01	0.01	0.01
	Sphere Multiplier	15.9663866	24.4332494	19.3548387	19.35483871	19.35483871
	Sphere Surface area [m ²]	0.81	0.81	0.81	0.81	0.81
pi	3.14 Sphere Radiance [mW/m ² * sr]	7.55029294	34.9429704	35.8368206	37.47754254	13.4711904
	Output Port Size [m]	0.00075503	3.49E-03	0.00358368	0.003747754	0.001347119
	Distance from Sphere [m]	1	1	1	1	1
	Detector Area [m ²]	0.0001	0.0001	0.0001	0.0001	0.0001
	Solid angle [sr]	0.03151	0.03151	0.03151	0.03151	0.03151
	Power arriving the Photo Diode [mW]	2.3791E-05	0.00011011	0.00011292	0.000118092	4.24477E-05
	Power of light @ 1cm² [W]	2.3791E-08	1.1011E-07	1.1292E-07	1.18092E-07	4.24477E-08

Table 3 Throughput calculation, integrating sphere section

3.2 Spectral dependence of the throughput

The throughput calculations are done with parameters varying with wavelength. The highly wavelength dependent parameters are:

- Spectral irradiance of the lamp
- Efficiency of the grating
- Difference in reflectivity of mirrors and sphere coating
- QE of photodiode and CCD

The QE has a minimum of <5% at 1100nm and a maximum of 92% at 950nm. The power output range of the Xenon lamp reaches from 6mW/m²*nm to 14mW/m²*nm [10]. The grating efficiency changes between 0.5 and 0.8. The problem is that these numbers are all getting worse at the same time, especially at the red and the blue end of the spectrum. At 1100nm, for example the lamp output is only 6mW/m²*nm, the lowest value in the whole range. At the same wavelength the QE of the CCD is something between 0 and 5%. The grating

efficiency is around 50%. Stray light at shorter wavelengths contributes over proportional to the signal. A similar thing happens at the blue end, but there all the figures are a little bit higher so that our critical point is definitely at the red end. Fig. 29 shows the calculated light flux on the detector versus the wavelength.

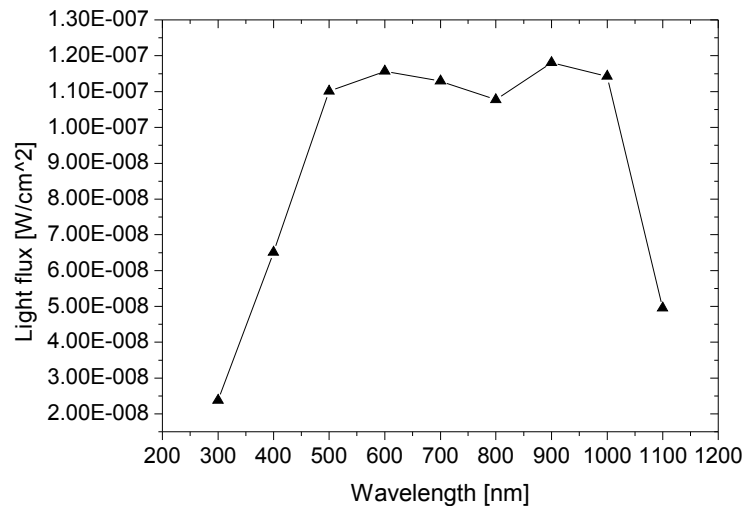


Fig. 29 Light flux on detector vs. wavelength

The light flux reaches its maximum at 900nm and two minima at 300nm and 1100nm. The low light flux at 300 nm is caused by a lower lamp output and bad UV reflection in the monochromator and especially in the integrating sphere. At 1100 a low lamp output, and losses due to low grating efficiencies at this wavelength are responsible for this low value.

3.3 Noise Measurements

3.3.1 Noise measurement of the photo diode

To verify the accuracy of the Keithley 6485 picoammeter and the noise of the Hamamatsu S2281 photo diode several noise measurements at different integration times were made. With the quoted NEP (Noise Equivalent Power) of 2×10^{-14} W/sqrt(Hz) at the peak sensitivity (960nm) for the S2281 photo diode. That means the output of the diode at this light level is equivalent to its noise level. To take measurements with less than 1% error the power of the light incident on the diode has to be at least 100 times the NEP. To convert the NEP

which is given in watts to amperes, it has to be multiplied by the sensitivity of the diode at 960nm [15].

$$I_{noise} = NEP * S \quad (19)$$

The S2281 has a peak sensitivity of 0.523 A/W which leads to a “noise equivalent current” of 1.046^{-14} A/ $\sqrt{\text{Hz}}$. To verify this number the diode was kept in total darkness and the photo current was measured. To determine the noise, 100 measurements were taken. The picoammeter was operated in buffered mode so that the measured values are stored and read out at the end of the measurement. In addition to the measurement values the meter calculates the mean value and the standard deviation of these 100 values.

Equation (20) describes the calculation of the mean value.[16]

$$M = \frac{1}{n} \sum_{i=1}^n X_i \quad (20)$$

where M is the mean value, X_i is a measurement sample and n is the number of samples.

The standard deviation is calculated by (21)

$$y = \sqrt{\left(\sum_{i=1}^n (M - X_i)^2 / (n - 1) \right)} \quad (21)$$

where y is the standard deviation, M is the mean value, X is the value of one sample and n is the number of samples

The measurements were taken at different integration times. The timing of the picoammeter is based on the line frequency of 60 Hz. The user has to specify the integration time in factors of this frequency. The range of integration times in this measurement reaches from 1.67 msec to 1000 msec. The optimal integration time for the picoammeter is between 16.67 and 166.7 msec. Fig. 30 shows the standard deviation in amperes over the integration time in msec.

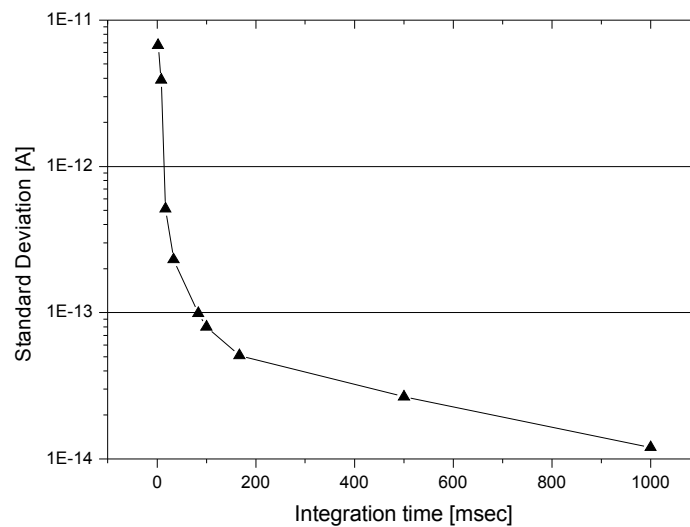


Fig. 30 Standard deviation of the measured values vs. integration time

As shown in Fig. 30 the quoted NEP of $1 \cdot 10^{-14} \text{ A}/\sqrt{\text{Hz}}$ is nearly reached by the measured standard deviation of $1.2 \cdot 10^{-14} \text{ A}$ for an integration time of 1 second, which is the maximum of the picoammeter. This result shows that the diode is within its specifications and the picoammeter is capable of measuring the diode current without adding significant noise.

3.3.1.1 Signal-to-noise ratio at 960nm

The next question concerns the ratio between the NEP noise and the measured signal of the photo diode during the exposure time. To calculate the amount of light the desired charge per pixel has to be known. We specified it to $\sim 20000 \text{ e}^-$ per pixel. An other variable in the following calculation is the exposure time which is set to five seconds to ensure a good measurable current. With (22) the number of electrons per pixel per second can be calculated.

$$n_{(e \text{ per pix} * \text{second})} = \frac{n_{(e \text{ per pix})}}{t_{\text{exposure}}} \quad (22)$$

Calculated with (22) we get 5000 e-h pairs per second per pixel. The number of electrons per cm^2 is given by

$$n_{(e \text{ per cm}^2 * \text{second})} = n_{(e \text{ per pixel} * \text{second})} * n_{(\text{pixel per cm}^2)} \quad (23)$$

which leads to $2.2 * 10^9$ e-h pairs per $\text{cm}^{-2} \text{s}^{-1}$. Assuming a QE of 0.87 for the SNAP CCD, the number of photons that are needed to generate this electron flux is then:

$$n_{(\text{photons per second})} = \frac{n_{(\text{electrons per second})}}{QE} \quad (24)$$

To follow from (24) we get an photon flux of $2.53 * 10^9$ photons per second per cm^2 . Knowing the required photon flux, the current of the photo diode is given by:

$$I_{pd} = n_{(\text{photons per second})} * QE_{pd} * e \quad (25)$$

With the values mentioned above the result is 271 pA. The fractional noise current is then:

$$Error_{NEP} = \frac{I_{NEP}}{I_{PD}} \quad (26)$$

This leads to an error of $4.43 * 10^{-3}$ % caused by the noise of the photo diode. An error of this size is negligible comparing to the error caused by non-perfect uniformity of the light or even the shutter error.

3.3.1.2 Signal-to-noise current ratios for different wavelengths

The NEP of the photo diode is given at the peak sensitivity which is at 960nm for the S2281. The noise current (19) is wavelength independent, but the photo current, according to (23) is highly wavelength dependent. There are two factors of dependency on the wavelength. Assuming a constant number of electrons per pixel, the photon flux has to be adjusted according to the QE of the CCD.

Fig. 31 shows the noise current and the error in the PD signal caused by the noise current for different wavelengths assuming an electron count of 20k per pixel, 15um pixel size, 5 second exposure time and a 1 cm^2 photo diode.

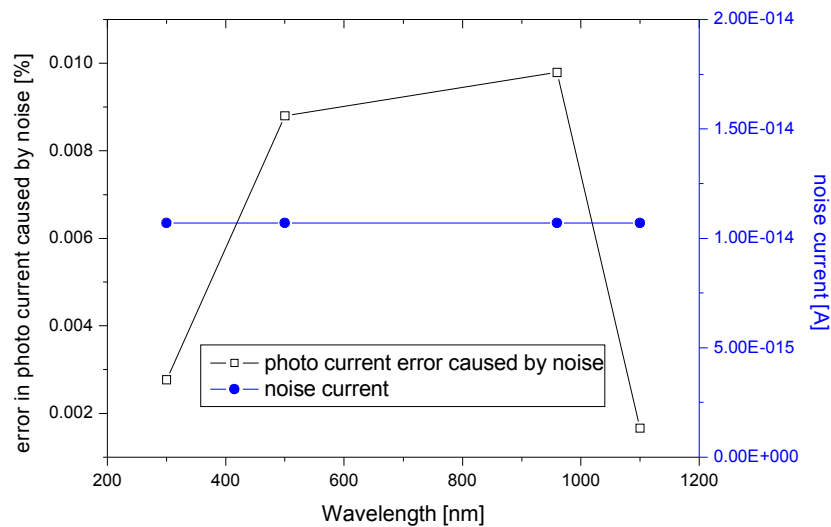


Fig. 31 Noise current and error caused by noise current vs. wavelength

The error at 300 and 1100 nm is low comparing to the error at 900nm. The reason for this behavior is the difference between the QE's of photo diode and CCD. While the CCD has very low QE values of 20% at 300nm and ~0% at 1100nm, the photo diode has higher QEs of 54% at 300nm and 13% at 1050nm. To maintain a constant charge of 20k electrons per pixel the photon flux has to be increased. This increased photon flux leads to an higher photo current in the pd. An higher photo current increases the signal/noise ratio of the photo diode, the error in the photo current caused by the noise current decreases.

3.3.1.3 Measurement strategies vs. Noise

The light intensity is monitored during exposure. Since the maximum integration time of the Keithley 6485 picoammeter is about one second the exposure time cannot be covered by one single measurement. To cover the exposure time, two measuring strategies are possible: a few long integration time measurements or a high number of short integration time measurements. As mentioned above, the optimal integration time determined by the picoammeter is between 16 and 166 msec. In this area the internal noise of the picoammeter is at a minimum. Integration times shorter than 16 msec are not recommended due to the high internal noise. To determine the optimal measuring strategy, a 5 second measurement of the photodiode in the dark was made. These 5 seconds were

covered by 50 x 100 msec and by 5 x 1 second. The standard deviations of these measurements were calculated and compared. The following graph shows the standard deviation divided by the square root of the samples for both cases, 5 * 1s and 50 * 0.1s.

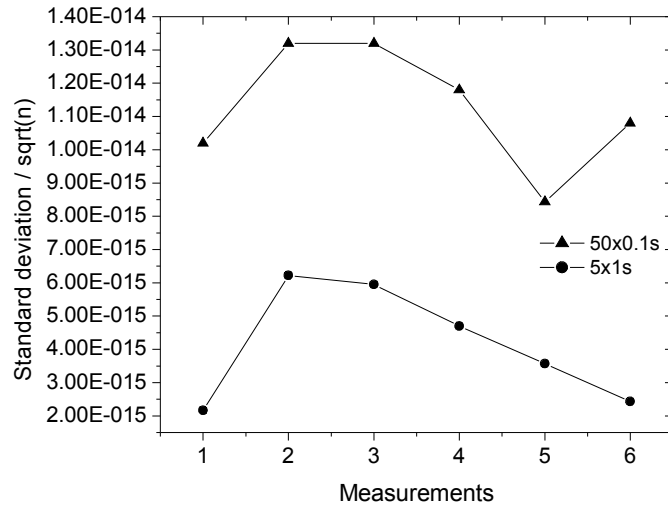


Fig. 32 Total integration time split into 5 long or 50 short measurements

As shown in Fig. 32 the strategy of making 5 samples with an integration time of 1 second each leads to a better performance than 50 measurements with 0.1 seconds. In the test setup an integration time of 0.5 sec for 5 sec exposures and an integration time of 1 sec for 10 sec exposures is used.

3.4 System Setup and performance measurements

In order to set up the system correctly and to verify the performance, several measurements were done. The test setup was assembled in two major steps. First the light source, monochromator and integrating sphere were set up. After that the dewar with the light monitoring system and the black box were assembled and put in place.

3.4.1 Light generation and manipulation system set up

This basic system generates the light in the light source, provides monochromatic light with the monochromator, and provides uniform CCD illumination via the integrating sphere. First the integrating sphere was positioned in the corner of the breadboard. The center height of the input port is the reference height of the beam line. In order to maintain this height, the monochromator was mounted on three height-adjustable posts. The same was done with the light source. The sphere and the monochromator were connected with the adapter specified in section 2.7.2.

3.4.1.1 Set up of the filter wheels

As a next step the filter wheels were equipped with filters. Here the first problem occurred. The dichroic filters are mounted in aluminum frames. The thickness of a frame was either 5.1 mm or 6.4 mm. The filter wheel is able to hold a stack of filters up to a combined thickness of 10mm. The coated filter substrates are thinner so that the combined thickness of two filters is $< 10\text{mm}$. After contacting the maker of the filters, Corion, we decided to remove the aluminum frame on one filter of each filter pair. To remove the frame, the filter was placed on a hot plate ($\sim 160\text{F}$) and was heated a few minutes until the glue became soft. Then the filter substrate was pushed gently out of the frame. To prevent lateral movement in the filter wheel the frame less filter was stacked with the framed filter so that it got held in place by the sticking out part of the frame. After these modifications the filter wheels were equipped with filters as planned.

The filter wheels were mounted on the input port of the monochromator. The connection between the second filter wheel and the shutter was made using by the shutter-to-filter wheel adapter.

3.4.1.2 Light source set up

As a next step, the light source was set up. The lamp and the appropriate adapter had to be installed. Also the adapter which holds the fiber for the light

intensity controller was mounted. After putting the focusing lens into the lens holder, it was mounted on the end of the condenser tube. The adjustable shutter to light source adapter completed the connections.

With installation of this adapter the covering of the beam line was completed. Before we could start with the measurements a few light leaks on the lamp housing had to be covered. To prevent the UV output from exceeding the maximum allowed dose of UV radiation per day within 20 seconds every substantial light, each leak had to be “sealed”. To do this a special metal cover for the lamp housing fan was designed. Other leaks were fixed with aluminum tape and rubber gaskets.

To adjust the system, a photo diode was mounted on one of the spheres' detector ports. To detect light leaks, parts of the setup had been illuminated with a strong halogen lamp. When the signal of the PD rose, a light leak had been found. By repeating this procedure on all parts of the system several light leaks had been found and covered. In the end the base signal of the PD was ~ 50 fA.

After a few measurements it was found that the lamp does not reach its theoretical light intensity. After some adjustments in place, the lamp housing was removed from the setup and taken apart. We found out that the movable condenser lens cannot be set to the right distance from the light source. After examining the lamp housing another level of adjustment of the lens was found. The lens was set one step closer to the light source.

To adjust the condenser and the reflector the lamp housing was placed on a table to shine on the wall of the opposite side of the room. There a piece of black cloth reduced the reflection. According to the manual's instructions the arc was projected on the wall. The reflector was set that the image of the arc overlaps with the projection. After this adjustment the housing put back in the setup and aligned until the diode indicates a maximum.

Then the lamp was adjusted. We monitored the light output with the PD and moved the lamp housing until we reached a maximal signal. Then the lamp position was adjusted. After that the reflector was adjusted.

3.4.2 Light detection system setup

The second part of the system includes the black box and the dewar including the CCD and the reference diode. First the black box was put in place and clamped to the optical table. During some light leak tests it was found that the box leaks light in the glued joints of the plywood. After some “treatment” with

black optical tape the box was light tight. The connection between box and sphere was made by the adapters specified in 2.7.2 and a black rubber bellows. The connection to the dewar was also made by an adapter flange. To keep the dewar in the right height it was mounted on a lab jack. To complete the setup the reference diode with the temperature controlled mount and the CCD had been mounted in the dewar.

3.4.3 Measurement of the dark level

To make sure the system is free from light leaks the “dark level” of the system was measured. At each measurement point, hundred measurements with an integration time of 1 second were taken. The mean value and the standard deviation have been recorded. First the S2881 photo diode was measured in an absolute dark environment. This measurement is the lowest possible value. The following table lists all measurements and the results:

Measurement	Result	Conclusion
Absolute dark, diode in metal housing light-tight sealed	Mean: 26 fA SDev: 12 fA	Lowest possible value/noise level
Diode measuring dark sphere, shutter closed, lamp off	Mean: 77 fA SDev: 22 fA	No major light leaks in sphere
Dark level in sphere with lamp on and shutter closed	Mean: 82 fA SDev: 15 fA	Shutter is really light-tight
Dark level in sphere with shutter open and lamp off	Mean: 51 fA SDev: 14 fA	No major light leaks up to the lamp housing
Dark level in sphere with shutter open, lamp off and mirror in monochromator	Mean: 51 fA SDev: 13 fA	No light leaks detectable, even with mono on max throughput

Table 4 Results of the dark level measurements

This test has proved that there are no major light leaks in the system up to the integrating sphere. The lowest currents in the QE measurements will be 10,000 times the dark level.

3.4.4 Measurement of the light output

To check if this system meet our calculated specs (see throughput calculation section 3.1.3) a performance measurement was done. The current at the key wavelengths (300, 500, 700, 900 and 1100 nm) was measured.

λ	Calculated PD current [A]	Measured PD current [A]	Ratio
300	9.59E-007	8.12E-009	118.1
500	5.75E-006	2.97E-006	1.94
700	6.81E-006	3.35E-006	2.03
900	1.06E-005	1.69E-005	0.63
1100	1.12E-006	1.10E-006	1.02

Table 5 Comparison of calculated and measured PD current at different wavelengths

As shown in Table 5 the measured values are mostly lower than the calculated ones. In the UV at 300nm the calculated value is over 100 times higher than the measured. An explanation for this UV drop is given in section 3.4.4.2.

3.4.4.1 Light output vs wavelength

This test was the first measurement to check the throughput of the system. The monochromator was set to a wavelength and the current of the PD was measured. After the first measurement the whole procedure was automated by a VODOO script. As result of the first measurement the filter ranges were corrected. The result of the first measurement is shown in Fig. 33.

The graph shows that above a wavelength of $\sim 450\text{nm}$ the current stays above 1 μA . This current is in the range of the expected values. The problem is the region from 300 nm to 450 nm. In this region the measured current is up to two magnitudes lower than expected. The “dip” in the curve at $\sim 400\text{nm}$ is caused by the change from the first to the second filter. It was difficult to find filters in this range, so the overlapping of filter one and two is not optimal. However the drop of the curve at shorter wavelengths cannot be fully explained by filter attenuation.

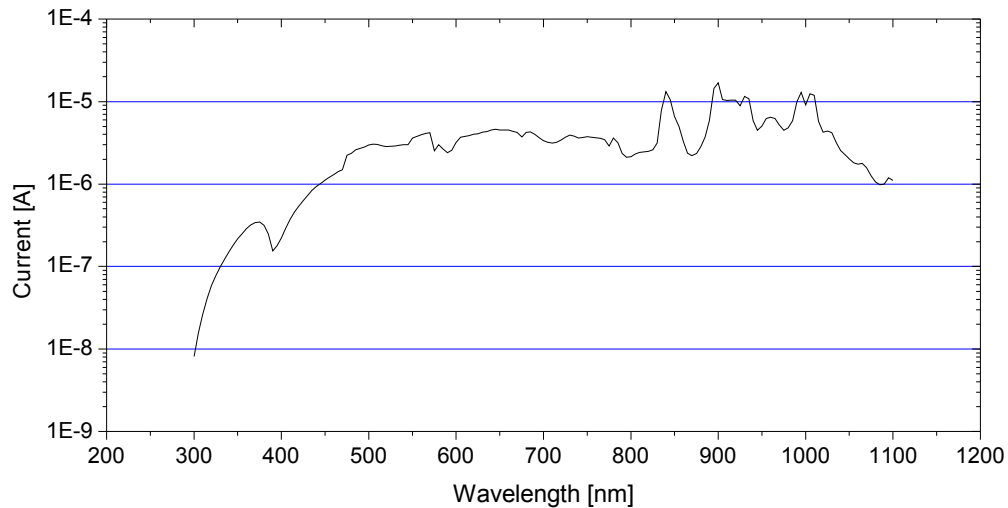


Fig. 33 First measurement of PD current vs. wavelength

3.4.4.2 Explanation of the UV drop

In order to get an explanation for the unexpected light intensity drop at 300nm some measurements were done to determine the reasons for the light loss. The measurements were done with two different 10nm wide bandpass filters. The center wavelengths of these filters are at 300nm and 600nm. To find the sources for the UV loss the ratios of the measured signals were calculated. This method provides good “common mode rejection”. Attenuations or offsets on both wavelengths are eliminated.

3.4.4.2.1 Base ratio

First the base ratio dependent on the PD sensitivities at different wavelengths was determined (27):

$$R_b = \left(\frac{PD_{600}}{PD_{300}} \right) * \left(\frac{Filter_{600}}{Filter_{300}} \right) \quad (27)$$

Where R_b is the base ratio, PD_{600} and PD_{300} are the PD sensitivities at a wavelength of 300nm and 600nm and $Filter_{300}$ and $Filter_{600}$ are the Filter transmittances at 300nm and 600nm. As calculated with specifications for the diode and the filters the base ratio is 8.33.

3.4.4.2.2 Drop in light source

To determine the ratio of UV and VIS light for the pure light source, the intensities at 300 and 600 nm were measured at the detector port of the lamp housing. The light from that port comes directly from the arc lamp. The ratio of the two measurements was about 15. To correct this number it has to be divided by the base ratio (28).

$$R_c = \frac{R_m}{R_b} \quad (28)$$

According to (28) where R_c is the corrected ratio, R_m is the measured ratio and R_b is the base ratio the corrected ratio was 1.8. The spectral plot of an high pressure xenon arc lamp showed that the intensity at 300 nm is approximately half of the intensity at 600 nm.

The next measurement was done after the focusing lens and lead to a ratio of 17.8. This small additional loss (1.18) is most likely caused by the condenser and the focusing lens.

3.4.4.2.3 Drop in monochromator

To determine the influence of the monochromator the ratio was measured at the second output port of the monochromator. This measurement showed a ratio of about 33. Divided by the previous ratio (17.8) leads to an differential ratio of 1.8. After reviewing the coating material of the mirrors a reflectivity at 300nm of about 0.77 and a reflectivity of 0.9 for 600nm was found. With

$$R_{reflectivity} = \left(\frac{R_{600}^n}{R_{300}^n} \right) \quad (29)$$

Where R_{600} is the reflectivity at 600 nm, R_{300} is the reflectivity at 300nm and n is the number of reflections (4 in our case). The result is a ratio of 1.87 which matches good with the measured differential ratio of 1.8.

3.4.4.2.4 Drop in the integrating sphere

Measured at the detector port of the integrating sphere, a ratio of 100 was detected. This leads to a differential ratio of 3 between monochromator and sphere. A closer look on a reflectance plot of the coating material showed a difference in reflectivity of about 3%. The value for 300 nm was 95%, for 600nm

98%. With

$$R_{sphere} = \frac{\left(\frac{\rho_{600}}{(1 - \rho_{600} * (1 - f))} \right)}{\left(\frac{\rho_{300}}{(1 - \rho_{300} * (1 - f))} \right)} \quad (30)$$

Where ρ_{300} is the reflectance of the sphere coating material at 300nm, ρ_{600} the reflectance at 600 nm and f is the port fraction [11]. This leads to a differential ratio of 2 which explains most of the UV drop by the sphere.

3.4.4.2.5 Multiplication of ratios

By multiplying these differential ratios with the base ratio leads to the measured ratio at the output of the sphere.

$$R_{overall} = R_b * Rd_{lamp} * Rd_{lens} * Rd_{mono} * Rd_{sphere} \quad (31)$$

Where R_b is the base ratio, Rd_{lamp} is the differential ratio caused by the lamp, Rd_{lens} is the differential ratio caused by the condenser and the focusing lens, Rd_{mono} is the differential ratio caused by the monochromator and Rd_{sphere} is the differential ratio caused by the integrating sphere. The result of (31) is an overall ratio of 98 which was shown in the measurement. An overview about the ratios is given in Table 6.

location	ratio	differential ratio	reason
		8.33	different PD sensitivities and filter transmissions
base ratio	8.33		
light source	15	1.8	Different light intensity of lamp
filter wheel	17.8	1.18	Different transmissivity of lens material
mono	33	1.85	different mirror reflectivity
sphere	100	3	different reflectivity of sphere coating
product		98.2	

Table 6 Summary of the different UV losses

3.4.5 Uniformity measurement

To ensure the uniform illumination of the CCD and the reference diode, the uniformity of the light was measured. The required area of uniform illumination is a 4" circle. Since the dewar with the CCD is ~90cm away from the sphere, the uniformity has to be measured in a similar distance. The measurement was done near the output port of the black box. The distance to the output port of the sphere was ~80cm. Two measurements were done, a horizontal and a vertical scan.

3.4.5.1 Horizontal scan

The uniformity was measured with a Hamamatsu S1337- 1010BQ photo diode. The diode was mounted in a lens holder and connected with a coaxial cable to the picoammeter. The lens holder was mounted on a post in a height of 11.5". This height is the same as the center height of the beam line. The post was mounted on an optical rail to move it across the output port. Aligned with the rest of the system the scale on the rail indicates the position of the PD. The measurement was done by moving the diode in 1 cm steps across the illuminated area and measuring the current. Since the light output of the lamp varies ~1% an absolute measurement of the light was not appropriate to detect uniformity errors >1%. To eliminate brightness variations over time, the light intensity was simultaneously measured in the integrating sphere. The picoammeters were triggered by the shutter signal. The ratio of the two diode readings was taken as a relative brightness level. Fig. 34 shows the ratio normalized to one and plotted versus the distance of the diode from the center of the beam line.

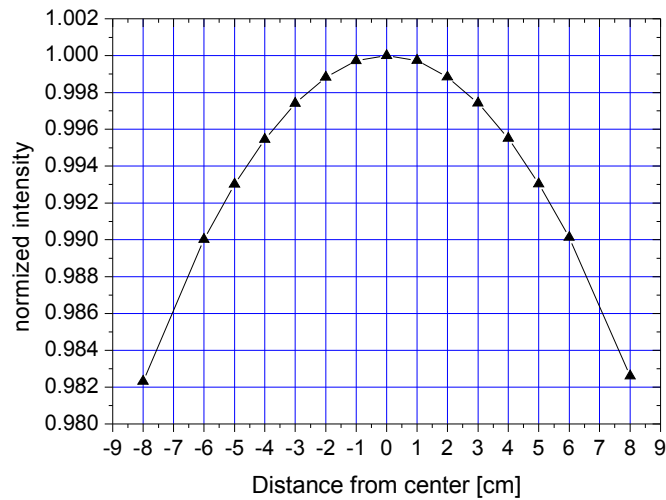


Fig. 34 Horizontal uniformity

3.4.5.2 Vertical scan

For the vertical scan the test setup had to be changed. The optical rail had to be mounted perpendicular to the table surface. Due to the limited length the rail was mounted on a lab jack which was used to center the scale of the rail with the beam line center.

3.4.5.3 Conclusion

The horizontal uniformity is >99.3% and the vertical uniformity is also better than 99.3%. These values are within our specifications. As shown in the graph the intensity drops from the center of the beam line to the edges. This intensity gradient can be covered by a mathematical fit. This function can then be used for correction.

In theory the brightness distribution follows the \cos^4 law [11].

$$I = \cos^4\left(\frac{x}{d}\right) \quad (32)$$

Where I is the intensity of the light, x is the distance from the beam line center and d is the distance from the spheres' output port. A fit of the measured curve gives:

$$I = \cos^{4.46} \left(\frac{x}{d} - 0.0002 \right) \quad (33)$$

The following graph (shows the horizontal uniformity and the fitted horizontal and the fitted vertical curve. The horizontal and vertical uniformity is nearly the same.

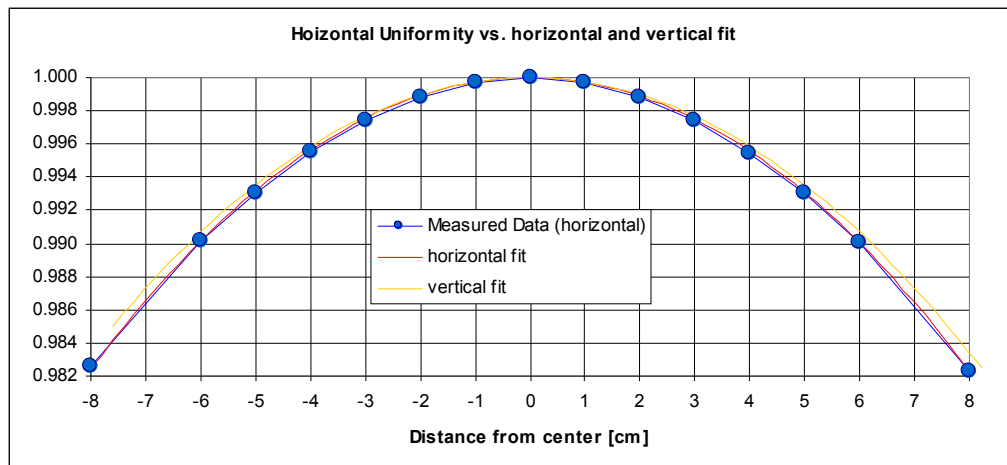


Fig. 35 Horizontal uniformity vs fitted curves

4 AUTOMATION

Everything that has to be moved or measured during the measurements is computer controlled. The following parts are equipped with a serial interface and connected to the computer:

- Light intensity controller
- Power supply of light source
- Monochromator (controls also the filter wheels)
- Keithley picoammeter (reading out the photodiode in the sphere)
- Keithley picoammeter (reading out the photodiode in the dewar)

Since all these computer connections require very low bandwidth, serial RS232 connections are the best light weight approach automate the system.

A wiring diagram of the setup is shown in the appendix at page 93.

The PC which controls the setup is a Dell Dimension 4600. This machine contains a 3 GHz Pentium 4 and is equipped with 1 Gbyte RAM. This PC is also equipped with two controller boards. One is a Digi Neo Classic serial board which provides 8 RS232 interfaces. The other board is the Leach controller board which communicates with the Leach controller, a device which runs the CCD. The operating system is Red Hat Enterprise Linux WS3 and the software which controls the whole system, VOODOO, is written in JAVA. To control the QE setup an extension to VOODOO has been programmed. The extension is able to control all adjustable parameters of the devices of our test setup.

4.0.1 The VOODOO software.

The VOODOO software was initially developed by Astronomical Research Cameras, Inc., the maker of the Leach CCD controller. The actual version in use at the LBNL is based on version 1.7.2.3.1 of VOODOO. Several changes in the software have been made by LBNL to support specific measurements and experiments. As mentioned above, VOODOO is written in JAVA, running on a Linux machine. VOODOO is a controlling and data acquisition software which directly communicates with the CCD Controller board.

4.0.1.1 Architecture

Since VOODOO is written in JAVA it follows the guidelines of object-oriented programming. VOODOO is organized in a structure of several abstraction layers.

The lowest layer in the architecture is a set of C++ libraries which are directly connected to the `astropci`⁷ driver. This driver provides the functions of the PCI Leach controller board, which communicates with the Leach controller. This controller is directly connected with the whole CCD operating environment. VOODOO itself consists of several layers with the `VOODOO.system` classes at the base and the `VOODOO.gui` classes at the top.

4.0.1.2 The VOODOO.qe add-on

To control and operate the QE test setup an add-on to VOODOO was written. Since VOODOO operates the whole CCD system, an extension of the existing VOODOO was the best way to control the test bench. The `VOODOO.qe` extension consist of a set of classes which are accessed with a graphical user interface or the internal scripting function. These classes are located in their package and in this way separated from the other code of the program. Due to its object-oriented architecture, where each class has its own variable space, the interference with other parts of the program is minimal. The only parts of the VOODOO main program which are used by the add-on are the `SerialInterface` class and a function to operate the shutter.

The following chapters are describing the different classes of the VOODOO.QE extension.

4.0.1.2.1 VOODOO.QE.main

This static class contains functions like the FITS file header support and the set light level function. The light level function is called with the desired number of photons per second. By dividing the measured light level with the desired level the slit width of the monochromator is increased or decreased by this ratio. To avoid over saturation of the CCD the light level function starts with a closed slit. Since the ratio with an closed slit is usually very large, limiting the ratio was necessary to avoid overshooting. If the measured light intensity is within +/- 3% of the desired intensity the loop breaks and the program continues.

4.0.1.2.2 Device control classes

Since the QE setup consist of several hardware parts which are controlled by VOODOO, every device is controlled by an specific device control class. Table 7 lists the class names and the functionality of the device classes.

⁷ `astropci`: Linux device driver for the leach controller board

Class name	Controls device	Description
Kei_1	Keithley 6485 (sphere)	Controls the picoammeter which measures the current of the PD located in the sphere Class contains several specialized functions supporting different measurements with the 6485
Kei_2	Keithley 6485 (dewar)	Identical to Kei_1 except the port identifier which is "ttyn1f" instead of "ttyn1e"
Mono	Monochromator (MS257)	Controls the MS257, supports a generic "send command" function, no specialized functions
LSource	Oriel 68907 arc lamp power supply	Controls the power supply, supports a generic "send command" function, no specialized functions
LIntense	Oriel 68950 digital exposure controller	Controls the digital exposure controller, supports a generic "send command" function, no specialized functions
LakeShore	LakeShore L321 Temperature regulator	Supports the L321, generic send command" currently not in use

Table 7 Listing of the device control classes

All classes in Table 7 have the same structure. They consist of an initialization part which sets up the serial port with the settings appropriate for the controlled device. They also implement the "SendCommand" function which sends a command specified in the function call to the device and waits for an answer. With an additional parameter a timeout can be specified. Since every device has different conventions regarding the format of the commands the "SendCommand" ensures that the appropriate device-specific terminator is sent. The rest of the functions in the device control classes are device specific specialized command blocks e.g. initiating a buffered measurement with the picoammeter. The classes `Kei_1` and `Kei_2` make use of these function since the command language of the meters requires multiple commands to control a certain function of the meter.

4.0.1.2.3 VODOO.QE.Calc

This class provides basic arithmetic functions like calculating the mean (38) and the standard deviation (37) of a given array. It also implements functions to calculate the photon flux. The photon flux is calculated with (34)(35)(36)

$$E = \frac{I_{PD}}{(S_{pd}/1000)} \quad (34)$$

$$E_{phot} = \frac{hc}{\lambda} \quad (35)$$

$$N_{phot} = \frac{E}{E_{phot}} \quad (36)$$

where E is the total energy of the photons [W] incident on the photodiode, I_{PD} is the photo current [A] of the PD, S_{PD} is the sensitivity [mA/W] of the PD at the given wavelength, E_{phot} is the energy per photon, h is the Planck constant, c the light speed [m/s], λ the wavelength [nm] and N_{phot} is the number of photons per PD area [photons/cm²].

Another function maintains the photo diode calibration data and interpolates the sensitivity for every given wavelength within the calibration range
The sensitivity of the PD calculated using a linear interpolation (37)(38)(39)

$$m = \frac{(S_b - S_a)}{(\lambda_b - \lambda_a)} \quad (37)$$

$$b = S_a - (m * \lambda_a) \quad (38)$$

$$S_i = m * \lambda + b \quad (39)$$

Where m is the slope between two data points S_a and S_b at the wavelengths λ_a and λ_b , b is the offset and S_i is the interpolated sensitivity value at wavelength λ
If the photo diode is changed, the new calibration data can be loaded from a file.

4.0.1.2.4 The "SerialInterface" Class

The `SerialInterface` class interfaces a C library which is used for communication with the serial ports. Due to the platform independent architecture of JAVA, it is relatively complicated and complex to access hardware directly. There is no direct way to communicate with the serial interface. Sun, which developed JAVA, provided a set of classes, the `JAVAX.comm` package, which enables the direct communication with the serial port. This package supports only Windows or Solaris, not Linux. To access the serial port, a C library was developed in our group which handles the low-level communication with the serial port. A

special interface class was written in JAVA to make the C library functions available for other JAVA classes.

4.0.1.2.5 *The architecture of the QE extension*

The path of information flow between the user inputs and the hardware device has to pass several layers of abstraction. The hardware is connected via RS232 serial connections with the PC. The driver provides a typical Linux hardware access to the RS232 ports. The C library interfacing the serial port uses the standard Linux way of accessing hardware. The “`SerialInterface`” class is an adapter which makes the functions of the C library available for all the other VOODOO classes. The QE extension creates one instance of the `SerialInterface` class per physical port. The `SerialInterface` objects are created by a device-specific static class. Static means that the functions provided by a static class can be accessed without creating an instance of the class. Since these classes are different for each device, instantiating them has no advantage. As shown in Fig. 36 every device class holds an own instance of the `SerialInterface` class. This provides undisturbed parallel access to the serial ports.

The device-dependent classes contain functions to initialize the hardware and send commands to the controlled devices. However, the provided functions are sending mostly single commands to the hardware. To perform e.g. a current measurement, a couple of those basic commands must be executed. The actual measurement is provided by another class which also implements the runnable interface.

The `RunMeas` class provides a set of functions which perform measurements and other complex hardware-related tasks like setting the monochromator to a certain wavelength. Since it implements the runnable interface it has to have the “`run()`” function implemented. If the run function of an instance of “`RunMeas`” is called, it is executed in its own thread, independent from the rest of the program flow. Threads can provide a simultaneous execution of two functions e.g. measurement of the photodiode currents on both Keithley picoammeters at the same time. This is essential when different devices in the setup have to be controlled at the same time.

As shown in Fig. 36 the QE extension provides a multi threaded access to the hardware. Another benefit from the multi threaded approach is the possibility to give the optical feedback about the progress of the action initiated by the user. In the QE extension, it is implemented by progress bars which are updated by the

specific function running in its own thread. Since the GUI provides status bars and indicators for every controlled device, the threads are prevented from interfering with each other by updating common objects as a global status bar. There is one

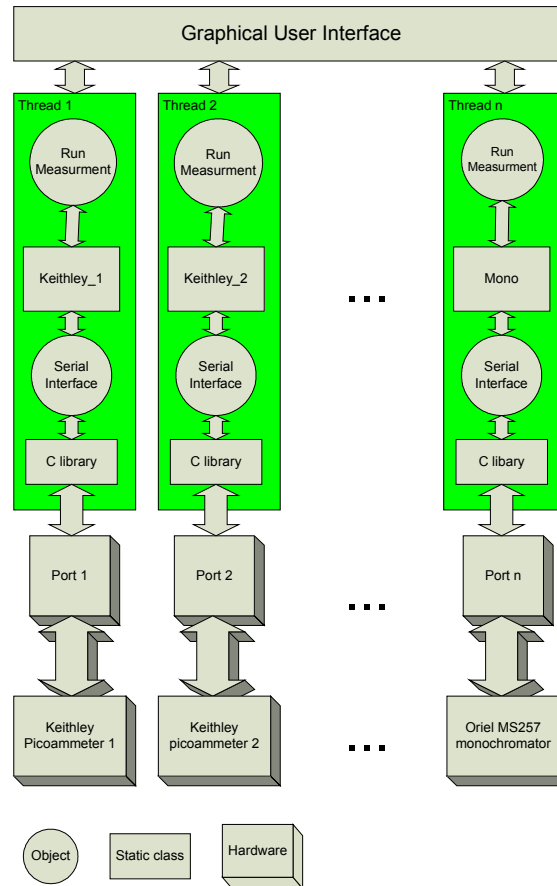


Fig. 36 Data flow in VOODOO.qe

global indicator, the log text area. Every running measurement or setting process is able to print messages to this log window. This is a second source of feedback and information for the user [17]. When running VOODOO script the multi-threaded approach of measuring is not used.

4.0.1.2.6 Data handling and visualization.

While the device control routines and measurements are able to run simultaneously, the internal data handling must also be multiprocess-ready. The measurement data is stored in the `DataStorage` object. This object is able to hold the measurement data and some additional information. By referencing this object to the data acquisition and data display objects each of these parts have access to the data. Apart from “store” the pure data the `DataStorage` object also contains a function to save its data to a text file. If a measurement is done, the

RunMeas object stores the data in the DataStorage object. Then RunMeas creates an instance of the Chart object which displays the measured data in a chart. It also assigns a reference of the DataStorage to the Chart object. The relationships among the objects are shown in Fig. 37.

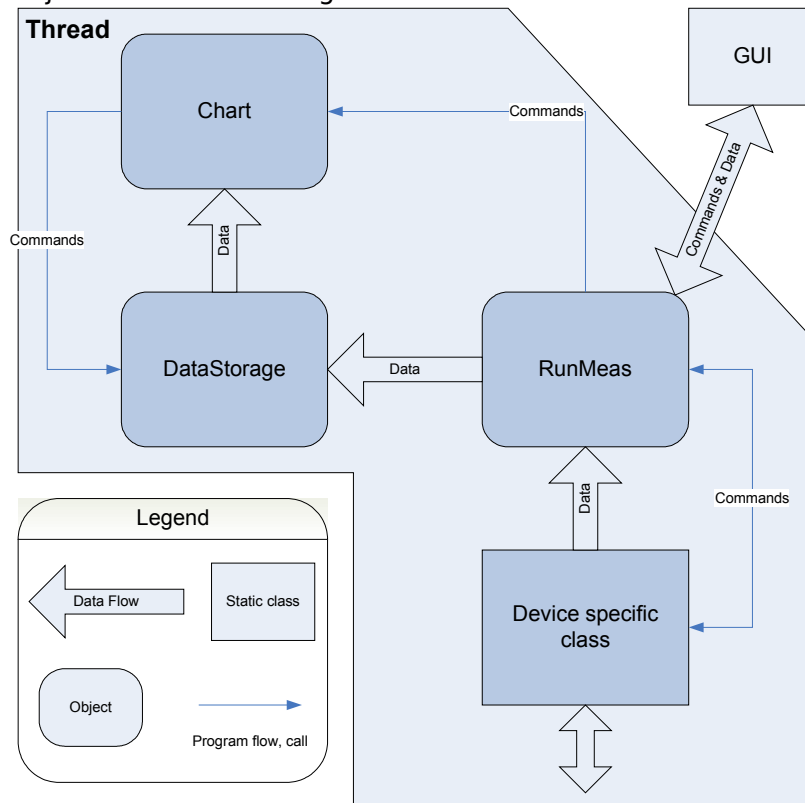


Fig. 37 Relationships among objects in VOODOO.qe

While each controlled device has its own chain of independent objects, the interference between the devices is reduced to a minimum.

4.0.1.3 VOODOO script

One modification on the original VOODOO which was added at LBNL is the ability to control nearly every function of VOODOO with a scripting language. This language is basically JAVA script and supports an set of functions provided by VOODOO. To make a function available in the script language, an interface function has to be implemented in the `VoodooControl` class. This was done for most of the functions in the VOODOO.QE extensions. The advantage of a scripting function is the ability to run complex measurements and tests fully automated.

4.0.1.4 Script controlled mode

To be as flexible as possible, all significant functions in the `VOODOO.qe` classes

are made available in VOODOO's scripting language which enables full access to most of the VOODOO functions in a pure procedural way. To program in VOODOO script, the user does not have to deal with object oriented programming. The `VOODOO.Command` class acts as a wrapper and makes the VOODOO functions accessible for the scripting language. Fig. 38 shows the concept of the VOODOO script architecture.

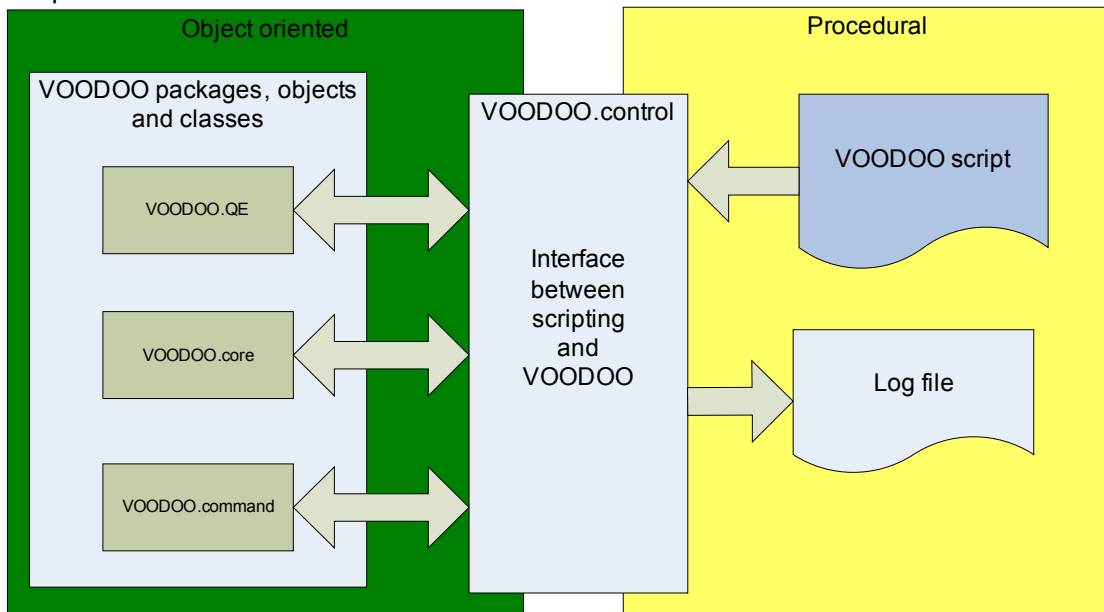


Fig. 38 Architecture of the VOODOO scripting interface

As mentioned above, the QE measurement is implemented as a VOODOO script. The commands in the script are calling directly the `VOODOO.script` wrapper functions. These functions are calling the "real" functions of the different VOODOO packages and classes. To support QE measurements a new set of wrapper functions for the `VOODOO.qe` package were written. Fig. 39 shows the flow chart of a QE measurement script

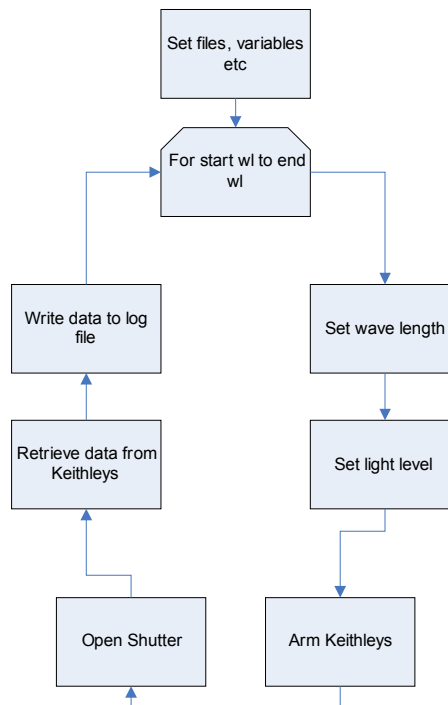


Fig. 39 Flow chart of the QE measurement script

After some initial settings like specification of the image and log file path, the main measurement loop begins. The loop is realized as a FOR loop. The loop variable “i” acts as the wavelength indicator. The loop usually starts with the lowest and ends at the highest wavelength. The increment is the step width, usually 10 nm or 20 nm.

Once the loop has started the wavelength is set by sending the “!GW” command to the monochromator. Then the light level is adjusted to the specified value. Therefore the “SetLightLevel” calls the `VOODOO.QE.MAIN.setLightLevel()` function. This functions measures the light intensity at the reference diode in the dewar and uses the motorized input slit of the monochromator to attenuate the light to the specified amount. The light intensity is specified by the user in photons per pixel per second. After the light intensity is set, the picoammeters are set up and armed for triggered mode. In the QE setup the “openShutter” signal of the Leach controller is used for triggering the Keithleys. After the exposure, the data is retrieved from the picoammeters by the “getKeiBufAmpDelMean” and the “getKeiBufAmpDelSDev” functions. The photons per pixel are calculated using the “calcPhotons” function. The data is then written into the log file. Once the loop is finished the log file is closed and the script ends.

4.0.2 IDL program

An IDL⁸ program was written in order to provide automatic analysis of the image files. IDL is an interpreted programming language which supports easy matrix calculations without loops and many functions for data analysis and manipulation.

The VOODOO script which controls the QE measurement saves the wavelength, the image file path, the diode readings and the photons per pixel value in a log file. The IDL program parses the log file and acquires all values needed to calculate the QE. Once the values are acquired the program loops over the images, calculates the QE and writes the results in a text file which can be read by a spread sheet program for displaying or for further calculations.

The most important value the IDL program acquires from the image files is the signal level in ADU⁹. To get this value, the program has to subtract the offset from the actual pixel value. Each image contains a region which consist of this offset data, the overscan. The IDL program calculates the mean value of a 100x100 pixel square in the overscan region and in the image region. To eliminate the influence of cosmic rays and hot pixels the mean is calculated once, and then every pixel in the array which is out of +/- 3 sigma is ignored in the second mean calculation. The two mean values, overscan and image, are subtracted and the result is the average amount of charge in the selected region of the CCD. To convert this number to e/h pairs, it is divided by the gain of the CCD. From the number of photons per pixel, the QE is calculated (40).

$$QE = \frac{PhotonsPerPixel}{(ADU / Gain)} \quad (40)$$

Where *PhotonsPerPixel* is the number of photons per pixel, *ADU* is the digital values read by the leach controller and *Gain* is the conversion factor from ADU to e/h pairs. The gain can be measured by several methods (section 5.1.2.1)

The results of the calculations and the raw values read from the VOODOO script log file are stored in a ";" separated text file.

8 IDL: Data analysis and visualization software by RSI (used in CCD group for CCD image characterization and analysis)

9 ADU: Analog-to-Digital Unit, unit defining integer values resulting from an analog to digital conversion.

5 QE MEASUREMENTS AND ERROR CALCULATION

This section shows the QE measurements we made followed by a discussion of the errors.

5.1 QE Measurements

After testing the setup and the software, a CCD was mounted in the dewar. This chapter will describe the tests and QE measurements we made with two different CCDs. One was a low voltage, back illuminated device (800x1980 pixel, 15 μm^2 pixel) equipped with an older version of the anti reflection (AR) coating used on the SNAP CCDs. The second device is an actual, high voltage, 200 μm thick backside illuminated device with 12 μm^2 pixels and a slightly different AR coating.

5.1.1 Reflectivity vs QE

In order to verify the results of the QE measurements samples of the wafers were sent to Lick observatory to measure the reflectivity of the devices. The surface of the CCDs is equipped with an AR coating (see section 1.1.3). In the range of $\sim 500\text{nm}$ to $\sim 900\text{nm}$ the internal QE of the CCD is likely to be 100%. In this region the measured external QE should be dominated by the reflection of the light at the surface of the device. The QE value in this region should be similar to the absorption (1-reflectivity).

5.1.2 Gain measurement

After cooling down and some test exposures, the gain of the CCD was measured. This measurement was required to acquire the conversion factor from ADU to e-h pairs in the CCD.

5.1.2.1 The ^{55}Fe method

To derive this number, the CCD was exposed to a radiation source of known energy. ^{55}Fe is used as soft gamma radiation source. In a beta+ decay the ^{55}Fe turns into ^{54}Mn . The ^{54}Mn is the actual x-ray source with two main emission lines, K_{α} with an energy of 5.9keV and K_{β} with 6.5keV. The x-rays are absorbed in the CCD, generating charge proportional to their energy [18].

The energy to generate an e-h pair in silicon is 3.76eV at 140K. Since the x-rays hitting the CCD perpendicular, the generated charge is distributed over a small

number of pixels. To generate an x-ray image the CCD was exposed about 10 sec to the x-rays. The result is an image with a large number of bright pixels, generated by the x-rays. An IDL program separates the x-ray events from the background noise and the base level. A histogram is calculated from the event pixels. Fig. 40 shows such an histogram.

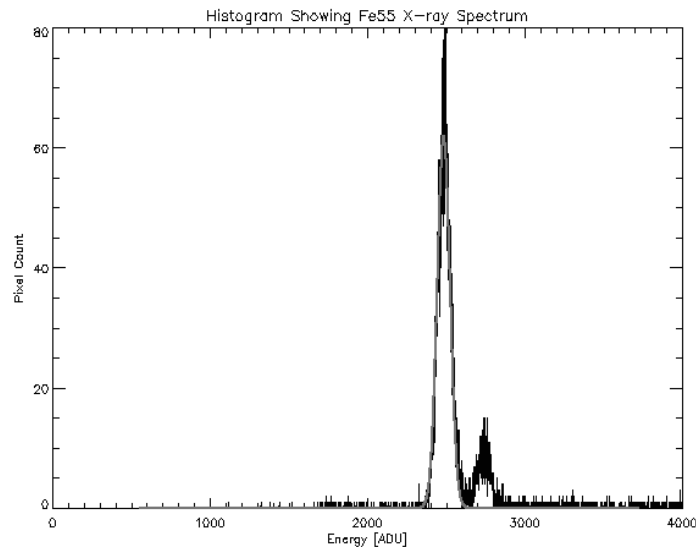


Fig. 40 Histogram of a x-ray exposure

To calculate the gain factor, the x-ray energy has to be divided by the e-h formation energy of 3.76eV. The result is the number of e-h pairs created by one event. The gain is the ratio of ADU and e-h pairs per event. Equation (41) shows the calculation of the gain.

$$Gain = \frac{ADU}{(E_{xray} / E_{eh})} \quad (41)$$

Where ADU are the measured analog digital units, E_{xray} is the xray energy and E_{eh} is the e-h formation energy.

After the exposure, the image has been analyzed in a software which compares the pixels hit by an x-ray with the background pixels. Since the amount of charge generated by such an event is known, the conversion factor from e-h pairs to ADUs can be derived. Once the gain is measured it can be used to calculate the quantum efficiency of the CCD.

5.1.2.2 Results of the Gain measurement

For the first CCD, a gain of 1.26 to 1.27, depending of the way the picture is analyzed, was measured. If a matrix of 3x3 pixel was used the gain was 1.26 if a

5x5 matrix was used the gain was 1.27 The fact that the 5x5 matrix shows a higher gain value indicates that a 3x3 matrix is not covering the whole event. Due to those and different problems (internal conversion factors are not very well known) [19] the gain is one of the largest sources of error.

5.1.3 Measurement of QE vs wavelength

These measurements are the proof of concept measurements for the QE measurement setup. To measure the QE a VODOO script program was written. This script controls, with the functions of VODOO, the whole test setup. The script runs in a loop and takes an exposure at each specified wavelength. The first real QE curve was taken with 10nm steps. For each step the image is saved in an folder, the image path is stored in a log file. Also stored in the log file are date and time, the mean values and standard deviations of both PDs and the wavelength where the exposure was taken. To maintain a constant light intensity over the wavelength range, a function adjusts the light level before each measurement.

5.1.3.1 Measurement of the QE on a low voltage (lv) device

The first CCD measured was the device no 86135-7-7 This device is a backside illuminated 250um thick high resistivity p-Si CCD. The size is 2000x800 pixel with an pixel size of 15um². The substrate voltage which depletes the device was set to 50V.

5.1.3.1.1 Measurement of the gain

First the gain of this device was determined. Measured with the ⁵⁵Fe method, the gain was 1.25 +/- 1.5%

The following image shows a 50x25 pixel sub image of an 10 sec x-ray exposure. As seen the x-ray events are distributed over a few pixels instead of only one. This is a typical effect of the backside illuminated low substrate voltage design.

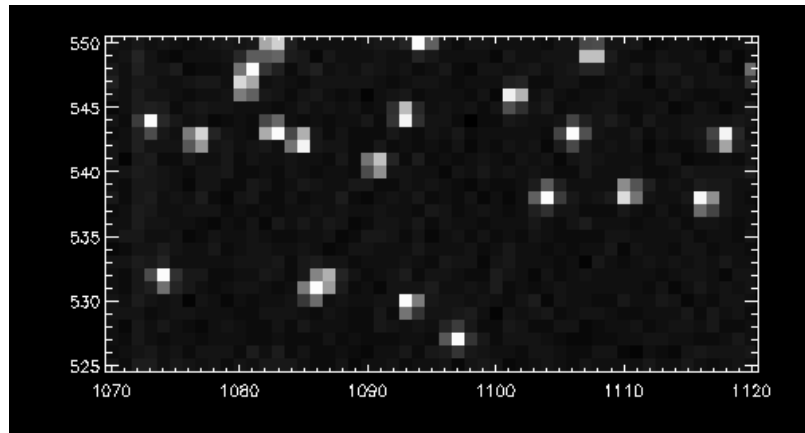


Fig. 41 10 sec x-ray exposure of a low voltage device. Every clusters represents an event (x-ray generating charge in silicon) Unit of x and y axis is [pixel]

5.1.3.1.2 QE measurement

The following QE plot (Fig. 42) was measured with 10nm steps, 5sec exposure time and a light intensity of 8000 photons/pixel * second. The curve is shown with error bands specified in section 5.2. In addition also the results of a reflectivity measurement, done with a sample of the same waver at Lick Observatory, are shown in this graph

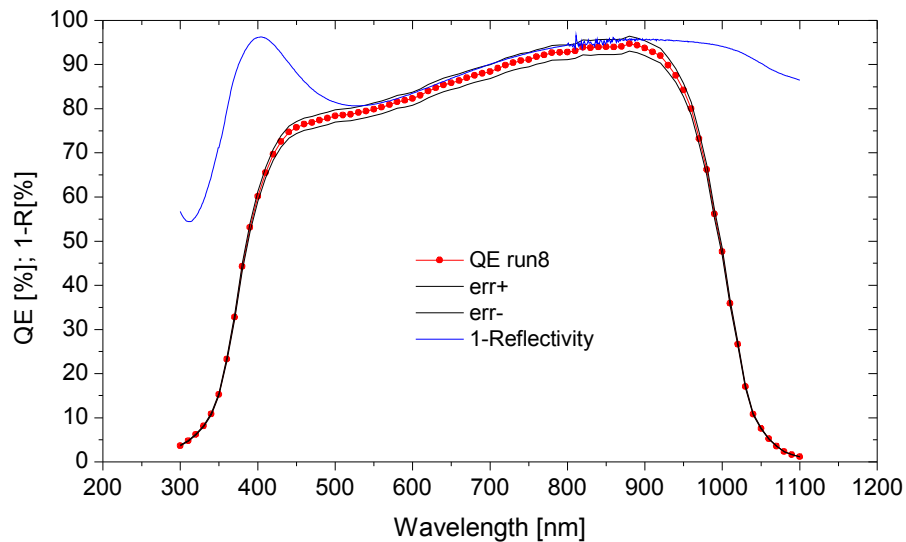


Fig. 42 Quantum Efficiency and 1-Reflectivity vs Wavelength

The shape of the QE curve is determined by 3 major effects. The slope at the blue end of the spectrum is caused by the decreasing penetration depth of the photons. The slope at the red end is determined by the increasing absorption length and limited by the band gap energy of Silicon which is at $\sim 1.45\text{eV}$. The area between this slopes shows a good QE of $\sim 75\%$ at $\sim 500\text{nm}$ to 95% at $\sim 900\text{nm}$. Since the internal QE in this region is nearly 100% , the QE is highly dependent on the AR coating which determines the shape of the curve in this area. The comparison with the 1-R data shows correlating values in the region with 100% internal QE. The measured curve is considered to be plausible and well understood.

5.1.3.1.3 Reproductivity measurements

In order to verify proper function of the the setup the QE curves have been measured several times with different step widths. The different curves for the low voltage device are shown in Fig. 43

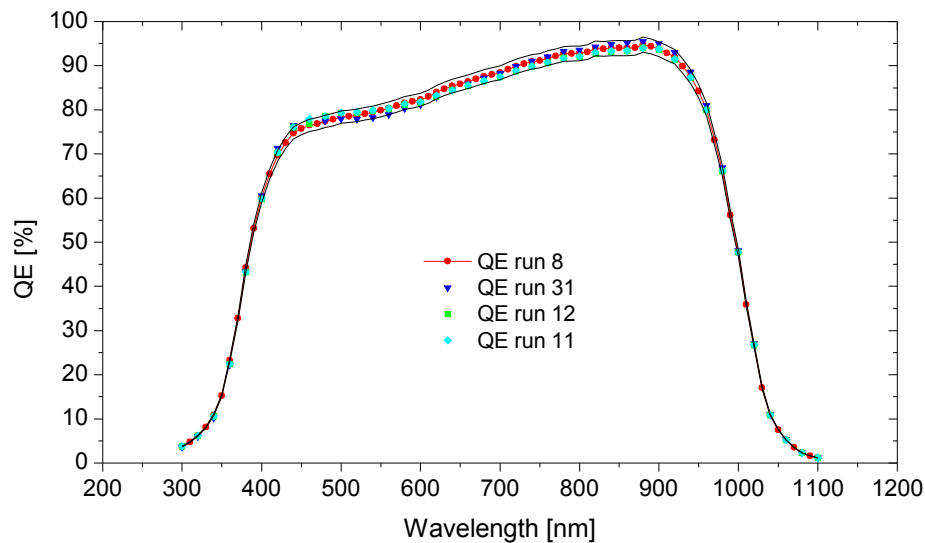


Fig. 43 Reproductivity measurement of the low voltage device

As shown in Fig. 43 the curves of the different measurements are staying always within the errors bands. QE run 8 was the first high resolution QE scan. Run 11 and 12 had nearly identical results, they had been measured with a step width of 20 nm . Run 31 was measured after the replacement of the hv device.

This QE curve shows the largest deviation to the first measurement. Reasons for this behavior could be mounting specific offsets or other changes in the setup.

5.1.3.2 Measurement of the QE on a high voltage (hv) device

The second CCD measured with the system device no. 82135-8-13, a backside illuminated, 200um thick fully depleted high resistivity p-channel CCD. The pixel size of this device is 12um in an 1980x1000 pixel array. To maintain the full depletion a substrate voltage of 100V was applied.

5.1.3.2.1 Gain measurement

The gain was also measured with the x-ray method and the result was 1.593 ADU/e-h

The following image shows a 50x25 pixel sub image of an 10 sec x-ray exposure. In comparison to the low voltage device, the charge deposition of the x-rays is concentrated to fewer pixels. This is caused by the higher e-Field which guides the e-h pairs faster to the wells.

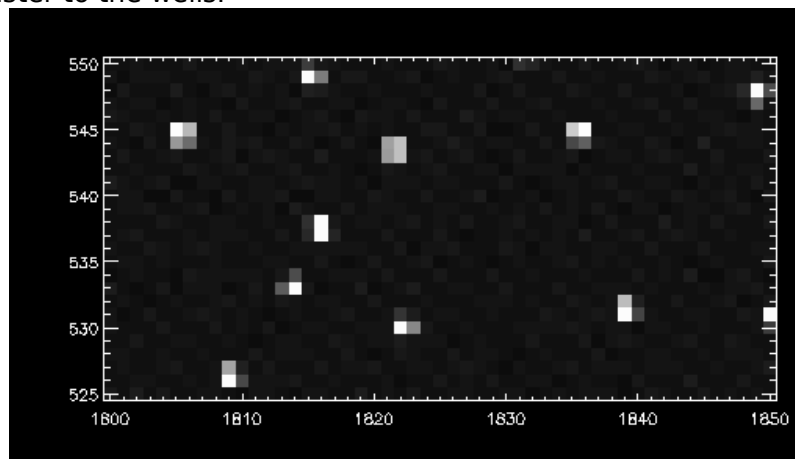


Fig. 44 10 second x-ray exposure of an high voltage device. The number of bright pixels created by an event i

5.1.3.2.2 QE measurement of the high voltage device

The following QE plot was measured in 10nm steps at an exposure time of 10sec and an average photon per pixel count of 4000 photons/pixel * sec.

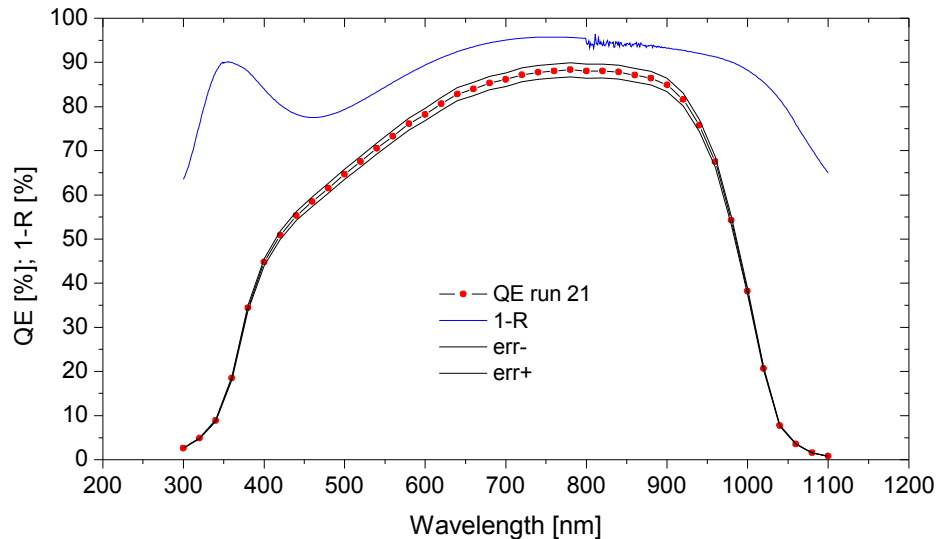


Fig. 45 Quantum efficiency vs 1-reflectivity

The result of this measurement was not expected to have this shape and QE. The QE measured on this device is always below 90% which is poor compared to the first device. Also the shape is totally different than expected. The reflectivity data from Lick does not correlate with the QE. There was no plausible explanation of this behavior. As mentioned above in the area from 500 to 900 nm the internal QE is usually \sim 1-reflectivity. This device shows a different behavior, the internal QE seems to be always lower than 90% and the shape of the curve does not correlate with the reflectivity data.

5.1.3.2.3 Reproductivity measurements

In order to verify the strange results of the QE measurements, several curves had been measured. The results are shown in Fig. 46.

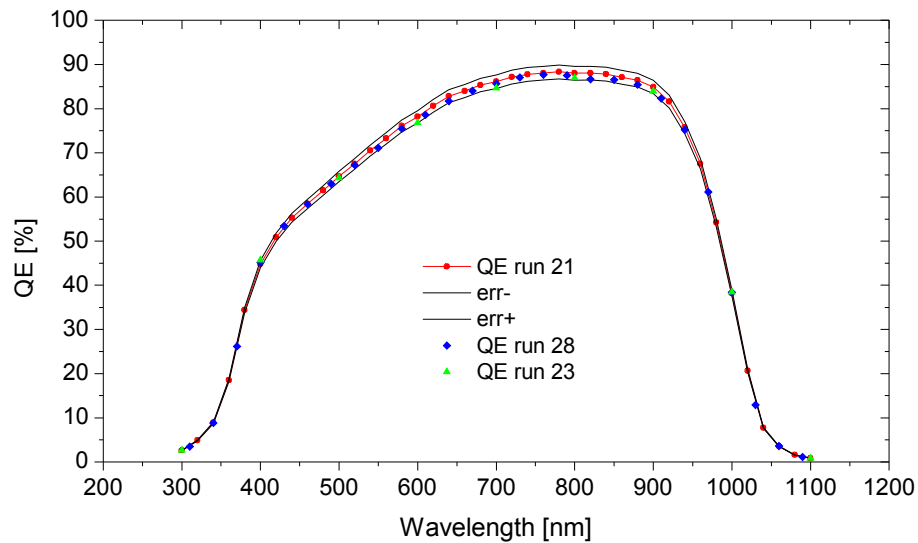


Fig. 46 Reproducibility measurement of the high voltage device

In this case the second measurement (run23) was done in reverse direction (from 1100 to 300nm) in 30 nm steps. The result of this measurement is consistent to the result of the first one (run21). To check the results a third run, (run28) with 100 nm steps was done. All values of this three measurements are within the error bars of the first one. The results are reproducible.

5.1.3.3 Re-measuring the first device

After the strange results of the second device, the first device, 82135-7-7, was remeasured to ensure that the QE setup works properly. The gain and the QE curve was measured again and the result was a good reproduction of the first measurement of this device. Fig. 47 shows the the data of the first (run8) and the second measurement (run31) of device 82135-7-7

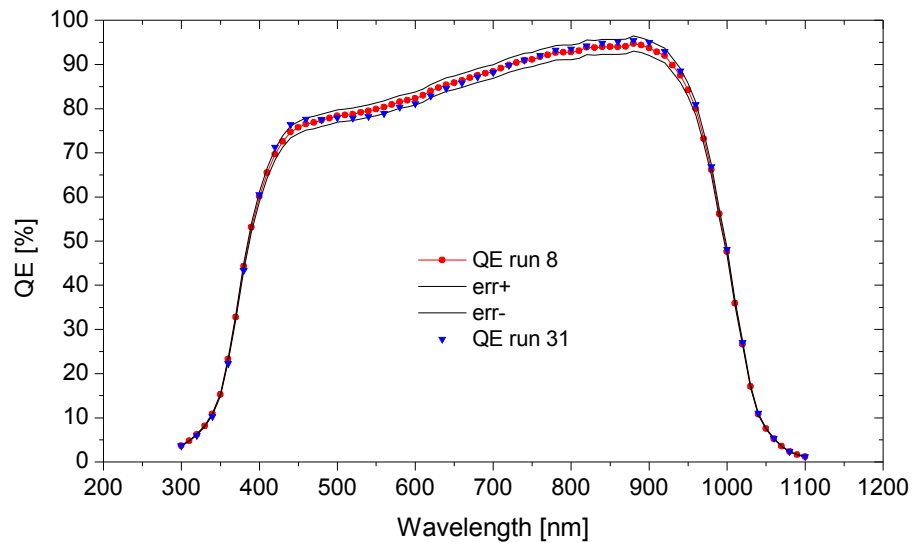


Fig. 47 QE curve of first meas (QE 8) vs QE after remounting (QE 31)

The data points of the second measurement are staying always within the error bars of the first measurement. A slight deviation of the results occurred in the region around 450-500 nm.

5.1.4 Conclusion

The QE of the Iv device was measured successfully, the QE was within the expected range and verified with the reflectivity measurement. The hv data does not correlate with the reflectivity data. Since the QE of this device was never measured before, there was no data for comparison available. Since the measurements are reproducible, even after changing the device, I consider the setup to be working. Some defect must have been occurred in the high voltage device.

5.2 Error Calculation

In this chapter the sources of errors and correction factors will be discussed. There are several types of errors. Each error type has another influence on the result of the measurement. The most predictable “errors” are correctable “errors” like the uniformity of the light. This uniformity was measured, a function was fitted and the influence on the resulting QE can be corrected. This correction factors are systematic, absolute and constant.

The next error class are the systematic absolute errors. They are independent from the actual measurement value. They have to be added in quadrature.

Systematic relative errors are caused by the test setup and are given as a percentage of the measured value. They are also added in quadrature.

The last class of errors are statistical errors. They are usually expressed as percentage of the measured value. They are completely random and they cannot be corrected. They are added in quadrature. In the QE test setup these errors contribute only a fraction of the total error.

5.2.1 Sources of errors and correction factors

5.2.1.1 Error caused by lamp and Housing

Since the light incident on the CCD is monitored “online”, variations in brightness and spectrum do not have any impact onto the QE measurement. Since the light source is stabilized by a light intensity controller, the biggest changes in intensity will be suppressed.

5.2.1.2 Error caused by the shutter

Shutter blades require a certain time to open and close. During this time, the position of the shutter blades is unknown and somewhere between open and closed position. That leads to an unknown amount of light passing the shutter during this time. To keep below the 1% error margin the amount of light passing during transfer time has to be under one percent of the light amount passing at the exposure time. Fig. 48 shows the timing diagram provided by Uniblitz, the maker of the shutter.

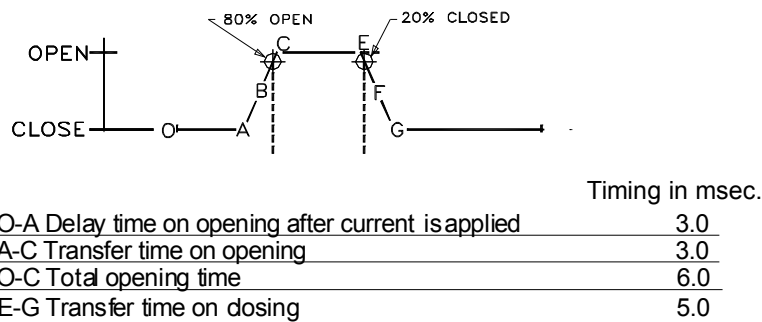


Fig. 48 Timing diagram of the Uniblitz shutter

Uniblitz quotes an opening time of 6ms and a closing time of 5 ms [20]. The total transfer time at one exposure is then 11ms. Assuming the worst case of full transparency of the shutter during transfer, the opening time has to be 100 times the transfer time, given by.

$$t_{exposure} = t_{transfer} * 100 \quad (42)$$

The exposure time has to be at least 1.1 seconds to meet the < 1% error criteria. The effective transfer time is about 8msec, so the minimal exposure time is about 0.8 seconds. Given an exposure time of 10 seconds the error in the amount of light caused by the shutter transfer time is about 0.08 %. This error is a systematic always positive error because there is always a light surplus. Since an exact (measured) timing diagram of the shutter is not available, this error cannot be corrected. With exposure times of min 5 seconds, this error has no big influence and is ignored in the error bars.

5.2.1.3 Error caused by the filter wheels

The possible sources of error at the filter wheels are light leakage through inaccurate mechanics and the limited blocking ability of the filters, since the filters are mostly used to block higher-order effects. Assuming that a 2nd order intensity is 50% of the first order intensity, blocking by the filters is important. Spectra Physics, the maker of most of our filters, claims a transmission <math> < 1 * 10^{-3}</math>. The 2nd order light is attenuated by a factor of 1000, which leads to an intensity of 0.05% of the 1st order light. This light counts as stray light and adds to the out-of-band light. Since this light has a relatively low intensity compared to the in-band-light, it is not a critical error [21].

5.2.1.4 Sources of error in the monochromator

The monochromator implies several sources of error, the most have only tiny impacts on the overall system error. One of the minor sources of error is the center wavelength accuracy of the monochromator. An other is the width of the band. The wavelength accuracy is below 0.1 nm. The accuracy of the slits which determines the bandwidth is about 0.5% of the maximum width and has only very low impact on the overall signal. The most important error source in the monochromator is the stray light as mentioned in the monochromator section. The relative amount of stray light at the worst case is about 0.75% of the in-band-light. This error can be increased by 2nd order effect light which can be about 0.05% of the signal. This systematic error is then worst case 0.8% of the light incident onto the CCD [10].

5.2.1.5 Error contribution by the integrating sphere

The integrating sphere as passive device adds no statistical or uncorrectable errors. The integrating sphere causes ~0.7% non-uniformity of light intensity over the illuminated area. Since we measured this non-uniformity and made a fit over the uniformity data, its influence on the QE can be corrected. Therefore the non-uniformity is not an error, its a correction factor.

5.2.1.6 Error contribution by light leaks in the setup

As shown in section 3.4.3, the light leakage of the system is very low. An current of ~50 fA is measured in the integrating sphere. Compared to the measurement signals of >0.1 nA the error contribution of light leaks is negligible.

5.2.1.7 Errors caused by the reference photo diode

The sources of error in our reference diode are the noise current of the diode, the temperature dependence of the output signal, and the errors caused by the measuring instrument.

As described above, the noise current of the Hamamatsu S1337 photo diode is very low. Measured with an integration time of 1 second, the noise current is about $1.2 \cdot 10^{-14}$ A. This is below the RMS noise of the picoammeter which is about 20fA. Due to this fact, the photo diode is not a severe source of error.

5.2.1.8 Measurement error of the Keithley 6485 picoammeter

In the lowest measurement range (max 2nA), Keithley quotes the following error numbers:

Offset: 0...400fA

Accuracy: +/-0.4%

RMS noise: +/-20fA

While the offset and the accuracy are systematic errors they can be added. The offset can be specified by measuring the 0A dark current of the PD. If no dark current is measured, then the meter has no offset. If any offset exists it can be measured and subtracted from the signal. The accuracy is also systematic and hard to correct. Since the accuracy is as good as 0.4 % of the measured value, it stays within the allowed 1% error. The RMS noise is a statistical error which can be reduced by increasing the number of repeated measurements. The following table shows the impact of the measurement errors on the measured value [16].

Current	Offset [%]	Accuracy [%]	RMS noise [%]
2pA	20	0.4	1
20pA	2	0.4	0.1
100pA	0.4	0.4	0.02
200pA	0.2	0.4	0.01

Table 8 Errors of the picoammeter relative to the measured current

During an exposure of 10s, a PD current of ~100pA is flowing. According to Table 8 the accumulated error remains below 1 %. Assuming the offset error is corrected, a current of 20pA can be measured with an error under 1%.

5.2.1.9 Maximum exposure time.

While the minimal exposure time is determined by the shutter speed, the maximum exposure time is dependent on the sensitivity of the photodiode. Assuming a noise current of the pd of $2 \cdot 10^{-14}$ A, the minimal photo current with less than 1% error is then

$$I_{min} = I_{noise} * 100 \quad (43)$$

which leads to an minimal photo current of 2pA. According to (36, 35, 34, 40) the maximum exposure time which maintains an photo current higher than 2pA is about 545 seconds [2]. Taking into account the imperfections and measurement errors of the picoammeter the lowest current <1% error is then 20pA. This leads to a maximum exposure time of ~50 seconds. [7][8] If the sphere diode is cross calibrated with the dewar diode and used as reference, much longer exposure times are possible.

5.2.2 Summary

Since the most known sources of error are listed in the previous section, the summation and weighting of these errors is discussed in this chapter. The QE is calculated with (44)

$$QE = \left(\frac{ADU}{gain} \right) * \left(\frac{nPixel}{area} \right) * \left(\frac{e}{I_{PD}} \right) * QE_{PD} * ept \quad (44)$$

Where ADU are the measured analog digital units, $gain$ is the CCD gain, $nPixel$ is the number of pixels, $area$ is the area of the PD, e is the elementary charge, I_{PD} is the current of the photo diode, QE_{PD} is the quantum efficiency of the PD and ept is the exposure time. Each of the equations' parameters can be measured with an error. To keep the error calculation simple and to avoid summing up nonexistent errors only a few parameters are taken into account for the QE error.

The following table lists the systematic errors in the equation.

Element	Type	Value
Gain	relative	1.50%
PD area	relative	0.50%
QE_{PD}	relative	0.50%
Meas accuracy	relative	0.40%
Geometric sum		1.78%

Table 9 Systematic errors and correction factors

The selected elements are listed in Table 9. The gain was chosen due to its relative large error which cannot be compensated. The PD area and the QE of the PD are also only known to this precision. The measurement accuracy is also claimed by Keithley. All the other systematic errors are not taken into account because they are either too small to be relevant or they are unknown.

Since (44) does not contain any nonlinear functions the errors can be simply added in quadrature. The addition has to be done quadratically because they are uncorrelated. As shown in Table 9 the overall systematic error is +/-1.78%. In addition to the systematic errors, also statistical errors occur. They are listed in Table 10

Element	Type	Value
PD noise	Relative	0.10%
Exposure time	Relative	0.10%
Light noise	Relative	0.10%

Table 10 Statistical errors

Statistical errors are added quadratically which leads to a total statistical error of 0.173% of the measured QE. To generate the error bands in the plot the relative errors for each data point were calculated. Then the absolute error was added.

The summation of the errors follows (45)

$$Err = \sqrt{(Systematic^2 + Statistic^2)} \quad (45)$$

With the values of Table 9 and Table 10 the error applied to the QE curves is +/-1.8

Constant correction factors like the light intensity distribution over the illuminated area or other factors like offsets are ignored in this error calculation. To correct the measured values with those correction factors they have to be quantified by measurements. The quantification was only done for the uniformity. The measurement results are uncorrected.

To meet the specifications the error calculation has to be refined and additional measurements to quantify offsets and other systematic errors have to be done.

6 CONCLUSION

The main goals in this project are the design and implementation of a QE setup with the performance specified in chapter three. After the design phase of the project and some delays due to late deliveries, the system was set up and several performance measurements including throughput, uniformity, and darkness were done.

The light throughput, especially in the blue end of the spectrum was lower than expected but still high enough to maintain a proper illumination of the CCD.

The uniformity within the 10cm diameter area is better than 99% and hence within our specifications.

Also the light leak test showed good results, after some improvements no mayor light leaks remained.

After the performance measurements, the QE's of two different CCDs were measured. The result was verified by a reflectivity measurement done at Lick Observatory.

The results of the measurement on the high voltage device are still not understood but it is likely that these results are caused by this specific device or some operational parameters.

The results of the low voltage device are consistent with theory and the reflectivity data. They could be reproduced even after changing devices.

Since most of the error sources remained uncompensated the total error of the QE is higher than specified. Therefore further work on specification and compensation of possible sources of errors has to be done.

The system is set up and its proper function was verified so the first step to a highly sophisticated quantum efficiency measurement system is done.

7 APPENDIX

7.1 Hardware

7.1.1 Pictures of the test setup

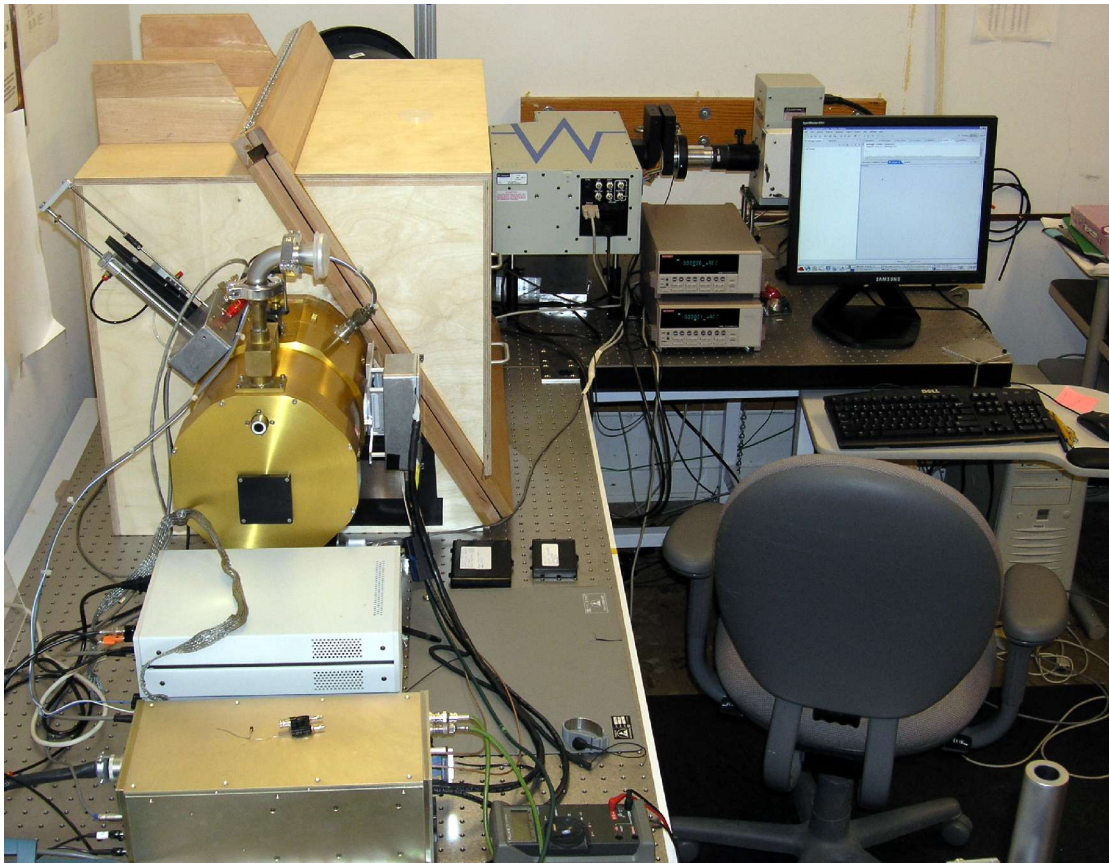


Fig. 49 Test setup, shown from the dewar side

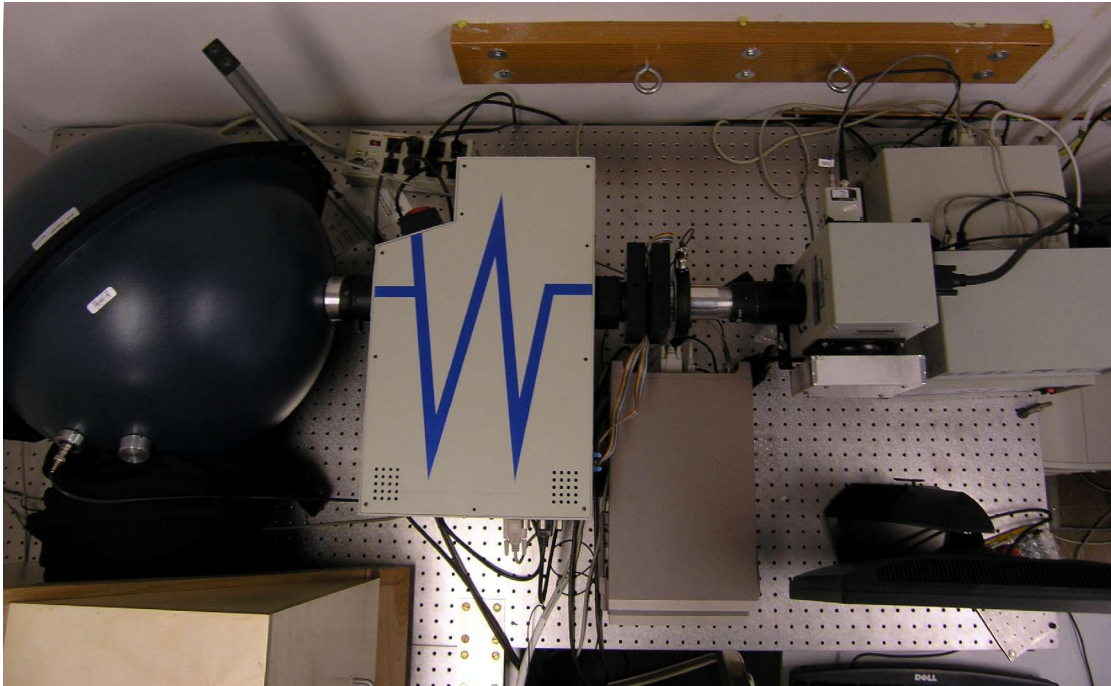


Fig. 50 Test setup, light generation section top view



Fig. 51 Test setup, view on the light generation part and the sphere

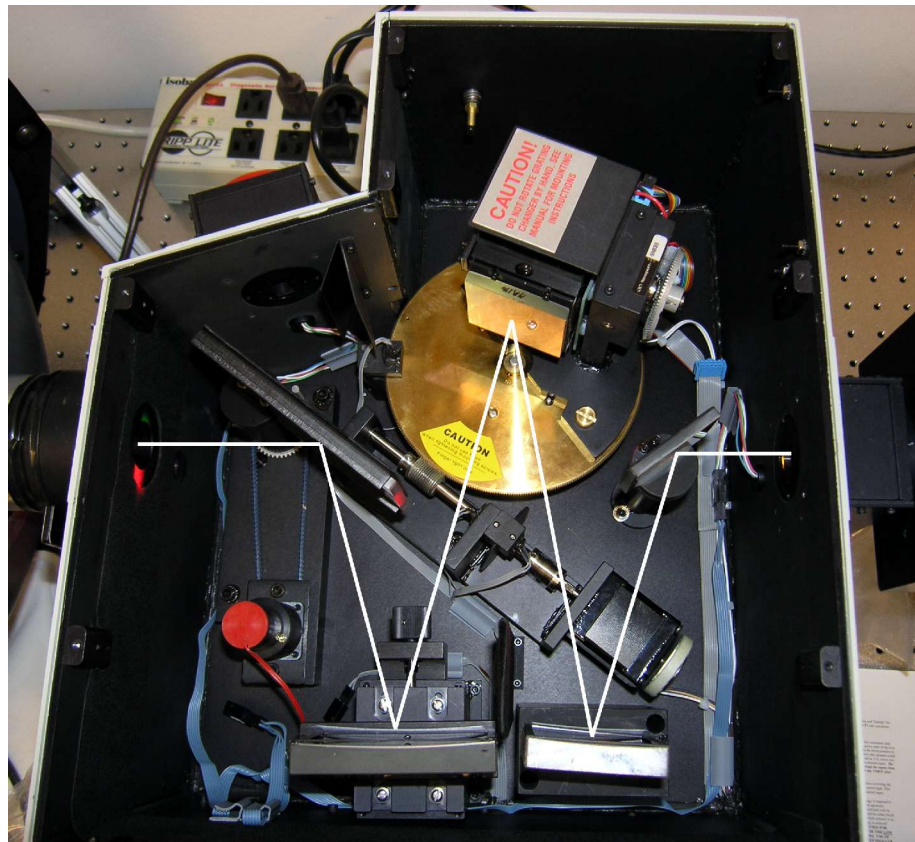


Fig. 52 Monochromator (open) with beamline

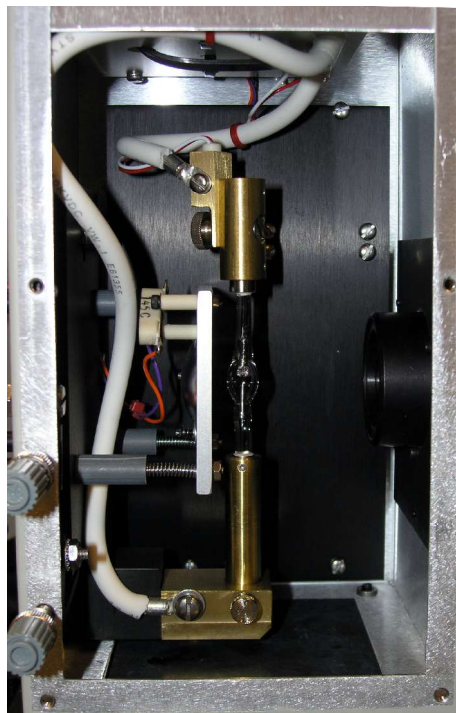


Fig. 53 Housing (open) with mounted arc lamp

7.1.2 Parts list

The following table lists all major parts used in the QE test setup.

Part	Part Number	Price	Sum	Description
Xenon Light Source				
Lamp	Oriel 6257	417		100W Xenon Lamp
socket adapter	Oriel 66150	77		Lamp Socket adapter
Lamp Housing	Oriel 66902	2440		50-500W Arc Housing with F/1 condenser
F/# matching Lens	Oriel 41575	289		F/4.6 152mm focal length
Power Supply	Oriel 68907	2689		Power supply for Arc lamps
Lens holder	Oriel 6195	67		Lens holder for 1.5" lenses
F/4.6 focusing lens	Oriel 41575	182		UVFS lens
			6161	
Stabilization				
Stabilization	Oriel 68950	2270		Light intensity controller system
Adapter for 66902 housing	Oriel 68855	210		
			2480	
Shutter				
Shutter	Uniblitz VS25S2ZM0R1	760		25mm aperture Shutter
			760	
Monochromator and Filter Wheel				
Monochromator	Oriel 77700	5655		Ms257 Oriel monochromator
Multiple Grating Turret	Oriel 77708	1429		Triple grating turret
Grating	Oriel 77742	706		1200g 350nm blaze
	Oriel 77752	706		1200g 750nm blaze
Mirror	SP45700-1738	160		Mirror 50x50x6m, coated one side
Motor driven Silt assembly	Oriel 77722	796		Variable input slit
Slit controller Board	Oriel 77712	347		Motorized single slit control

Part	Part Number	Price	Sum	Description
Fixed slit	Oriel 77212	137		3.16mm fixed slit
Output Mirror	Oriel 77716	927		Motorized flip output mirror
Motorized Filter Wheel	Oriel 77737	1075		
Motorized Filter Wheel	Oriel 77737	1075		
Dielectric filters	LS-600-F	122		Short pass 600nm
	LS-700-F	122		Short pass 700nm
	LS-800-F	122		Short pass 800nm
	LS-900-F	122		Short pass 900nm
	LS-1000-F	122		Short pass 1000mm
	LL-450-F	101		Long pass 450nm
	LL-550-F	101		Long pass 550nm
	LL-650-F	101		Long pass 650nm
	LL-750-F	101		Long pass 750nm
	LL-850-F	101		Long pass 850nm
Colored glass filters	Hoya U340	36		
	Schott BG 28	54		
			14319	
Integrating Sphere				
Integrating Sphere	LabSphere CSTM US2000	7500		20" Integrating Sphere
			7500	
Light Measurement				
Photo Diode	Hamamatsu S1337-1010BQ	640		Calibrated Photo Diode
Photo Diode	Hamamatsu S2281	250		
Picoammeter	Keithley 6485	1495		Picoammeter for Diode Readout
Picoammeter	Keithley 6485	1495		Picoammeter for Diode Readout
			2385	
Optical Table				
	Newport IG-35-2	1525		90x150 cm Breadboard
	Newport IG-36-2	1683		90x180 cm Breadboard

Part	Part Number	Price	Sum	Description
			3208	
Automation				
Linux PC +Monitor		1500		Fast PC compatible with the leach controller board.
Serial board	DIGI Neo Classic 8	150		8-Port RS232 Board
Breakout Cable	Opt8-M9	70		8 Port DB9 Breakout Cable
			1720	
Total		40028		

7.1.3 Additional Autocad drawing of the mechanical parts

- Changes:
 1.) Outer diameter 9"
 2.) O-Ring groove where specified
 3.) Thread on inside of tube
 4.) 5 holes on a new bolt circle

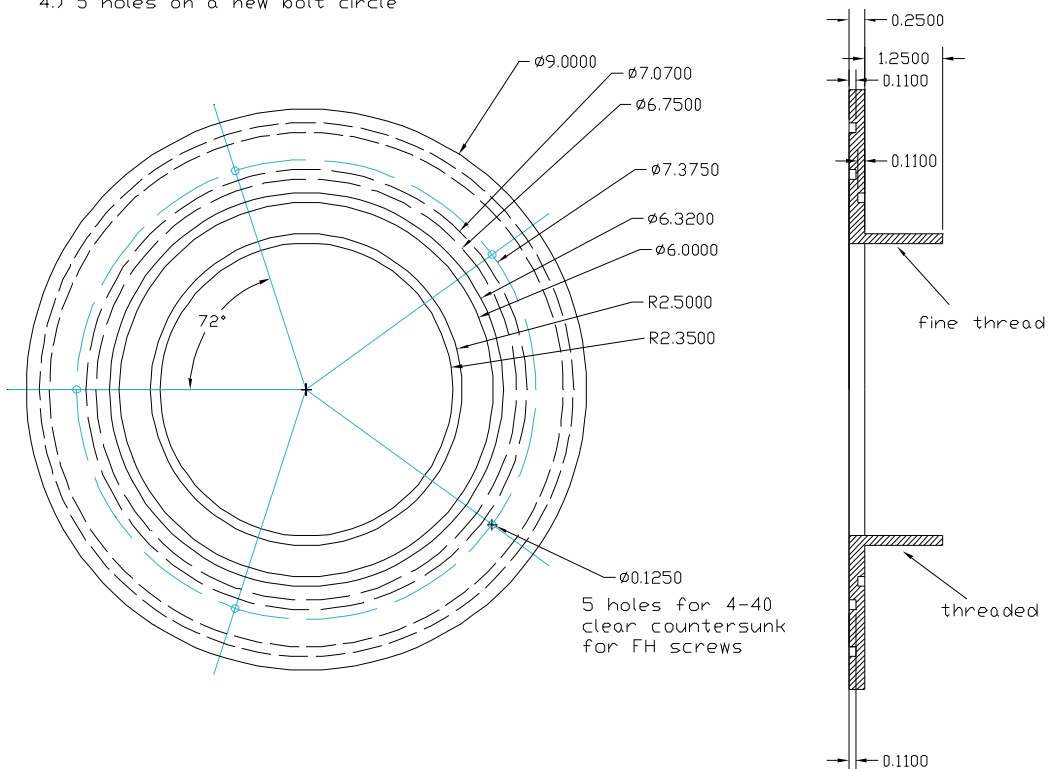


Fig. 54 Dewar-to-Black-Box adapter

7.1.4 Wiring diagram of the setup

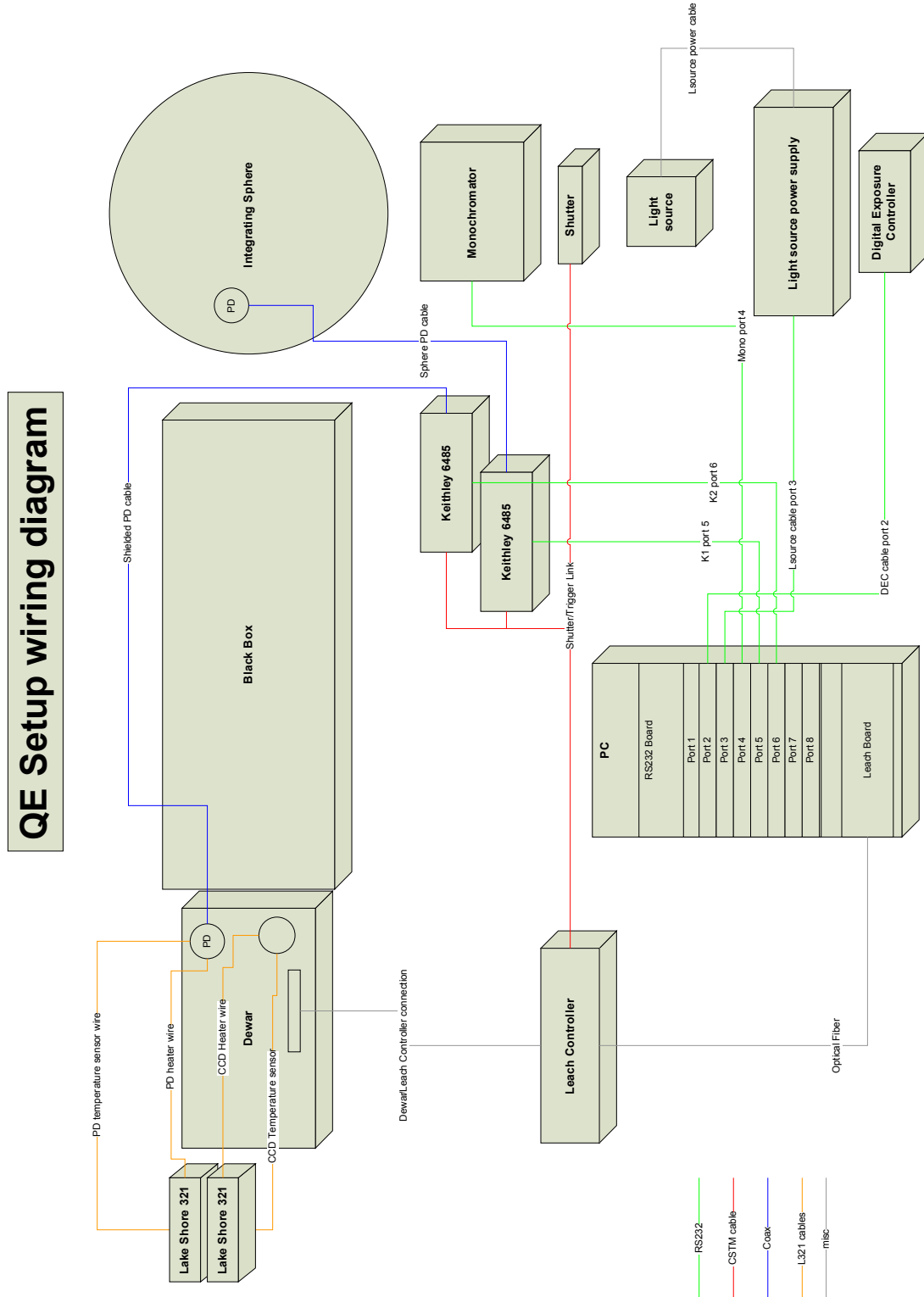


Fig. 55 Wiring diagram of the test setup

7.2 Software

7.2.1 Qe measurement script

This script was used to measure the QE with VOODOO

```

/*****
VOODOO QE measurement script
fullscan 300-1100nm, 20nm steps
5 sec exposure time, 10 measurements, 0.5 sec integration time, first meas discarded
15um pixel size, 1cm^2 = 444444 pixel
*****/

double mkei1 = 0;
double skei1 = 0;
double mkei2 = 0;
double skei2 = 0;
double ppp;
double pixel = 444444;
double exptime;
int wl;

String mans;
String logfilename;
String imagename;
String path;
String fn;

VoodooControl.setDoOpenShutter(true);

VoodooControl.setupKei(1);
VoodooControl.setupKei(2);

//specify path
path = "/home/jens/Images/02242005";
fn = "qe_run32_";

//set up log file
logfilename = "Qe_run32.txt";
VoodooControl.openLog(logfilename);

//start main loop

for( int i = 300; i <= 1100; i = i + 10){

    //set exposure time and filename
    VoodooControl.setDoSaveToDisk(true, path, fn + Integer.toString(i) + ".fit",
false);
    VoodooControl.setExposureTime(5);

```

```
//set wl and slw
mans = VoodooControl.scMono("!gw " + Integer.toString(i), false);
VoodooControl.sleep(1);

//set light level to 7000 photons per second on a 15um pixel
VoodooControl.scMono("slita 0",false);
VoodooControl.openShutter();
VoodooControl.setLightLevel(7000, 15e-6,i);
VoodooControl.closeShutter();

//clears the ccd
VoodooControl.clear();
VoodooControl.clear();
VoodooControl.clear();

//wait a second...
VoodooControl.sleep(1);

//reset keithley
VoodooControl.setupKei(1);
VoodooControl.setupKei(2);

//set keithley autozero off
VoodooControl.azeroKei(1,false);
VoodooControl.azeroKei(2,false);

//arms the keithley for a triggered operation, 10 buffers, 0.5 sec
//integration time, and two different meas ranges
VoodooControl.armKeiExtTrigBuf(1,10,30,2e-6);
VoodooControl.armKeiExtTrigBuf(2,10,30,2e-9);

//wait a second
VoodooControl.sleep(1);

//expose and wait2
VoodooControl.expose(true);
VoodooControl.sleep(2);

//get meas values
mkei1 = VoodooControl.getKeiBufAmpDelMean(1,10,1);
skei1 = VoodooControl.getKeiBufAmpDelSDevi(1,10,1);
mkei2 = VoodooControl.getKeiBufAmpDelMean(2,10,1);
skei2 = VoodooControl.getKeiBufAmpDelSDevi(2,10,1);

//calculations
dewarwatts = VoodooControl.calcWatts(mkei2, i);
dewarphotons = VoodooControl.calcPhotons(mkei2, i);
//calculate photons per pixel per second
ppp= dewarphotons /pixel;
//calculate the amount of photons per pixel per exposure
```

```
ppp = ppp * 5;

//reset keithley
VoodooControl.setupKei(1);
VoodooControl.setupKei(2);

//write results to the log file
VoodooControl.log('\t' + "Wavelength" + '\t' + Integer.toString(i));
    VoodooControl.log('\t' + "Image_file_name " + '\t' + path + '/' + fn +
Integer.toString(i) + ".fit");
VoodooControl.log('\t' + "mkei1" + '\t' + Double.toString(mkei1));
VoodooControl.log('\t' + "skei1" + '\t' + Double.toString(skei1));
VoodooControl.log('\t' + "mkei2" + '\t' + Double.toString(mkei2));
VoodooControl.log('\t' + "skei2" + '\t' + Double.toString(skei2));
VoodooControl.log('\t' + "photons_per_pixel" + '\t' + Double.toString(ppp));

}
//close log File
VoodooControl.closeLog();
```

7.2.2 VOODOO qe script log file

The following lines are a sample of a voodoo qe script log file

```
Thu Feb 24 19:19:44 PST 2005>      Wavelength  300
Thu Feb 24 19:19:44 PST 2005>      Image_file_name
/home/jens/Images/02242005/qe_run32_300.fit
Thu Feb 24 19:19:44 PST 2005>      mkei1 -8.807597111111111E-8
Thu Feb 24 19:19:44 PST 2005>      skei1 2.902217645734003E-10
Thu Feb 24 19:19:44 PST 2005>      mkei2 -2.722432666666666E-10
Thu Feb 24 19:19:44 PST 2005>      skei2 1.1049132711690593E-12
Thu Feb 24 19:19:44 PST 2005>      photons_per_pixel 34996.3413860301
Thu Feb 24 19:20:44 PST 2005>      Wavelength  310
Thu Feb 24 19:20:44 PST 2005>      Image_file_name
/home/jens/Images/02242005/qe_run32_310.fit
Thu Feb 24 19:20:44 PST 2005>      mkei1 -8.977561555555555E-8
Thu Feb 24 19:20:44 PST 2005>      skei1 1.426360085525421E-10
Thu Feb 24 19:20:44 PST 2005>      mkei2 -2.768314111111111E-10
Thu Feb 24 19:20:44 PST 2005>      skei2 4.824628851745756E-13
Thu Feb 24 19:20:44 PST 2005>      photons_per_pixel 34920.498413957
Thu Feb 24 19:21:50 PST 2005>      Wavelength  320
Thu Feb 24 19:21:50 PST 2005>      Image_file_name
/home/jens/Images/02242005/qe_run32_320.fit
Thu Feb 24 19:21:50 PST 2005>      mkei1 -8.982119111111111E-8
Thu Feb 24 19:21:50 PST 2005>      skei1 9.130202042390752E-11
Thu Feb 24 19:21:50 PST 2005>      mkei2 -2.760359888888889E-10
Thu Feb 24 19:21:50 PST 2005>      skei2 3.846268052554274E-13
Thu Feb 24 19:21:50 PST 2005>      photons_per_pixel 34937.98246054
Thu Feb 24 19:22:59 PST 2005>      Wavelength  330
Thu Feb 24 19:22:59 PST 2005>      Image_file_name
/home/jens/Images/02242005/qe_run32_330.fit
Thu Feb 24 19:22:59 PST 2005>      mkei1 -9.183870444444444E-8
Thu Feb 24 19:22:59 PST 2005>      skei1 2.5312458580971003E-11
Thu Feb 24 19:22:59 PST 2005>      mkei2 -2.812770333333333E-10
Thu Feb 24 19:22:59 PST 2005>      skei2 1.5755517596137181E-13
Thu Feb 24 19:22:59 PST 2005>      photons_per_pixel 35000.570822
Thu Feb 24 19:23:59 PST 2005>      Wavelength  340
Thu Feb 24 19:23:59 PST 2005>      Image_file_name
/home/jens/Images/02242005/qe_run32_340.fit
Thu Feb 24 19:23:59 PST 2005>      mkei1 -9.180626555555555E-8
Thu Feb 24 19:23:59 PST 2005>      skei1 2.2848584285635163E-11
Thu Feb 24 19:23:59 PST 2005>      mkei2 -2.806935888888888E-10
Thu Feb 24 19:23:59 PST 2005>      skei2 9.701112200778117E-14
Thu Feb 24 19:23:59 PST 2005>      photons_per_pixel 35051.682015828
Thu Feb 24 19:24:59 PST 2005>      Wavelength  350
Thu Feb 24 19:24:59 PST 2005>      Image_file_name
/home/jens/Images/02242005/qe_run32_350.fit
Thu Feb 24 19:24:59 PST 2005>      mkei1 -8.735507222222222E-8
Thu Feb 24 19:24:59 PST 2005>      skei1 2.618141424762954E-11
Thu Feb 24 19:24:59 PST 2005>      mkei2 -2.665324888888889E-10
Thu Feb 24 19:24:59 PST 2005>      skei2 7.187347593661041E-14
Thu Feb 24 19:24:59 PST 2005>      photons_per_pixel 34262.2320317827
...
```

7.2.3 IDL Program for calculation of the QE

This IDL program was used to extract the QE from the image data.

```
pro QE_script2, INFILE, OUTFILE
;*****
;QE calculation script for VOODOO.qe log files
;*****

;check parameters
IF n_params(0) LT 1 THEN BEGIN
    print, 'Qe_script, INFILE, OUTFILE'

    RETALL
ENDIF

;log file name
file = INFILE

;first get image file names
readcol, file, c1, c2, c3, c4, c5, c6, c7, c8, $
    f='(a,a,a,a,a,a,a,a )'

;get wavelength
w = where(c7 eq 'Wavelength')
wl = c8[w]

;get filenames
w = where(c7 eq 'Image_file_name')
fn = c8[w]

;get photons per pixel
w = where(c7 eq 'photons_per_pixel')
photons = c8[w]

;get keithley 1 mean
w = where(c7 eq 'mkei1')
mkei1 = c8[w]

;get keithley 1 standard deviation
w = where(c7 eq 'skei1')
skei1 = c8[w]

;get keithley 2 mean
w = where(c7 eq 'mkei2')
mkei2 = c8[w]

;get keithley 2 standard deviation
w = where(c7 eq 'skei2')
skei2 = c8[w]

;open outputfile
get_lun, hallo
openw, hallo, OUTFILE

;print header
printf, hallo, 'wavelength' + ';' + 'photons_per_pixel' + ';' +
'counts' + ';' + 'electrons' + ';' + 'QE' + ';' + 'mkei1'
+';'+'skei1'+';'+'mkei2'+';'+'skei2'
```

```
;dimension array
arlength = n_elements(wl)
print, 'arraylength' + string(arlength)

;start main for loop

FOR i= 0, arlength-1 DO BEGIN

    ;read image
    im = readfits( fn[i])
    im = float(im)

    ;specify overscan area
    overscan = im(2500:2599,600:700)

    ;specify image area
    image = im(1500:1900,300:700)

    ;calc statistics
    momov = moment(overscan)
    momim = moment(image)

    ; make a first pass, including outliers (xrays in this case)
    momov = moment(overscan)
    meanlov = momov[0]
    siglov = sqrt(momov[1])

    a = 3.
    lower = meanlov-a*siglov
    upper = meanlov+a*siglov
    w = where(overscan gt lower and overscan lt upper)

    ; now do it again with  $\pm a*\text{sigl}$  of the mean
    momov2 = moment(overscan[w])

    mean2ov = momov2[0]
    sig2ov = sqrt(momov2[1])

    ; do the same with the image...

    ; second pass, only pixels within +/- three sigma are taken for
c ;alculation
    momim = moment(image)
    meanlim = momim[0]
    siglim = sqrt(momim[1])

    a = 3.
    lower = meanlim-a*siglim
    upper = meanlim+a*siglim
    w = where(image gt lower and image lt upper)

    ; now do it again with  $\pm a*\text{sigl}$  of the mean
    momim2 = moment(image[w])

    ;print, 'n_elements(im[w] = ', n_elements(w)
    mean2im = momim2[0]
    sig2im = sqrt(momim2[1])
```

```
;calculating the ADUs
counts = mean2im - mean2ov
electrons = counts / 1.5959D
print, string(photons[i])

ph = 0.0D
ph = photons[i] *1.00D

qe = (electrons/ph)*100D

wavel = wl[i]

;print results into output file
printf, hallo, string(wavel) + ';' + string(ph) + ';' + string
(counts) + ';' + string(electrons) + ';' + string(qe)+ ';' + string
(mkeil[i]) + ';' + string(skeil[i])+';' + string(mkei2[i])+';' + string
(skei2[i])

ENDFOR

;close output file
close, hallo

END
```

7.2.4 Selected parts of the VOODOO extensions

The VOODOO.QE extensions consist of several classes which contain several functions. Since the JAVA source code of the extensions has a length of over 4000 lines it is too large to be attached in this appendix. Instead several important excerpts of the code are presented in the next chapters.

7.2.4.1 VOODOO.QE.Main.setLightLevel_closedSlit

This function sets the light level to an specified value. Therefore it calls some VOODOO.QE.Calc functions.

```
/******
adjusts the light level to a specified number of photons per pixel
*****/
public static boolean setLightLevel_closedslit(double ppp, int wl, double pixelsize){
    //variable declarations
    double mphotons;
    double amps;
    double photons;
    int i = 0;
    int percent = 3 ;
    int slw;
    double ratio;
```

```
slw = 4;
Mono.setISlit( slw);

//calculate photons per cm^2
photons = ppp * (0.01 / pixelsize)* (0.01 / pixelsize);

//measure the light level
amps = Kei_2.measAmp() ;
//convert A to photons
mphotons = QeCalc.calcPhotons( wl,amps);

if( mphotons> photons){
    System.out.println("firstloop mphotons: " + Double.toString( mphotons) + "
    photons: " + photons);
    return false;
}

//while light not within +/- 3% of ppp
while(mphotons < (photons - ((photons/100) *percent)) || mphotons > (photons
+ ((photons/100) *percent))){
    if (i >= 10){
        break;
    }
    //calculate ratio
    ratio = photons/mphotons;
    //limit ratio (prevents overshooting)
    if (ratio >= 4)
        ratio = 4;

    //calculate slit width
    slw = (int) ((double)slw * ratio);

    i++;
    //set slit width
    if (slw <= 2000)
        Mono.setISlit( slw);
    else
        return false;
    //measure light level
    mphotons = QeCalc.calcPhotons(wl, Kei_2.measAmp() );
}

//if light to bright
while(mphotons > photons){
    slw = slw - 1;
    Mono.setISlit( slw);
    mphotons = QeCalc.calcPhotons(wl, Kei_2.measAmp() );
}
return true;
}
```

7.2.4.2 VOODOO.QE.Calc

This class contains some functions which perform essential calculations

```
/* Created on Nov 2, 2004 */
package voodoo.qe;

import java.io.File;
import java.io.FileInputStream;
import java.io.FileReader;
import java.io.BufferedReader;

import javax.swing.JOptionPane;

import sun.awt.CharsetString;
/**
 * This class contains the main calculation functions for the Qe test setup
 * @author jens
 *
 */
public class QeCalc {
    //planck
    public static final double h = 6.63e-34;
    //light speed
    public static final double c = 3e+8;
    //electron charge
    public static final double e = 1.6e-19;

    //sensitivity values of the pd (s2281 uncalibrated)
    //have to be replaced by real calibration values
    public static final double [] pdwl = {300, 310, 320, 330, 340, };
    public static final double [] pdqe = {131, 138, 141, 149, 153, };

    public static FileInputStream f1 = null;
    public static BufferedReader fin = null;

    static{
        QeCalc.loadCalibration( QeInfo.cinf.qeDiodeCalibration );
    }

    /*****
    calculates the settings for the QE simple gui
    *****/
    public static void calcSettings(){
        int meascount;
        float integTime = (float)0.5;
        meascount = (int)(QeInfo.expTime /(integTime *1));

        QeInfo.kei1Buf = meascount;
        QeInfo.kei2Buf = meascount;
        QeInfo.kei1SkipBuf = 1;
    }
}
```

```

QeInfo.kei2SkipBuf = 1;

QeInfo.kei1Integ = 30;
QeInfo.kei2Integ = 30;

}
/*****
converts current to photons
*****/
public static double calcPhotons(int wl, double current){
    double pdsens;
    double energy;
    double photons;
    double Ephoton;

    pdsens = calcSensitivity(wl);
    energy = current/(pdsens/1000);

    Ephoton = h * c/(wl * 1e-9);

    photons =energy/Ephoton;
    if (photons<0){
        photons = photons * (-1);
    }

    return photons;
}
/*****
converts current to energy in watt
*****/
public static double calcWatts(int wl, double current){
    double pdsens; //pd sensitivity (has to be calculated with the calcsens function)
    double watts;
    pdsens = calcSensitivity(wl); //calcs the pd sensitivity for wl

    watts = current/(pdsens/1000); //pdsens is given in mA/W, divided by 1000 to get
A/W

    return watts;
}
/*****
calculates the mean of a given array
*****/
public static double calcMean(double[] ar){
    double buf=0;
    int i;
    for( i = 0; i< ar.length ; i++){
        buf = buf + ar[i];
        System.out.println("calcMean:" + Double.toString( ar[i]));
    }
}

```

```
System.out.println("bufout " + buf + "count: " + Integer.toString(i));
return buf/((double)i);

}
/*****
calculates the standard deviation of an given array
*****/
public static double calcSDevi(double[] ar){
    double mean;
    double sdev =0;
    double mulfac= 10;
    mean = calcMean(ar);
    int i;

    for ( i =0; i< ar.length; i++){
        sdev =+ (ar[i]-mean)*(ar[i]-mean);
    }

    sdev = sdev * ((double) 1/((double)ar.length - (double) 1));
    sdev =Math.sqrt( sdev);
    return sdev;
}

/*****
loads the PD calibration data
*****/
public static void loadCalibration(String fn){
    String line = "sdf";
    String [] sLine = new String[2];
    double wl=0;
    double sens=0;
    int i = 0;

    try{
        BufferedReader cfile = new BufferedReader(new FileReader(fn));
        line = cfile.readLine();
        sens = 0;
        while (line != null)
        {

            System.out.println(line) ;
            sLine = line.split( Character.toString( '\t'));
            wl = Double.parseDouble( sLine[0]) ;
            sens = Double.parseDouble( sLine[1]);
            pdwl[i]=wl;
            pdqe[i]=sens;
            i++;
            line = cfile.readLine();
        }
    }
}
```

```

cfile.close() ;

QeInfo.cinf.qeDiodeCalibration = fn;
QeInfo.cinf.qeMainGui.stm("Loading photo diode calibration file
successful");

}catch(Exception ex){
    System.out.println (ex.toString());
    QeInfo.cinf.qeMainGui.stm("Loading photo diode calibration file failed");
}

}
/*****
calculates the diode sensitivity at the given wavelength
(linear interpolation)
*****/
public static double calcSensitivity(int wl){
    double wla=0; //wavelength a
    double wlb=0; //wavelength b
    int i=0;
    double m; //slope
    double b; //offset
    double sa;
    double sb;

    //searching the proper wl
    while (wl >= pdwl[i]){
        i++ ;
    }

    //select wavelength b
    wlb = pdwl[i];

    //select wavelength a
    wla = pdwl[i-1];

    //select sensitivity a
    sa = pdqe[i-1];

    //select sensitivity b
    sb = pdqe[i];

    //calculating the slope
    m=(sb-sa) /(wlb-wla);
    //calculate offset
    b= sa - (m* wla);

    //interpolates the sensitivity value for the given wavelength
    return m * wl + b;
}

```

7.2.4.3 VOODOO.QE.Mono.SendCommand

This function is identical in all device control classes. It sends an string to the device and waits for the answer. A timeout can be specified.

```

/*****
 * This is the generic send-command-to-the-device function. It gives back the answer of the
 * device
 * @param cmd the command to send (without terminator)
 * @param delay (the time to wait for an answer of the device in milliseconds)
 * @return The answer of the device (if there is one)
 *****/
public static String sendCommand(String cmd, long timeout){
    String question;
    String answer = "";

    //get date and time
    GregorianCalendar gc1 = new GregorianCalendar();
    Date d1 = gc1.getTime();
    long l1 = d1.getTime();

    //assembles the command of command and terminator
    question = cmd + term;

    //opens the serial interface
    serPort.open( INTERFACE_NAME);

    //sends the command
    serPort.write(question);

    //watis for answer
    while(answer.indexOf( '>' ) < 1){
        //read serial port
        answer = answer + serPort.strRead(50);
        delay(1);

        //get actual time
        GregorianCalendar gc2 = new GregorianCalendar();
        Date d2 = gc2 .getTime();
        long l2 = gc2.getTimeInMillis();

        //check timeout
        if (l1 + timeout < l2 ){
            answer = "timeout-1";
            break;
        }
    }

    //close serial connection
    serPort.close() ;
    return answer;
}

```

7.2.5 Software Screenshots

The following image is a screenshot of the VOODOO main window

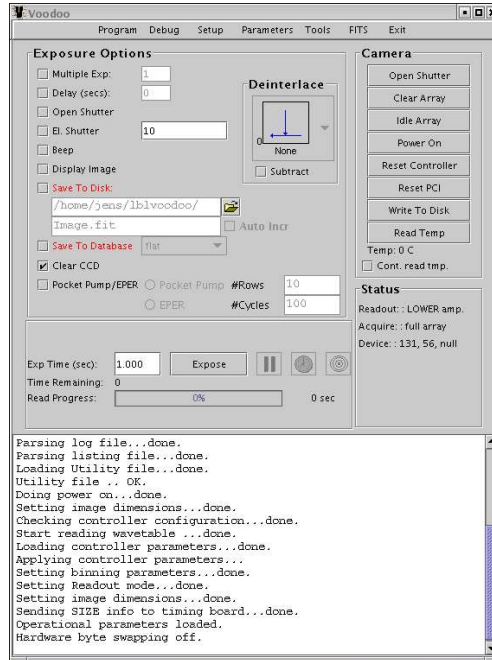


Fig. 56 Main window of the VOODOO software

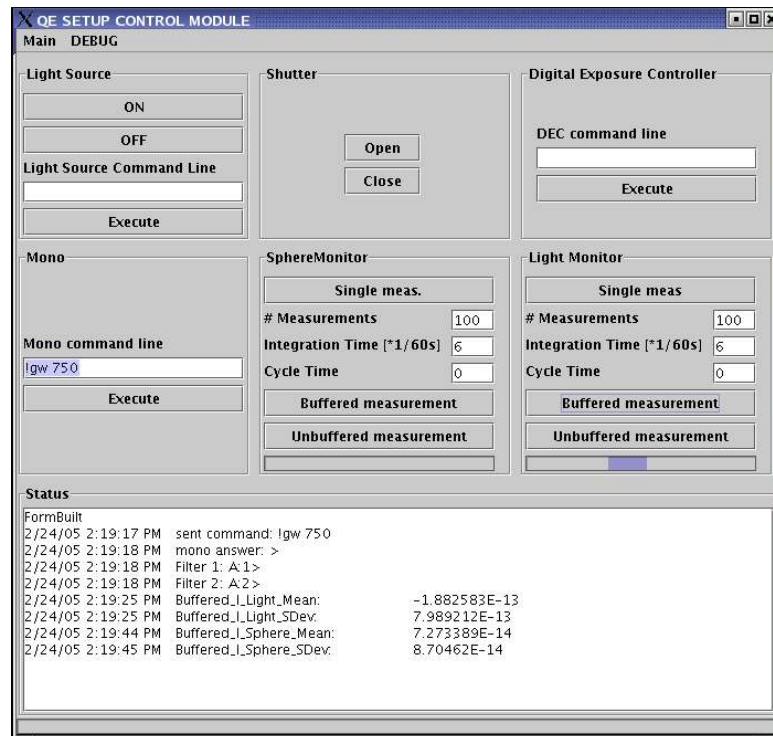


Fig. 57 The QE setup control window

Fig. 57 shows a screenshot of the VOODOO.QE extension

Acknowledgements

The work described in this thesis was done from September 2004 to February 2005 at the Lawrence Berkeley National Laboratory. I want to thank all people who supported me there.

Especially:

Armin Karcher who was my supervisor and first address for questions, comments and Linux problems...

Bill Kolbe who was the “lab guru” and shared his huge experience in every lab related aspects.

Chris Bebek for comments ideas and all the administrative support.

Don Groom for his engagement in this project and he was the one who read and annotated the thesis, thanks !

Joao Pequano who introduced me to the wonderful espresso machine....

Richard Kuiper who did a great job in manufacturing the mechanical parts.

All the others I didn't mentioned in person

I also want to thank **Prof. Dr. Bantel** who was my Professor at the Fachhochschule Karlsruhe and made the link to the LBNL.

It was a great time and a wonderful project !

Ich versichere hiermit, daß ich die vorliegende Diplomarbeit selbständig erarbeitet und dabei keine anderen als die angegebenen Quellen verwendet habe.

Datum: 31.03.2005

Illustration Index

<i>Fig. 1 Cross section of the SNAP satellite [2]</i>	8
<i>Fig. 2 Exploded drawing of the SNAP imager [4]</i>	9
<i>Fig. 3 Different types of CCDs</i>	10
<i>Fig. 4 Quantum efficiency of a LBNL CCD vs. wavelength [6]</i>	11
<i>Fig. 5 Absorption length of photons in Si vs. wavelength [6]</i>	12
<i>Fig. 6 Block diagram of the QE test bench</i>	14
<i>Fig. 7 Photo of the QE setup</i>	15
<i>Fig. 8 Illustration of an optical grating. The angle b is the blaze angle</i>	20
<i>Fig. 9 Grating efficiencies of the used gratings</i>	22
<i>Fig. 10 Stray light vs wavelength</i>	24
<i>Fig. 11 Bandpass resulting of the combination of a short wave pass and a long wave pass filter</i>	25
<i>Fig. 12 The bandpass filters used</i>	26
<i>Fig. 13 Uniformity vs. distance from sphere calculated with (9)</i>	28
<i>Fig. 14 Sketch of the integrating sphere</i>	29
<i>Fig. 15 Photograph of the integrating sphere</i>	29
<i>Fig. 16 open black box</i>	30
<i>Fig. 17 Dewar with CCD and photo diode</i>	31
<i>Fig. 18 Typical QE of a Hamamatsu 1010BQ photo diode</i>	32
<i>Fig. 19 Temperature controlled photo diode mount for dewar</i>	33
<i>Fig. 20 PD mount built into Dewar</i>	34
<i>Fig. 21 Shutter- filter wheel adapter</i>	35
<i>Fig. 22 Focusing lens to shutter adapter</i>	36
<i>Fig. 23 Shutter-to-filter wheel adapter</i>	36
<i>Fig. 24 Monochromator- integrating sphere adapter</i>	37
<i>Fig. 25 Monochromator to integrating sphere adapter</i>	37
<i>Fig. 26 Flange for sphere and black box supporting a bellows</i>	38
<i>Fig. 27 Dewar with attached black box adapter flange</i>	38
<i>Fig. 28 Photo diode housing</i>	39
<i>Fig. 29 Light flux on detector vs. wavelength</i>	45
<i>Fig. 30 Standard deviation of the measured values vs. integration time</i>	47
<i>Fig. 31 Noise current and error caused by noise current vs. wavelength</i>	49
<i>Fig. 32 Total integration time split into 5 long or 50 short measurements</i>	50
<i>Fig. 33 First measurement of PD current vs. wavelength</i>	55

<i>Fig. 34 Horizontal uniformity</i>	59
<i>Fig. 35 Horizontal uniformity vs fitted curves</i>	60
<i>Fig. 36 Data flow in VOODOO.qe</i>	66
<i>Fig. 37 Relationships among objects in VOODOO.qe</i>	67
<i>Fig. 38 Architecture of the VOODOO scripting interface</i>	68
<i>Fig. 39 Flow chart of the QE measurement script</i>	69
<i>Fig. 40 Histogram of a x-ray exposure</i>	72
<i>Fig. 41 10 sec x-ray exposure of a low voltage device. Every clusters represents an event (x-ray generating charge in silicon) Unit of x and y axis is [pixel]</i>	74
<i>Fig. 42 Quantum Efficiency and 1-Reflectivity vs Wavelength</i>	74
<i>Fig. 43 Reproductivity measurement of the low voltage device</i>	75
<i>Fig. 44 10 second x-ray exposure of an high voltage device. The number of bright pixels created by an event i</i>	76
<i>Fig. 45 Quantum efficiency vs 1-reflectivity</i>	77
<i>Fig. 46 Reproductivity measurement of the high voltage device</i>	78
<i>Fig. 47 QE curve of first meas (QE 8) vs QE after remounting (QE 31)</i>	79
<i>Fig. 48 Timing diagram of the Uniblitz shutter</i>	81
<i>Fig. 49 Test setup, shown from the dewar side</i>	87
<i>Fig. 50 Test setup, light generation section top view</i>	88
<i>Fig. 51 Test setup, view on the light generation part and the sphere</i>	88
<i>Fig. 52 Monochromator (open) with beamline</i>	89
<i>Fig. 53 Housing (open) with mounted arc lamp</i>	89
<i>Fig. 54 Dewar-to-Black-Box adapter</i>	92
<i>Fig. 55 Wiring diagram of the test setup</i>	93
<i>Fig. 56 Main window of the VOODOO software</i>	107
<i>Fig. 57 The QE setup control window</i>	107

References

- [1] "Supernova", <http://en.wikipedia.org/wiki/Supernova>
- [2] M. Scholl, M.Lampton et al., "SNAP Telescope", *Proceedings of SPIE*, vol. 5487, pp. 1473-1483, 2004
- [3] "SNAP Homepage" , <http://snap.lbl.gov>
- [4] "SNAP Brochure", <http://snap.lbl.gov>
- [5] C.J. Bebek et al., "Fully depleted back-illuminated p-channel CCD development", *Proceedings of SPIE*, vol. 5167, pp. , 2003
- [6] S.E. Holland, "Fully Depleted, Back-Illuminated Charge-Coupled Devices Fabricated on High-Resistivity Silicon", *IEEE TRANSACTIONS ON ELECTRON DEVICES*, vol. 50, pp. 225-238, 2003
- [7] Yukiko Kamata, Satoshi Miyazaki et al., "Development of thick back illuminated CCD to improve quantum efficiency in optical longer wavelength using high resistivity n-type silicon", *Proceedings of SPIE*, vol. 5499, pp. 210-218, 2004
- [8] M.P. Lesser, B.L. McCarthy, "Quantum Efficiency Characterization of Scientific CCDs", *Proceedings of SPIE*, vol. 2654, pp. 278-286, 1996
- [9] P. Amico, T. Bohm, C. Cavadore, "The ESO CCD testbench", <http://www.eso.org/projects/odt/CCDtestbench/Testbench.html>
- [10] "The Book of Photon Tools" ,Oriel Instruments,
- [11] "Sphere Systems and Instrumentation" ,Labsphere, 2001
- [12] "Data Sheet Si photodiode S1337 series" ,Hamamatsu,
- [13] "Waermeleitfaehigkeit" , <http://de.wikipedia.org/wiki/W%C3%A4rmeleitf%C3%A4higkeit>
- [14] "Data Sheet Si photodiode S2281 series" ,Hamamatsu,
- [15] "Photo Diode Technical Information" ,Hamamatsu,
- [16] "Model 6485 Picoammeter Instruction Manual" ,Keithley Instruments Inc.,
- [17] Patrik Niemeyer, Jonathan Knudsen, "Learning Java", pp. 807, 2002
- [18] James R. Janesick, "Scientific Charge-Coupled Devices",, vol. , pp. ,
- [19] Don Groom, "Temperature dependence of mean number of e-h pairs per eV of x-ray energy deposit", 2004
- [20] "VS14 & VS25 Shutters Specifications" ,Uniblitz (Vincent Associates),

- [21] "Spectra Physics Filter Catalogue" , <http://www.spectra-physics.com/com/cda/product/detail/1,1055,117057,00.html>